NASA TECHNICAL MEMORANDUM

NASA TM X-3276

NASA TM X-3276

LOW-SPEED AERODYNAMIC CHARACTERISTICS OF A TRANSPORT MODEL HAVING 42.33° SWEPT LOW WING WITH SUPERCRITICAL AIRFOIL, DOUBLE-SLOTTED FLAPS, AND T-TAIL OR LOW TAIL

Paul G. Fournier

Langley Research Center

Hampton, Va. 23665

NATIONAL AERONAUTICS AND SPACE ADMINISTRATION • WASHINGTON, D. C. • NOVEMBER 1975

1. Report No.	2. Government Accession No.	3. Recipient's Catalog No.
NASA TM X-3276		

4. Title and Subtitle	5. Report Date
LOW-SPEED AERODYNAMIC CHARACTERISTICS OF A TRANSPORT MODEL HAVING 42.33° SWEPT LOW WING WITH SUPERCRITICAL AIRFOIL, DOUBLE-SLOTTED FLAPS, AND T-TAIL OR LOW TAIL	November 1975
	6. Performing Organization Code
7. Author(s)	8. Performing Organization Report No.
Paul G. Fournier	L-9957
	10. Work Unit No.
9. Performing Organization Name and Address	505-11-11-01
NASA Langley Research Center Hampton, Va. 23665	11. Contract or Grant No.
	13. Type of Report and Period Covered
12. Sponsoring Agency Name and Address	Technical Memorandum
National Aeronautics and Space Administration Washington, D.C. 20546	14. Sponsoring Agency Code

15. Supplementary Notes

16. Abstract

A low-speed investigation was conducted in the Langley V/STOL tunnel over an angle-of-attack range from approximately -4° to 24° to determine the static longitudinal stability characteristics and high-lift performance of a general research model which represented an advanced subsonic transport configuration. The model had a 42.33° swept, aspect-ratio-7.05 wing with a supercritical airfoil and high-lift system consisting of a leading-edge device (slat or Kruger flap) and a double-slotted flap. The flaps were deflected for take-off and landing configurations and were not deflected for tests of the clean configuration. The model was tested with the horizontal tail in either a T-tail or low-tail position. The effects of various arrangements of flowthrough nacelles which represent a three-engine configuration (two large wing-mounted nacelles and a vertical-tail mounted nacelle) and a four-engine configuration (four smaller wing-mounted nacelles) were determined.

17. Key Words (Suggested by Author(s))	18. Distribution Statement
High-lift systems Supercritical wing (Boeing) Low-speed aerodynamics Swept wing Tail height Transport configuration	Unclassified – Unlimited Subject Category 02

19. Security Classif. (of this report)	20. Security Classif. (of this page)	21. No. of Pages	22. Price*
Unclassified	Unclassified	93	$4.75

*For sale by the National Technical Information Service, Springfield, Virginia 22161

LOW-SPEED AERODYNAMIC CHARACTERISTICS OF A TRANSPORT MODEL HAVING 42.33° SWEPT LOW WING WITH SUPERCRITICAL AIRFOIL, DOUBLE-SLOTTED FLAPS, AND T-TAIL OR LOW TAIL

Paul G. Fournier
Langley Research Center

SUMMARY

A low-speed investigation was conducted in the Langley V/STOL tunnel over an angle-of-attack range from approximately -4° to 24° to determine the static longitudinal stability characteristics and high-lift performance of a general research model which represented an advanced subsonic transport configuration. The model had a 42.33° swept, aspect-ratio-7.05 wing with a supercritical airfoil and high-lift system consisting of a leading-edge device (slat or Kruger flap) and a double-slotted flap. The flaps were deflected for take-off and landing configurations and were not deflected for tests of the clean configuration. The model was tested with the horizontal tail in either a T-tail or low-tail position. The effects of various arrangements of flowthrough nacelles which represent a three-engine configuration (two large wing-mounted nacelles and a vertical-tail-mounted nacelle) and a four-engine configuration (four smaller wing-mounted nacelles) were determined.

The maximum lift coefficient for the model with the high-lift system deflected was 2.22 for the landing configuration. In general, slightly greater lift was obtained with the Kruger flap than with the leading-edge slat. The model configuration with both of the tail heights and for all flap deflections became unstable at fairly low angles of attack (α = 6° to 9°); however, the low-tail configuration became stable near an angle of attack of 17° to 18°. For the maximum flap deflection, stall occurred at angles of attack above 20° for the four-engine configuration and was not reached in the test angle-of-attack range for the three-engine configuration.

INTRODUCTION

Extensive research effort by the National Aeronautics and Space Administration to improve the performance of subsonic aircraft has shown that the drag rise can be delayed to Mach numbers approaching unity by the use of supercritical airfoil sections and by careful integration of the wing, engines, and tail surfaces with a properly shaped fuselage. (See refs. 1 and 2.) Much research effort has been undertaken at near-sonic speeds to develop

aerodynamic configurations that could provide realistic focal points for developing the technology applicable to advanced subsonic commercial transports. Research has also been conducted at low speeds to develop high-lift systems for wings employing supercritical airfoils that would enable these advanced configurations to have take-off and landing performance equal to or better than subsonic transports employing wings with conventional airfoils. Some work has been reported in reference 3 on a rectangular wing with a slotted supercritical airfoil having several high-lift devices and in references 4 to 6 for more recent adaptation of a supercritical airfoil. Also, data which would be more applicable to a transport configuration are presented in references 7 and 8.

The present investigation was conducted to obtain an overall assessment of the low-speed, static-stability, and high-lift performance of a general research model which represented an advanced subsonic transport configuration with a high-lift system. The present model had a wing with 42.33° sweep of the quarter-chord line, an aspect ratio of 7.05, a taper ratio of 0.35, and supercritical airfoil sections. The wing was located in a low position near the bottom of the fuselage.

The high-lift system consisted of a partial-span, double-slotted flap which extended from the wing-body juncture to the 73-percent wing semispan and a leading-edge device which extended from the 38-percent wing-semispan station to the 90-percent wing-semispan station. The model was tested with either a leading-edge slat or a leading-edge Kruger flap deflected 45°. Combinations of flap deflections and a leading-edge device were investigated to represent clean, take-off, and landing configurations. The horizontal tail was located either near the top of the vertical tail (T-tail) or in a low-tail position; both were tested for a limited range of stabilizer settings. Effects of various arrangements of flowthrough nacelles which represented a three-engine configuration (two large wing-mounted nacelles and a vertical-tail-mounted nacelle) and a four-engine configuration (four smaller wing-mounted nacelles) were determined.

SYMBOLS

The static longitudinal stability data are presented about the stability-axis system. The positive directions of forces, moments, and angles are indicated in figure 1. The model moment reference was located at the quarter chord of the wing mean aerodynamic chord (theoretical wing) and on the fuselage center line. (See fig. 2(a).)

The measurements of this investigation are presented in the International System of Units (SI). Details concerning the use of SI units, together with physical constants and conversion factors, are presented in reference 9.

b wing span, cm

C_D drag coefficient, $\frac{\text{Drag}}{qS}$

C_L	lift coefficient, $\frac{\text{Lift}}{qS}$
C_m	pitching-moment coefficient, $\frac{\text{Pitching moment}}{qS\bar{c}}$
c	local chord, cm
c_f	chord of flap, cm
$c_{f,1}$	forward section of flap, cm
$c_{f,2}$	aft section of flap, cm
c'	local chord perpendicular to leading edge or trailing edge, cm
c'_K	chord of leading-edge Kruger flap perpendicular to leading edge, cm
c'_s	chord of leading-edge slat perpendicular to leading edge, cm
$\bar{c}$	mean aerodynamic chord of theoretical wing, cm
$\bar{c}_H$	mean aerodynamic chord of horizontal tail, cm
$\bar{c}_V$	mean aerodynamic chord of vertical tail, cm
i_t	horizontal-tail incidence, positive when trailing edge is down (see fig. 1), deg
q	free-stream dynamic pressure, Pa
S	wing area (based on theoretical planform), m^2
T	temperature, K
t_{max}	maximum thickness of airfoil, cm
x	distance along chord of wing, slat, Kruger flap, or flap element, cm
x'	distance along chord perpendicular to leading edge or trailing edge of wing, slat, Kruger flap, or flap element, cm

y	spanwise distance measured from fuselage center line, cm
z_l	lower coordinate of airfoil section, cm
z_u	upper coordinate of airfoil section, cm
α	angle of attack of wing reference line, deg
δ_f	flap deflection, deg
$\delta_{f,1}$	vane-deflection angle of double-slotted flap with respect to wing chord line, deg
$\delta_{f,2}$	aft flap-deflection angle with respect to wing chord line, deg
δ_K	leading-edge Kruger flap-deflection angle with respect to wing chord line, deg
δ_s	leading-edge slat deflection angle with respect to wing chord line, deg
Λ	sweepback angle, measured at quarter-chord line, deg
ϕ	wing twist, positive when trailing edge is down, deg

MODEL DESCRIPTION

The model used in the present investigation was a general research model representing an advanced subsonic transport configuration. Drawings of the complete model are presented in figure 2(a). Details of the high-lift system are shown in figure 2(b); details of the nacelles are shown in figure 2(c). The basic geometric characteristics of the model are summarized in table I.

Wing

The basic wing planform had supercritical airfoil sections, 42.33° sweep of the quarter-chord line, an aspect ratio of 7.05, and a taper ratio of 0.35. The basic wing (theoretical planform) was modified over the inboard part which resulted in the planform shown in figure 2(a). The twist, maximum-thickness variation, and chordwise location of maximum thickness for the complete wing are shown in figure 2(d). Detailed coordinates for the wing are presented in table II. Transition strips, 0.32 cm wide, of No. 80 carborundum were applied to the upper and lower surfaces of the wing 3.81 cm behind the leading edge.

High-Lift System

The high-lift system of the model consisted of a partial-span, double-slotted flap which extended from the wing-body juncture (10-percent wing semispan) to the 73-percent wing semispan station (see fig. 2(b)) and a leading-edge device which extended from the 38-percent wing semispan station to the 90-percent wing semispan station. (See fig. 2(b).) There were two types of leading-edge devices used, one a leading-edge slat and the other a leading-edge Kruger flap. Coordinates of the leading-edge elements of the high-lift system are presented in table III and those of the flap elements are presented in table IV. Deflections of the high-lift system were measured in the streamwise plane relative to their respective reference chord line. Transition strips, 0.32 cm wide, of No. 80 carborundum were applied to the upper and lower surfaces of the leading-edge devices 2.54 cm behind the leading edge of the slat or Kruger flap.

Fuselage

The overall dimensions of the fuselage are shown in figure 2(a). A fiberglass—resin shell formed the outer shape of the fuselage and was attached to a metal strongback which housed the six-component strain-gage balance. An electronic angle-of-attack sensor was mounted to the internal strongback to provide the measured geometric angle of attack of the model during the tests. The rear of the fuselage was constructed so that the horizontal tail could be mounted near the center line of the fuselage (using the same horizontal tail as the T-tail arrangement). Transition strip, 0.32 cm wide, of No. 80 carborundum was applied to the nose of the fuselage 5.00 cm behind the apex of the nose.

Tail Surfaces

The location and principal dimensions of the horizontal and vertical tails are given in figure 2(a) and table I. The horizontal-tail incidence could be varied through a large range of incidence angles, but only a limited range was used for this investigation ($i_t = 0^o$ and -10^o). Transition strips, 0.32 cm wide, of No. 80 carborundum were applied 3.81 cm behind the leading edge of the tail surfaces.

Nacelles

The present model was tested with two sizes and arrangements of flowthrough nacelles. One was a three-engine configuration (two large wing-mounted nacelles and a simulated vertical-tail-mounted nacelle) and the other, a four-engine configuration (four smaller wing-mounted nacelles). Drawings of these nacelles are presented in figure 2(c). When the four-engine configuration was tested, the tests were made with and without part of the flap system directly behind the inboard nacelles removed and are noted as no-flap cutout and flap cutout. No transition strips were applied to the nacelles.

TESTS AND CORRECTIONS

The investigation was conducted in the Langley V/STOL tunnel (4.42 m by 6.63 m) at a dynamic pressure of 2394 Pa. The test Reynolds number at this dynamic pressure was 1.35×10^6 (T = 288.9 K or 520° R) based on the wing mean aerodynamic chord of 0.329 m.

Longitudinal aerodynamic characteristics were obtained from tests conducted through an angle-of-attack range from approximately -4° to 24° in increments of 2°. Limited stabilizer incidences were investigated over the test angle-of-attack range as well as tests made with the horizontal tail removed to define the tail-off aerodynamic characteristics.

Aerodynamic characteristics were determined for the clean-wing configuration with the flaps undeflected and the leading-edge device (slat or Kruger flap) on and retracted. Tests were also made with three different deflections of the double-slotted flap, all with either the leading-edge slat or Kruger flap deflected 45°. The double-slotted flap deflections were 15°/nested, 22°/32°, and 30°/55°; the first number being the vane deflection $\delta_{f,1}$ and the last being the flap deflection $\delta_{f,2}$. (See fig. 2(b).)

Jet-boundary corrections, determined from reference 10, and blockage corrections, obtained from reference 11, were applied to the measured data. The drag data were corrected for balance chamber pressure at the base of the fuselage (0.0098 m^2) but were not corrected for effects of the flow through the nacelles because it was felt that this correction would be negligible. The angle of attack was also corrected for a small flow angularity in the tunnel. This correction was obtained from upright and inverted tests of the clean tail-off model.

PRESENTATION OF RESULTS

The longitudinal aerodynamic characteristics obtained on the present model for the various test conditions and model configurations are presented in the figures as follows:

DISCUSSION OF RESULTS

Longitudinal Aerodynamic Characteristics

Except for a few preliminary runs, transition strips were applied near the leading edges of the basic wing and the wing leading-edge devices. A comparison of the data of figure 5 (fixed transition) with that in figure 3 (no transition strips) show that there were no effects of the addition of transition strips except for a slight decrease in lift at the higher angles of attack.

High-Lift Performance

Comparison of leading-edge devices.- Results obtained for the horizontal-tail-off configuration with the high-lift system having various leading-edge devices are presented

in figure 5. These data indicate that the configuration with the high-lift system having the leading-edge Kruger flap had slightly higher lift at a given angle of attack than the configuration with the leading-edge slat. (See summary in fig. 16.) The overall trend in pitching-moment characteristics for the tail-off configuration with the high-lift system was about the same with either leading-edge device and was about what would be expected for the tail-off condition.

Effect of engine arrangement.- The basic horizontal-tail-off results for the various engine arrangements with the high-lift system are presented in figures 6 to 9. Comparison of the lift data with Kruger flap at $\delta_K = 45^o$ for the four-engine configuration (no flap cutout, fig. 7) with the data for the three-engine configuration (fig. 9) shows that the aerodynamic trends were about the same, except that for the maximum flap-deflection condition, stall occurred for the four-engine configuration above $\alpha = 20^o$.

Comparison of the data with nacelles off (figs. 3 and 4) with the data for the nacelles on (figs. 6, 7, and 9) shows that the overall change in drag due to addition of the nacelles was very small at low and moderate lift coefficients. It is therefore believed that the drag increment associated with the internal flow was probably negligible.

Effect of flap cutout.- The effect of flap cutout behind the inboard nacelle of the four-engine configuration is presented in figure 8, and the data indicate that for the flap-cutout condition the lift was decreased throughout the angle-of-attack range. This decrease was greater as the flap deflection was increased. There were no significant changes in stability associated with the flap cutout.

Effect of horizontal-tail height.- Results obtained on the model without nacelles with various leading-edge devices for the range of trailing-edge flap deflections are presented in figures 10 and 12 for the T-tail configuration and figures 11 and 13 for the low-tail configuration. Only a limited range of horizontal-tail incidence was investigated. These data indicate that the low-tail configuration developed slightly higher lift than the T-tail configuration for all flap deflections including $\delta_f = 0^o$ (figs. 14 and 15), especially at the higher angles of attack. These data also indicate that for the $\delta_f = 0^o$ configuration a slightly higher lift was experienced with a Kruger leading-edge flap for both horizontal-tail heights.

The maximum untrimmed lift coefficient for the various high-lift system configurations are summarized as follows:

Configuration (wing)	Leading-edge device, δ_s or $\delta_K = 45^o$	Horizontal tail off	Horizontal tail on; $i_t = 0^o$	
			T-tail	Low tail
Clean	Off	1.38	1.37	1.58
$\delta_f = 0^o$	Slat	1.46	1.46	1.66
15^o/nested	Slat	1.83	1.83	1.97
$22^o/32^o$	Slat	2.08	2.09	2.19
$30^o/55^o$	Slat	2.15	2.16	2.20
0^o	Kruger	1.53	1.54	1.73
15^o/nested	Kruger	1.88	1.88	2.02
$22^o/32^o$	Kruger	2.14	2.15	2.22
$30^o/55^o$	Kruger	2.16	2.17	2.18

Static Longitudinal Stability

A summary of the effect of leading-edge devices and horizontal-tail height on the static longitudinal stability characteristics for the test range of trailing-edge flap deflections is presented in figure 17.

Effect of leading-edge devices.- The results obtained on the model with the horizontal tail on ($i_t = 0^o$) (fig. 17) and with the complete high-lift system (figs. 17(b) and 17(c)) indicated that the leading-edge devices had no significant effect on the longitudinal stability for either the clean configuration or with the flaps deflected.

Effect of horizontal-tail height.- The results obtained on the flaps-retracted configuration (leading-edge devices off and on, fig. 17(a)) indicate that between $\alpha = 13^o$ and $\alpha = 14^o$, the tail contribution of the T-tail decreased rapidly, whereas the low-tail contribution increased rapidly. This difference in tail configuration seems to indicate that the T-tail moved into an adverse downwash field near $\alpha = 14^o$ and that the low tail was moving out of this adverse flow field.

The results obtained on the flap-deflected configurations with slat at $\delta_s = 45^o$ and Kruger flap at $\delta_K = 45^o$ are presented in figures 17(b) and 17(c), respectively. These data show that the model configuration with both tail heights and all flap deflections became unstable at fairly low angles of attack ($\alpha = 6^o$ to 9^o); however, the low-tail configuration became stable at higher angles of attack (near $\alpha = 17^o$ to 18^o). The stability increase of the low-tail configuration at the higher angles of attack with flaps deflected seems to

indicate the same characteristics observed with the clean configuration in that the low tail was leaving the adverse downwash flow field for angles above 17°, whereas the T-tail remained in this adverse flow field. The contribution of the low tail to stability reduced as the flap deflection increased. In general, both tail positions gave marginal longitudinal stability, especially at the higher flap deflections and angles of attack, and the low tail seemed to be located in the least adverse flow condition at moderate angles of attack.

SUMMARY OF RESULTS

A low-speed investigation was conducted in the Langley V/STOL tunnel to determine the static longitudinal stability characteristics and high-lift performance of a general research model which represented an advance subsonic transport configuration with a T-tail or a low tail. The model had a 42.33° swept, aspect-ratio-7.05 wing with a supercritical airfoil and a high-lift system consisting of a leading-edge device and a double-slotted flap. Effects of various arrangements of flow through wing-mounted nacelles and a vertical-tail-mounted nacelle were determined (four-engine or three-engine configurations). The results of this investigation may be summarized as follows:

1. The maximum untrimmed lift coefficient for the tail on the clean wing configuration (low tail at zero incidence) was 1.58 (1.38 for tail off). Deflection of the high-lift system for the landing condition (Kruger flap at 45°, flap at 22°/32°) increased the value of maximum lift coefficient to 2.22. For all flap deflections, except the highest, the configuration with the Kruger flap had slightly higher lift for both tail off or tail on (either height).

2. The model configuration with either tail height and for all flap deflections became unstable at fairly low angles of attack (α = 6° to 9°); however, the low-tail configuration became stable at the higher angles of attack (near α = 17° to 18°).

3. The stability of the low-tail configuration at the higher angles of attack seems to indicate that the low tail was leaving an adverse downwash flow field, whereas the T-tail remained in the adverse flow field.

4. There was insignificant difference in the longitudinal stability and high-lift performance between the four-engine and three-engine configurations. At the maximum flap deflection (landing condition), the four-engine configuration stalled above an angle of attack of 20°.

Langley Research Center
National Aeronautics and Space Administration
Hampton, Va. 23665
July 9, 1975

REFERENCES

1. Whitcomb, Richard T.; and Clark, Larry R.: An Airfoil Shape for Efficient Flight at Supercritical Mach Numbers. NASA TM X-1109, 1965.

2. Langhans, Richard A.; and Fiechner, Stuart G.: Wind-Tunnel Investigation at Mach Numbers From 0.25 to 1.01 of a Transport Configuration Designed To Cruise at Near-Sonic Speeds. NASA TM X-2622, 1972.

3. Goodson, Kenneth W.: Low-Speed Aerodynamic Characteristics of a Rectangular, Aspect-Ratio-6, Slotted Supercritical Airfoil Wing Having Several High-Lift Flap Systems. NASA TM X-2317, 1971.

4. Harris, Charles D.: Wind-Tunnel Investigation of Effects of Trailing-Edge Geometry on a NASA Supercritical Airfoil Section. NASA TM X-2336, 1971.

5. Fournier, Paul G.; and Sleeman, William C., Jr.: Effects of Wing Height on Low-Speed Aerodynamic Characteristics of a Model Having a 42° Swept Wing, a Supercritical Airfoil, Double-Slotted Flaps, and a Low Tail. NASA TM X-2794, 1973.

6. Fournier, Paul G.; and Goodson, Kenneth W.: Low-Speed Aerodynamic Characteristics of a 42° Swept High-Wing Model Having a Double-Slotted Flap System and a Supercritical Airfoil. NASA TM X-3036, 1974.

7. Fournier, Paul G.; and Sleeman, William C., Jr.: Low-Speed Aerodynamic Characteristics of a Transport Configuration Having a 42° Swept Supercritical Airfoil Wing and Three Tail Height Positions. NASA TM X-3149, 1974.

8. Fournier, Paul G.; and Sleeman, William C., Jr.: Low-Speed Aerodynamic Characteristics of a Model Having a 42° Swept Low Wing With a Supercritical Airfoil Double-Slotted Flaps, and a T-Tail. NASA TM X-2582, 1972.

9. Mechtly, E. A.: The International System of Units – Physical Constants and Conversion Factors (Second Revision). NASA SP-7012, 1973.

10. Gillis, Clarence L.; Polhamus, Edward C.; and Gray, Joseph L., Jr.: Charts for Determining Jet-Boundary Corrections for Complete Models in 7- by 10-Foot Closed Rectangular Wind Tunnels. NACA WR L-123, 1945. (Formerly NACA ARR L5G31.)

11. Herriot, John G.: Blockage Corrections for Three-Dimensional-Flow Closed-Throat Wind Tunnels, With Consideration of the Effect of Compressibility. NACA Rep. 995, 1950. (Supersedes NACA RM A7B28.)

TABLE I.- GEOMETRIC CHARACTERISTICS

Wing (theoretical):	
Area, m^2	0.656
Mean aerodynamic chord, cm	32.845
Span, cm	215.067
Aspect ratio	7.046
Taper ratio	0.354
Horizontal tail (low tail):	
Area, m^2	0.186
Mean aerodynamic chord, cm	24.237
Span, cm	83.108
Aspect ratio	3.715
Taper ratio	0.379
Horizontal tail (T-tail):	
Area, m^2	0.141
Mean aerodynamic chord, cm	21.885
Span, cm	68.996
Aspect ratio	3.368
Taper ratio	0.336
Vertical tail:	
Area, m^2	0.209
Mean aerodynamic chord, cm	49.195
Span, cm	43.231
Aspect ratio	0.896
Taper ratio	0.608
Base area of fuselage, m^2	0.010

TABLE II.- WING COORDINATES

[Coordinates perpendicular to wing leading edge except where noted]

x'/c'	z_u/c'	z_l/c'
	$\frac{y}{b/2}$ = 0.1379; c' = 15.2070 cm	
0	-0.4034	-0.4034
.0060	-.3252	-.4824
.0217	-.2654	-.5385
.0493	-.2116	-.5886
.0937	-.1563	-.6365
.1732	-.0884	-.6897
.2444	-.0416	-.7267
.3232	.0005	-.7615
.4087	.0367	-.7929
.4999	.0666	-.8199
.5624	.0827	-.8355
.6606	.1012	-.8559
.7685	.1057	-.8746
.8503	.1201	-.8868
.8959	.1224	-.8929
1.0000	.1256	-.9056

x'/c'	z_u/c'	z_l/c'
	$\frac{y}{b/2}$ = 0.1795; c' = 20.0863 cm	
0	-0.3203	-0.3203
.0039	-.2792	-.3628
.0154	-.2443	-.3964
.0319	-.2184	-.4217
.0699	-.1803	-.4574
.1242	-.1440	-.4894
.1875	-.1096	-.5211
.2529	-.0808	-.5506
.3189	-.0578	-.5765
.3910	-.0395	-.6001
.4713	-.0258	-.6216
.5000	-.0224	-.6286
.5871	-.0159	-.6480
.6956	-.0132	-.6622
.8324	-.0144	-.6916
.9186	-.0172	-.7022
1.0000	-.0209	-.7097

TABLE II.- Continued

x'/c'	z_u/c'	z_l/c'
	$\frac{y}{b/2}$ = 0.2315; c' = 26.6776 cm	
0	-0.2419	-0.2419
.0031	-.2200	-.2607
.0104	-.2051	-.2805
.0331	-.1835	-.3033
.0665	-.1651	-.3227
.1167	-.1456	-.3432
.1822	-.1270	-.3186
.2588	-.1109	-.3917
.3345	-.0982	-.4186
.4190	-.0908	-.4400
.4998	-.0876	-.4614
.5297	-.0876	-.4689
.6252	-.0903	-.4905
.6929	-.0942	-.5035
.7917	-.1023	-.5185
.8920	-.1082	-.5295
1.0000	-.1264	-.5366

x'/c'	z_u/c'	z_l/c'
	$\frac{y}{b/2}$ = 0.3071; c' = 40.0025 cm	
0	-0.1497	-0.1497
.0025	-.1406	-.1604
.0077	-.1352	-.1667
.0169	-.1302	-.1731
.0417	-.1226	-.1841
.0789	-.1160	-.1950
.1272	-.1113	-.2044
.2062	-.1079	-.2165
.2734	-.1075	-.2281
.3572	-.1105	-.2459
.4515	-.1146	-.2670
.4680	-.1177	-.2780
.5235	-.1196	-.2834
.5912	-.1272	-.2980
.6588	-.1375	-.3097
.7277	-.1490	-.3187
.7999	-.1620	-.3252
.8815	-.1773	-.3299
1.0000	-.2005	-.3339

TABLE II.- Continued

x'/c'	z_u/c'	z_l/c'
	$\frac{y}{b/2}$ = 0.4143; c' = 43.5635 cm	
0	-0.1127	-0.1127
.0020	-.1065	-.1196
.0056	-.1037	-.1235
.0148	-.1002	-.1289
.0354	-.0960	-.1366
.0731	-.0926	-.1459
.1255	-.0916	-.1543
.1908	-.0936	-.1609
.2579	-.0982	-.1650
.3628	-.1104	-.1701
.4734	-.1260	-.1739
.5000	-.1298	-.1748
.5508	-.1373	-.1775
.6108	-.1467	-.1833
.6752	-.1572	-.1920
.7727	-.1739	-.2061
.8434	-.1873	-.2143
.9117	-.2016	-.2195
1.0000	-.2192	-.2224

x'/c'	z_u/c'	z_l/c'
	$\frac{y}{b/2}$ = 0.5315; c' = 28.6588 cm	
0	-0.1305	-0.1305
.0027	-.1220	-.1399
.0046	-.1197	-.1419
.0107	-.1163	-.1466
.0348	-.1095	-.1578
.0791	-.1034	-.1703
.1560	-.0995	-.1828
.2548	-.1005	-.1929
.2974	-.1045	-.1986
.4308	-.1126	-.2009
.4999	-.1218	-.2006
.5704	-.1330	-.1986
.6835	-.1544	-.1960
.7472	-.1677	-.1969
.8284	-.1849	-.2019
.9184	-.2038	-.2113
1.0000	-.2211	-.2230

TABLE II.- Continued

x'/c'	z_u/c'	z_l/c'
	$\frac{y}{b/2}$ = 0.6486; c' = 21.6560 cm	
0	-0.1192	-0.1192
.0039	-.1078	-.1294
.0089	-.1036	-.1341
.0188	-.0999	-.1390
.0429	-.0938	-.1485
.0965	-.0864	-.1609
.2056	-.0807	-.1749
.3347	-.0813	-.1850
.4348	-.0847	-.1891
.4999	-.0884	-.1888
.5531	-.0942	-.1863
.6670	-.1072	-.1785
.7669	-.1254	-.1714
.8275	-.1392	-.1703
.8991	-.1582	-.1740
.9639	-.1772	-.1832
1.0000	-.1885	-.1908

x'/c'	z_u/c'	z_l/c'
	$\frac{y}{b/2}$ = 0.7658; c' = 18.8366 cm	
0	-0.0707	-0.0707
.0043	-.0596	-.0810
.0092	-.0562	-.0847
.0299	-.0489	-.0943
.0645	-.0423	-.1036
.0619	-.0330	-.1170
.3030	-.0300	-.1265
.4234	-.0328	-.1302
.4999	-.0367	-.1296
.5762	-.0429	-.1262
.6970	-.0574	-.1169
.8139	-.0778	-.1103
.8749	-.0910	-.1108
.9524	-.1098	-.1172
1.0000	-.1220	-.1247

TABLE II.- Concluded

x'/c'	z_u/c'	z_l/c'
	$\frac{y}{b/2}$ = 0.8829; c' = 16.0553 cm	
0	0.0025	0.0025
.0038	.0114	-.0081
.0082	.0146	-.0115
.0226	.0199	-.0184
.0587	.0275	-.0280
.1449	.0375	-.0394
.2242	.0418	-.0449
.2780	.0432	-.0475
.4164	.0437	-.0505
.4998	.0410	-.0489
.5825	.0359	-.0443
.7151	.0225	-.0326
.8366	.0025	-.0259
.9305	-.0174	-.0290
1.0000	-.0335	-.0367

x'/c'	z_u/c'	z_l/c'
	$\frac{y}{b/2}$ = 0.9264; c' = 9.3878 cm; perpendicular to wing trailing edge	
0	0.1531	0.1477
-.1266	.1775	.1550
-.2738	.1997	.1480
-.4451	.2132	.1258
-.5005	.2148	.1190
-.6548	.2132	.1077
-.7984	.2043	.1101
-.9207	.1907	.1223
-.9754	.1786	.1361
-.9962	.1786	.1485
-.9976	.1691	.1507
-.9989	.1672	.1529
-.9995	.1650	.1548
-.9997	.1613	.1569
-1.0000	.1601	.1601

TABLE III.- LEADING-EDGE DEVICE COORDINATES

[Perpendicular to leading edge]

(a) Slat

x/c'_s	z_u/c'_s	z_l/c'_s
	$\frac{y}{b/2}$ = 0.3808;	c'_s = 4.5771 cm
0	-1.1459	-1.1459
.0011	-1.1299	-1.1687
.0083	-1.1060	-1.1964
.0139	-1.0955	-1.2098
.0239	-1.0821	-1.2259
.0400	-1.0677	-1.2447
.0649	-1.0527	-1.2658
.0977	-1.0377	-1.2863
.1398	-1.0233	-1.3091
.1915	-1.0089	-1.3330
.2481	-.9967	-1.1837
.3113	-.9856	-1.1193
.3812	-.9750	-1.0710
.4589	-.9656	-1.0322
.5466	-.9567	-.9933
.6448	-.9484	-.9767
.7214	------	-.9634
.7525	-.9423	------
.8324	------	-.9440
.8707	-.9373	------
.8879	------	-.9378
1.0000	-.9340	------

x/c'_s	z_u/c'_s	z_l/c'_s
	$\frac{y}{b/2}$ = 0.5527;	c'_s = 3.8049 cm
0	-0.9286	-0.9286
.0013	-.9065	-.9479
.0060	-.8852	-.9700
.0120	-.8732	-.9833
.0240	-.8578	-1.0007
.0481	-.8391	-1.0236
.0841	-.8211	-1.0474
.1262	-.8057	-1.0708
.1776	-.7911	-1.0948
.2377	-.7764	-1.1175
.3077	-.7630	-.9426
.3865	-.7503	-.8758
.4720	-.7397	-.8284
.5668	-.7294	-.7857
.6756	-.7190	-.7530
.8178	-.7089	-.7323
1.0000	-.7003	-.7042

TABLE III.- Continued

(a) Concluded

x/c'_s	z_u/c'_s	z_l/c'_s
	$\frac{y}{b/2}$ = 0.7247; c'_s = 4.3713 cm	
0	-0.4079	-0.4079
.0006	-.3928	-.4201
.0029	-.3817	-.4300
.0058	-.3748	-.4370
.0110	-.3649	-.4457
.0227	-.3533	-.4573
.0447	-.3388	-.4736
.0750	-.3260	-.4898
.1116	-.3138	-.5067
.1563	-.3027	-.5230
.2144	-.2905	-.5410
.2876	-.2783	-.3940
.3719	-.2667	-.3451
.4660	-.2562	-.3062
.5752	-.2470	-.2754
.6984	-.2394	-.2615
.8390	-.2324	-.2394
1.0000	-.2284	-.2313

x/c'_s	z_u/c'_s	z_l/c'_s
	$\frac{y}{b/2}$ = 0.8966; c'_s = 4.6203 cm	
0	0.0396	0.0396
.0005	.0451	.0335
.0027	.0599	.0247
.0055	.0654	.0187
.0110	.0731	.0110
.0209	.0819	.0011
.0418	.0929	-.0115
.0737	.1039	-.0258
.1160	.1149	-.0401
.1743	.1264	-.0544
.2468	.1385	.0352
.3315	.1495	.0808
.4370	.1594	.1182
.5734	.1688	.1457
.7268	.1754	.1638
1.0000	.1820	.1814

TABLE III.- Concluded

(b) Kruger flap

x/c'_K	z_u/c'_K	z_l/c'_K
	c'_K = 3.9471 cm	
0	0	0
.0026	.0103	-.0277
.0116	.0348	-.0418
.0257	.0599	-.0496
.0502	.0888	-.0405
.0798	.1120	-.0090
.1203	.1345	.0193
.1647	.1532	.0438
.2201	.1680	.0476
.2800	.1783	.0476
.3500	.1840	.0476
.4247	.1840	.0476
.5000	.1763	.0476
.5747	.1628	.0476
.6500	.1441	.0476
.7246	.1197	.0476
.8000	.0914	.0476
.8752	.0586	.0315
.9402	.0302	.0142
.9801	.0122	.0026
1.0000	.0026	-.0026

TABLE IV.- FLAP COORDINATES (STREAMWISE)

(a) Flap, nested

x/c_f	z_u/c_f	z_l/c_f
	$\frac{y}{b/2}$ = 0.1105; c_f = 10.8509 cm	
0	0	0
.0047	.0239	-.0131
.0094	.0360	-.0178
.0140	.0440	-.0201
.0187	.0515	-.0211
.0234	.0576	-.0215
.0351	.0707	-.0215
.0468	.0805	-.0220
.0702	.0955	-.0220
.0936	.1063	-.0220
.1170	.1147	-.0220
.1404	.1208	-.0215
.1873	.1290	-.0211
.2941	.1330	-.0197
.2809	.1334	-.0192
.3277	.1320	-.0187
.3745	.1278	-.0182
.4213	.1222	-.0173
.4682	.1156	-.0164
.5150	.1086	-.0154
.5618	.1011	-.0145
.6086	.0929	-.0138
.7022	.0754	-.0122
.7959	.0545	-.0096
.8895	.0304	-.0075
.9831	.0049	-.0035
1.0000	-.0007	-.0030

x/c_f	z_u/c_f	z_l/c_f
	$\frac{y}{b/2}$ = 0.3439; c_f = 12.8372 cm	
0	0	0
.0040	.0174	-.0115
.0079	.0269	-.0158
.0119	.0336	-.0182
.0158	.0392	-.0194
.0198	.0439	-.0202
.0297	.0536	-.0194
.0396	.0617	-.0178
.0594	.0728	-.0146
.0791	.0815	-.0119
.1187	.0922	-.0067
.1583	.1001	-.0024
.1979	.1057	.0024
.2374	.1088	.0067
.3166	.1108	.0146
.3957	.1088	.0226
.4749	.1036	.0297
.5540	.0958	.0336
.6331	.0867	.0352
.7123	.0756	.0348
.7915	.0631	.0334
.8706	.0503	.0301
.9497	.0362	.0267
.9893	.0289	.0249
1.0000	.0263	.0243

TABLE IV.- Continued

(a) Concluded

x/c_f	z_u/c_f	z_l/c_f
	$\frac{y}{b/2}$ = 0.4422; c_f = 9.7130 cm	
0	0	0
.0052	.0209	-.0131
.0105	.0314	-.0173
.0157	.0382	-.0194
.0209	.0450	-.0199
.0262	.0497	-.0199
.0392	.0607	-.0188
.0523	.0685	-.0173
.0785	.0790	-.0141
.1046	.0868	-.0110
.1569	.0973	-.0047
.2092	.1025	.0005
.2615	.1041	.0052
.3138	.1041	.0089
.3661	.1020	.0115
.4184	.0983	.0136
.4707	.0931	.0146
.5230	.0868	.0146
.5753	.0795	.0141
.6276	.0717	.0131
.6799	.0633	.0120
.7322	.0544	.0099
.7845	.0450	.0078
.8368	.0353	.0055
.8891	.0248	.0029
.9414	.0141	.0016
1.0000	.0013	-.0013

x/c_f	z_u/c_f	z_l/c_f
	$\frac{y}{b/2}$ = 0.7247; c_f = 7.1730 cm	
0	0	0
.0071	.0198	-.0170
.0142	.0283	-.0205
.0212	.0354	-.0212
.0283	.0411	-.0205
.0354	.0460	-.0198
.0531	.0538	-.0177
.0708	.0595	-.0156
.1062	.0673	-.0113
.1416	.0730	-.0078
.2125	.0800	-.0007
.2833	.0829	.0057
.3541	.0829	.0120
.4249	.0822	.0163
.4958	.0800	.0205
.5666	.0758	.0234
.6374	.0701	.0248
.7082	.0630	.0248
.7790	.0531	.0234
.8499	.0418	.0227
.9207	.0298	.0177
1.0000	.0177	.0142

TABLE IV.- Continued

(b) Forward flap element

x/c_f	z_u/c_f	z_l/c_f
	$\frac{y}{b/2}$ = 0.1105; c_f = 10.8503 cm	
0	0	0
.0047	.0239	-.0131
.0094	.0360	-.0178
.0140	.0440	-.0201
.0187	.0515	-.0211
.0234	.0576	-.0215
.0351	.0707	-.0215
.0468	.0805	-.0220
.0702	.0955	-.0220
.0936	.1063	-.0220
.1170	.1147	-.0220
.1404	.1208	-.0215
.1873	.1290	-.0211
.2341	.1330	-.0197
.2809	.1334	-.0192
.3277	.1320	-.0187
.3745	.1278	-.0182
.4213	.1222	-.0173
.4682	.1156	-.0164
.4991	.1114	-.0154
.5150	.1086	.0267
.5618	.1011	.0571
.6086	.0927	.0669
.6554	.0843	.0688
.7022	.0751	.0662
.7500	.0653	.0630

x/c_f	z_u/c_f	z_l/e_f
	$\frac{y}{b/2}$ = 0.3439; c_f = 12.8372 cm	
0	0	0
.0040	.0174	-.0115
.0079	.0269	-.0158
.0119	.0336	-.0182
.0158	.0392	-.0194
.0198	.0439	-.0202
.0297	.0538	-.0194
.0396	.0617	-.0178
.0594	.0728	-.0146
.0791	.0815	-.0119
.1187	.0922	-.0067
.1583	.1001	-.0024
.1979	.1057	.0024
.2374	.1088	.0067
.3166	.1106	.0146
.3957	.1088	.0226
.4749	.1036	.0297
.5006	.1017	.0313
.5046	.1013	.0495
.5085	.1009	.0534
.5144	.1001	.0570
.5540	.0966	.0673
.6332	.0871	.0740
.7123	.0760	.0712
.7500	.0704	.0685

TABLE IV.- Continued

(b) Concluded

x/c_f	z_u/c_f	z_l/c_f
	$\frac{y}{b/2} = 0.4422$; $c_f = 9.7130$ cm	
0	0	0
.0052	.0209	-.0131
.0105	.0314	-.0173
.0157	.0382	-.0194
.0209	.0450	-.0199
.0261	.0497	-.0199
.0392	.0607	-.0188
.0523	.0685	-.0173
.0785	.0790	-.0141
.1046	.0868	-.0110
.1570	.0973	-.0047
.2092	.1025	.0005
.2615	.1041	.0052
.3138	.1041	.0089
.3661	.1020	.0115
.4184	.0983	.0136
.4707	.0931	.0146
.4995	.0900	.0146
.5021	.0894	.0293
.5047	.0889	.0314
.5099	.0884	.0350
.5230	.0868	.0424
.5753	.0795	.0539
.6276	.0717	.0549
.6799	.0633	.0528
.7322	.0544	.0502
.7500	.0512	.0486

x/c_f	z_u/c_f	z_l/c_f
	$\frac{y}{b/2} = 0.7247$; $c_f = 7.1730$ cm	
0	0	0
.0035	.0198	-.0170
.0142	.0283	-.0205
.0212	.0354	-.0212
.0283	.0411	-.0205
.0354	.0460	-.0198
.0531	.0538	-.0177
.0708	.0595	-.0156
.1062	.0673	-.0113
.1414	.0730	-.0078
.2125	.0800	-.0007
.2833	.0829	.0057
.3541	.0829	.0120
.4245	.0822	.0163
.5011	.0793	.0205
.5011	.0793	.0305
.5046	.0786	.0375
.5081	.0786	.0404
.5152	.0786	.0460
.5223	.0786	.0489
.5365	.0779	.0517
.5666	.0758	.0574
.6374	.0701	.0602
.7082	.0630	.0581
.7500	.0574	.0538

TABLE IV.- Continued

(c) Rear flap element

x/c_f	z_u/c_f	z_l/c_f
	$\frac{y}{b/2}$ = 0.1105; c_f = 10.8509 cm	
0.4991	-0.0047	-0.0047
.5037	.0103	-.0131
.5084	.0183	-.0155
.5131	.0248	-.0155
.5178	.0295	-.0152
.5225	.0342	-.0150
.5342	.0436	-.0150
.5459	.0501	-.0145
.5693	.0595	-.0145
.5927	.0651	-.0140
.6395	.0688	-.0126
.6863	.0674	-.0117
.7331	.0646	-.0108
.7800	.0576	-.0098
.8268	.0459	-.0084
.8736	.0342	-.0075
.9204	.0218	-.0059
.9672	.0094	-.0042
1.0000	-.0007	-.0030

x/c_f	z_u/c_f	z_l/c_f
	$\frac{y}{b/2}$ = 0.3439; c_f = 12.8372 cm	
0.5006	0.0421	0.0421
.5046	.0501	.0350
.5085	.0536	.0330
.5144	.0576	.0326
.5334	.0643	.0338
.5540	.0683	.0342
.5936	.0726	.0354
.6332	.0742	.0360
.6727	.0738	.0360
.7123	.0722	.0358
.7519	.0691	.0350
.7915	.0639	.0342
.8310	.0572	.0326
.8706	.0505	.0311
.9102	.0433	.0295
.9497	.0362	.0265
1.0000	.0263	.0243

TABLE IV.- Concluded

(c) Concluded

x/c_f	z_u/c_f	z_l/c_f
	$\frac{y}{b/2} = 0.4422$; $c_f = 9.7130$ cm	
0.4995	0.0235	0.0235
.5021	.0293	.0167
.5047	.0314	.0146
.5099	.0350	.0146
.5152	.0378	.0146
.5230	.0424	.0146
.5492	.0507	.0146
.5753	.0539	.0141
.6276	.0549	.0136
.6799	.0533	.0126
.7322	.0502	.0105
.7845	.0455	.0084
.8368	.0356	.0063
.8891	.0248	.0042
.9414	.0141	.0016
1.0000	.0013	-.0013

x/c_f	z_u/c_f	z_l/c_f
	$\frac{y}{b/2} = 0.7247$; $c_f = 7.1730$ cm	
0.5011	0.0319	0.0319
.5046	.0390	.0248
.5085	.0418	.0234
.5152	.0475	.0227
.5223	.0503	.0234
.5365	.0567	.0234
.5666	.0588	.0212
.6374	.0616	.0248
.7082	.0644	.0248
.7790	.0524	.0234
.8499	.0418	.0227
.9207	.0305	.0177
1.0000	.0177	.0142

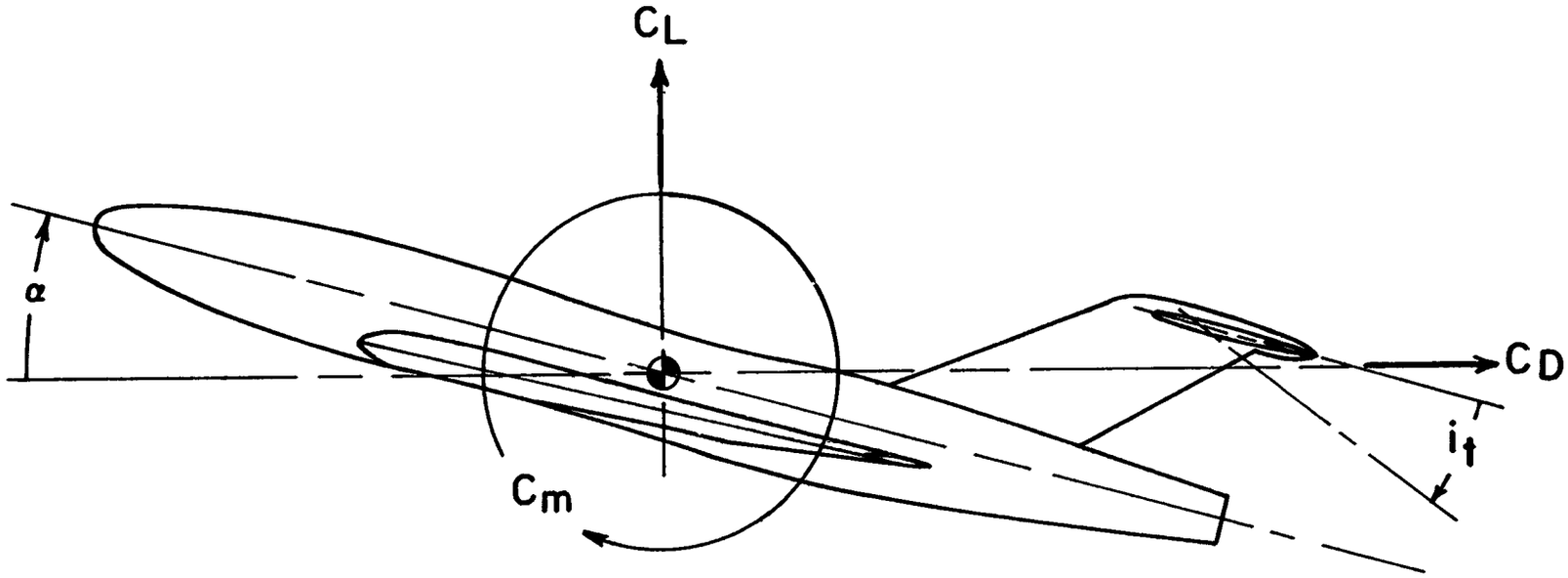

Figure 1.- System of axes. Positive directions of forces, moments, and angles are indicated by arrows.

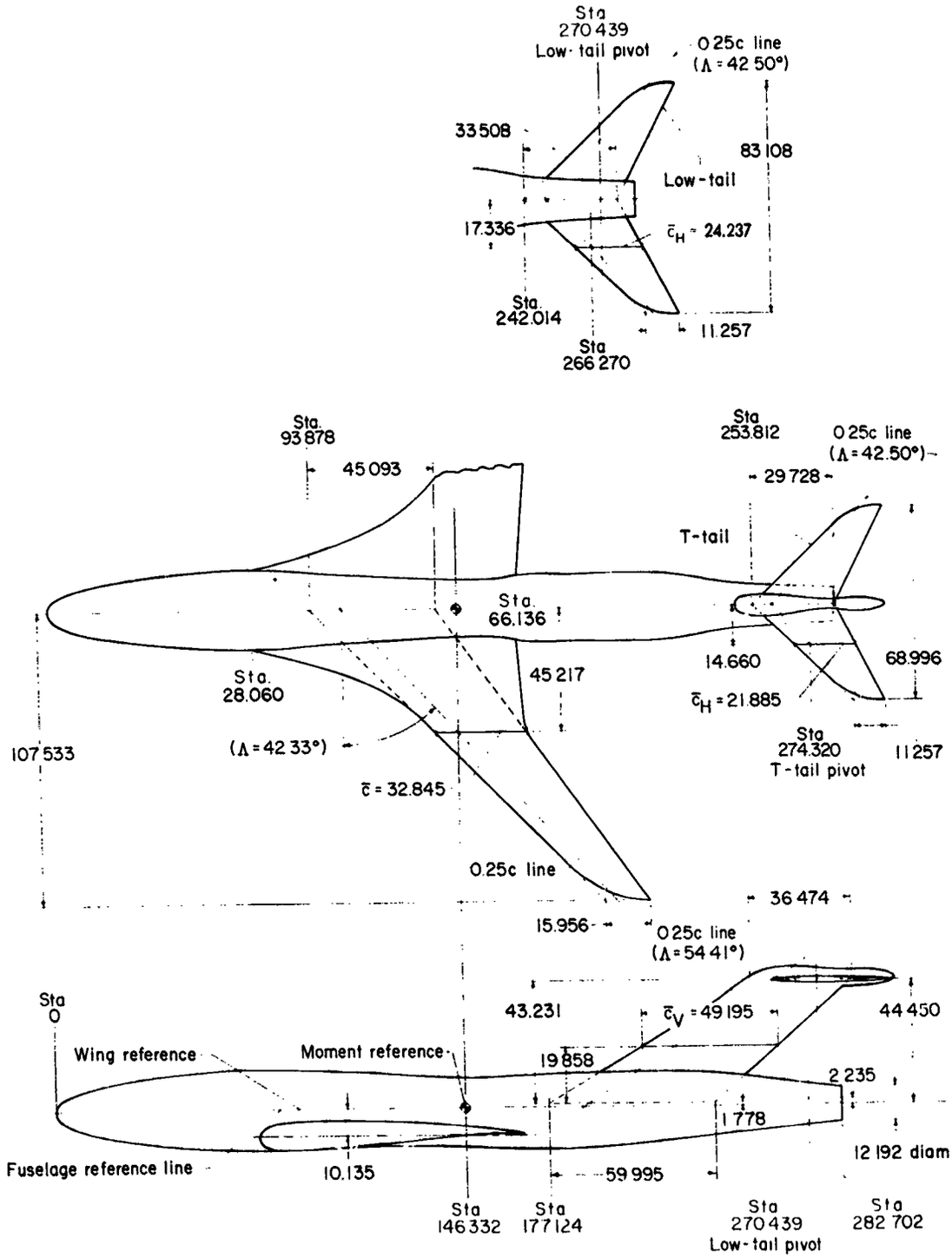

(a) Clean model geometric characteristics.

Figure 2.- Details of model. Dimensions are in centimeters.

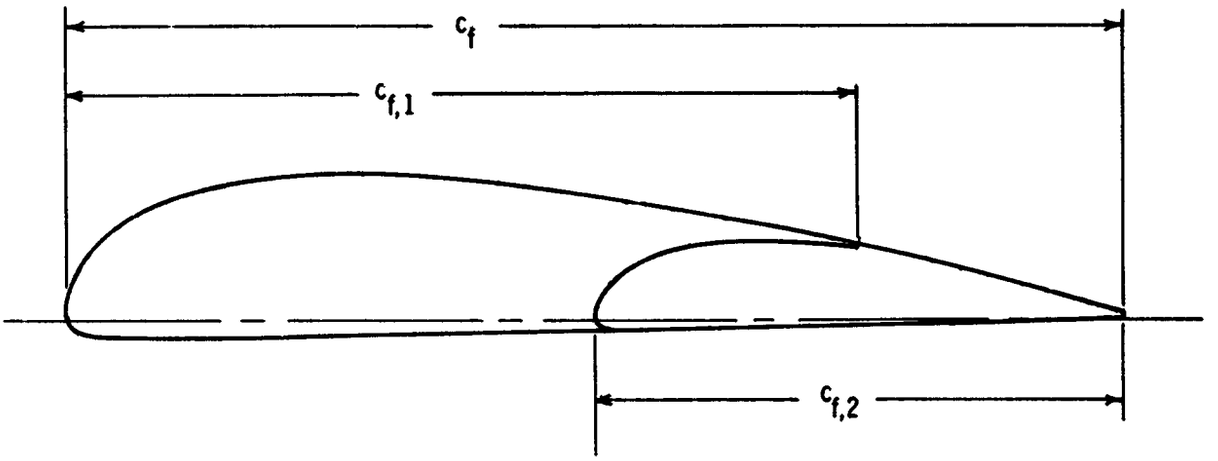

Semispan station, $y/b/2$	c_f, cm	$c_{f,1}$, cm	$c_{f,2}$, cm
0.111	10.850	8.138	5.426
.344	12.844	9.633	6.422
.442	9.715	7.286	4.858
.725	7.179	5.384	3.590

(b) Details of flaps (undeflected).

Figure 2.- Continued.

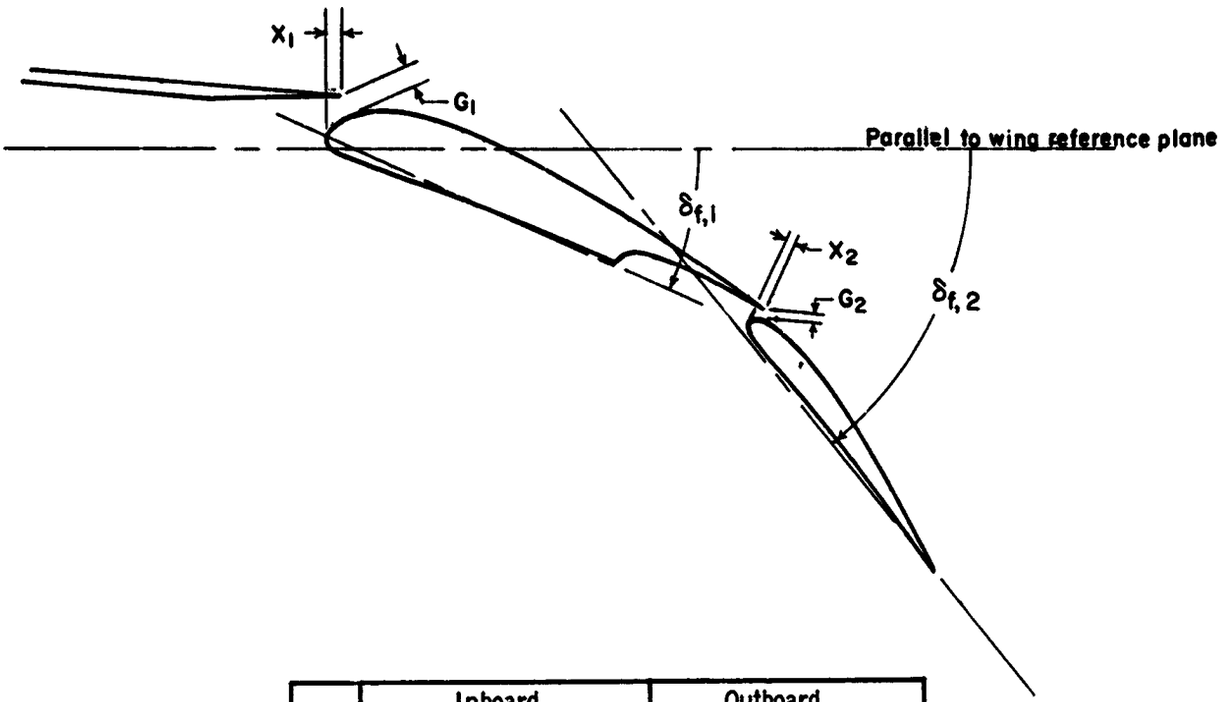

	Inboard		Outboard	
	Semispan station, $y/b/2$		Semispan station, $y/b/2$	
	0.111	0.344	0.442	0.725
$\delta_{f,1}$	10.0^0	11.5^0	13.0^0	12.0^0
G_1	.457	.488	.318	.348
x_1	1.664	1.651	1.189	1.168
$\delta_{f,2}$	10.0^0	11.5^0	13.0^0	12.0^0
G_2	Nested	Nested	Nested	Nested
x_2	Nested	Nested	Nested	Nested
$\delta_{f,1}$	17.0^0	18.5^0	20.0^0	19.0^0
G_1	.500	.488	.356	.348
x_1	1.123	1.222	.726	.871
$\delta_{f,2}$	27.0^0	28.5^0	30.0^0	29.0^0
G_2	.373	.244	.356	.175
x_2	.206	.175	.157	.125
$\delta_{f,1}$	25.0^0	26.5^0	28.0^0	27.0^0
G_1	.627	.528	.475	.373
x_1	.206	.279	.107	.201
$\delta_{f,2}$	50.0^0	51.5^0	53.0^0	52.0^0
G_2	.417	.351	.356	.249
x_2	0	0	0	0

(b) Continued. Flaps deflected. G_1, G_2, x_1, and x_2 are in centimeters.

Figure 2.- Continued.

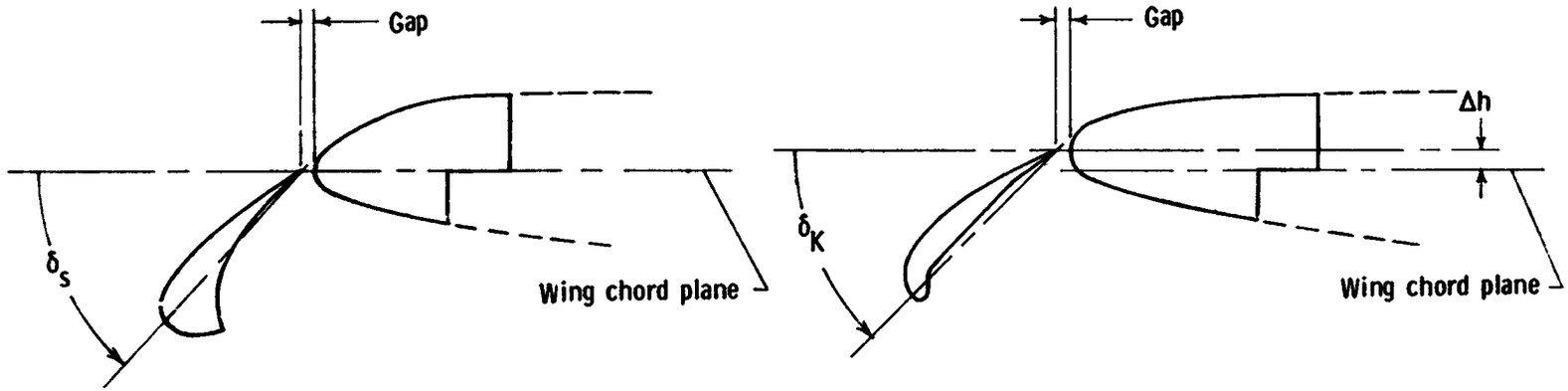

Slat	
Semispan station $y/b/2$	Gap (0.015c), cm
0.448	0.480
.567	.427
.604	.412
.757	.343
.827	.312
.885	.290

Kruger flap		
Semispan station, $y/b/2$	Gap (0.015c), cm	Δh, cm
0.448	0.480	0.711
.558	.427	.508
.596	.412	.483
.753	.343	.432
.826	.312	.381
.885	.290	.356

(b) Continued. Leading-edge devices.

Figure 2.- Continued.

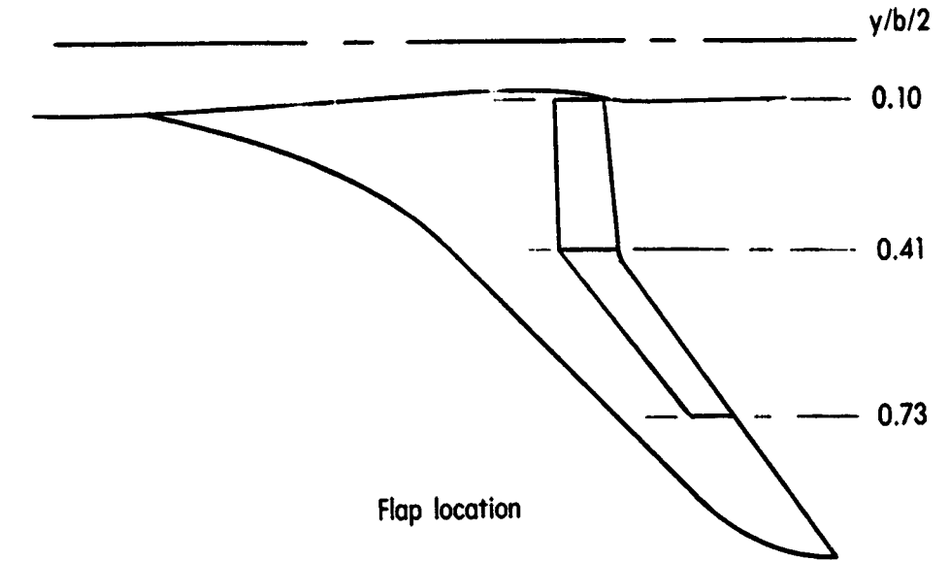

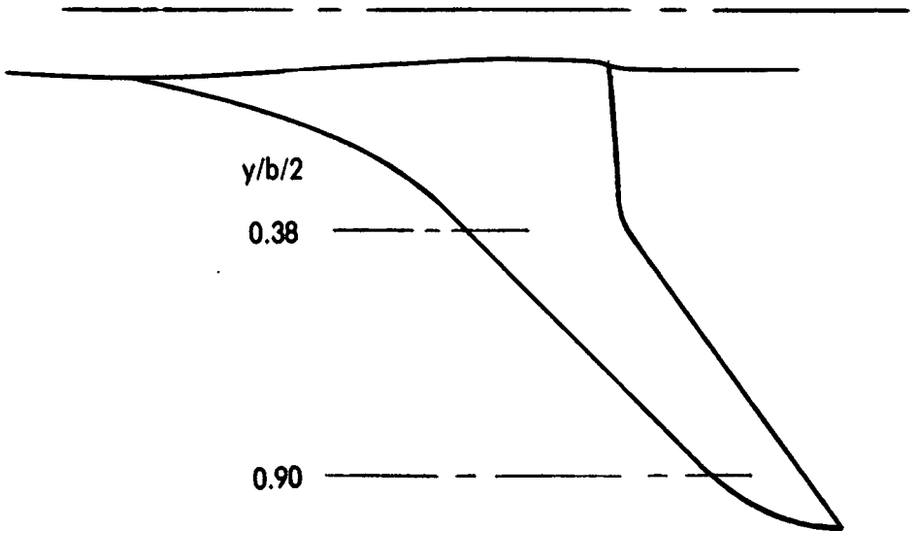

(b) Concluded. Leading-edge devices and flap span.

Figure 2.- Continued.

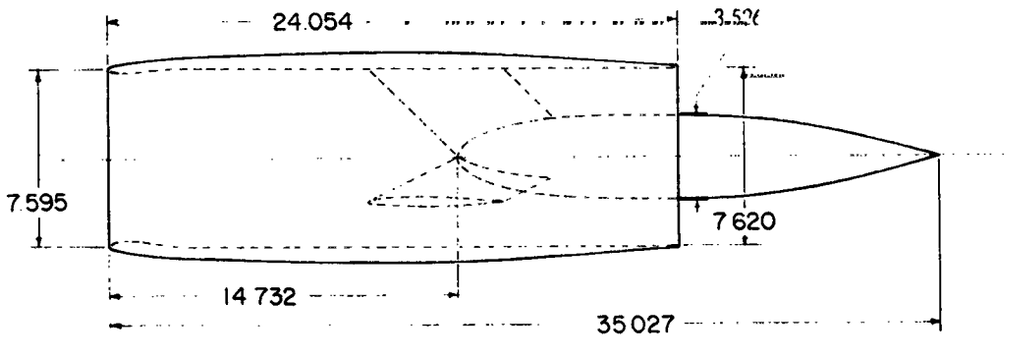

4 - Nacelle configuration

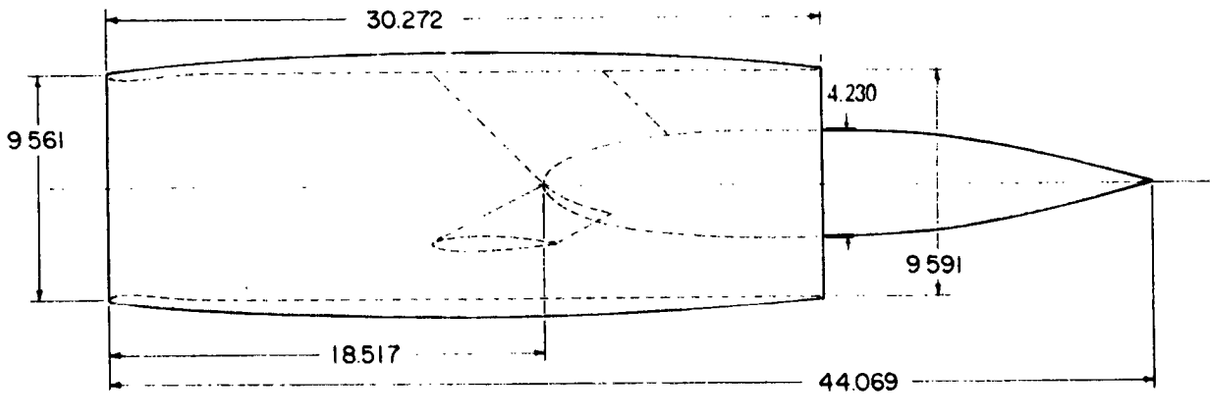

3 - Nacelle configuration

(c) Details of wing-mounted nacelles.

Figure 2.- Continued.

	Inboard	Outboard
y	40.874 cm	83.805 cm
A	13.030 cm	8.915 cm
B	128.930 cm	171.450 cm
C	3.50°	3.60°
D	1.40°	1.00°

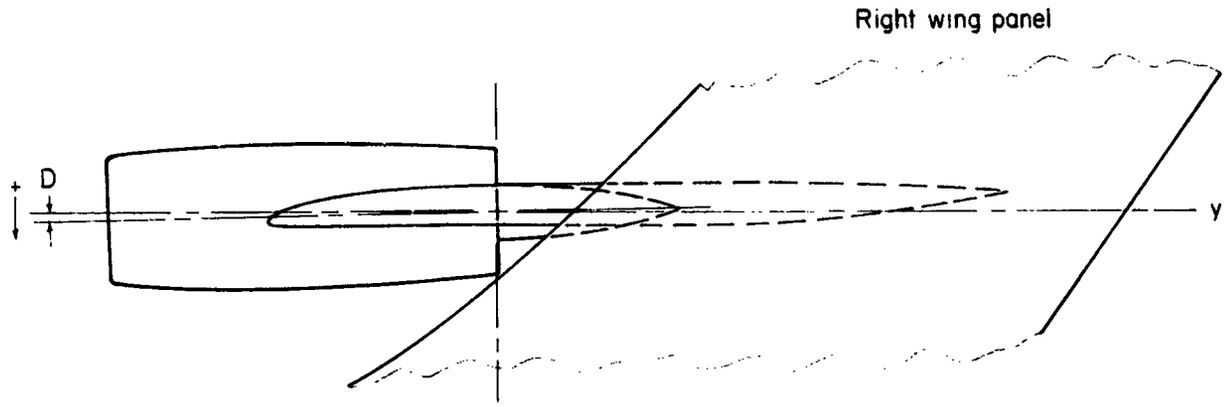

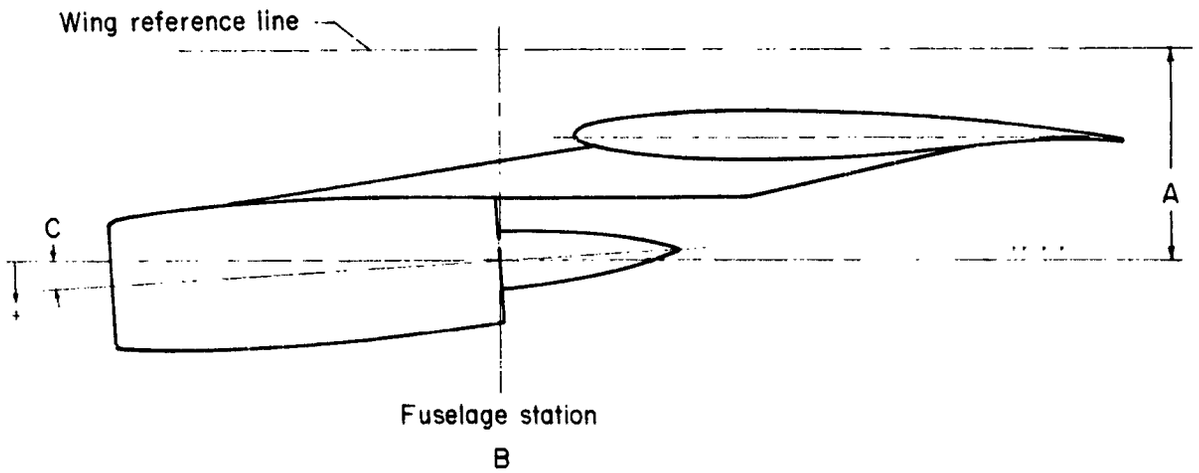

(c) Continued. Location of four wing-mounted nacelles.

Figure 2.- Continued.

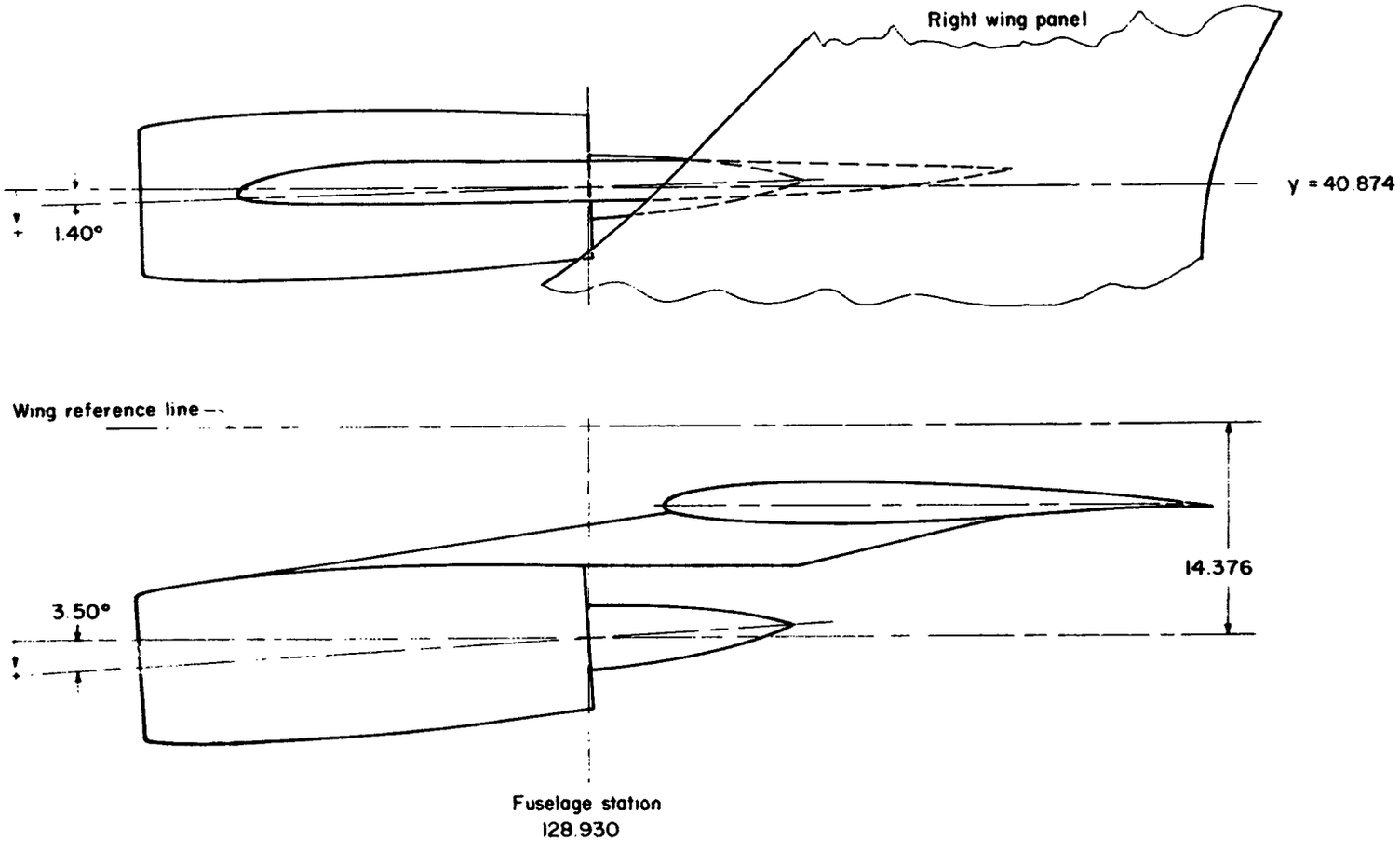

(c) Continued. Location of wing-mounted nacelle for three nacelle configurations.

Figure 2.- Continued.

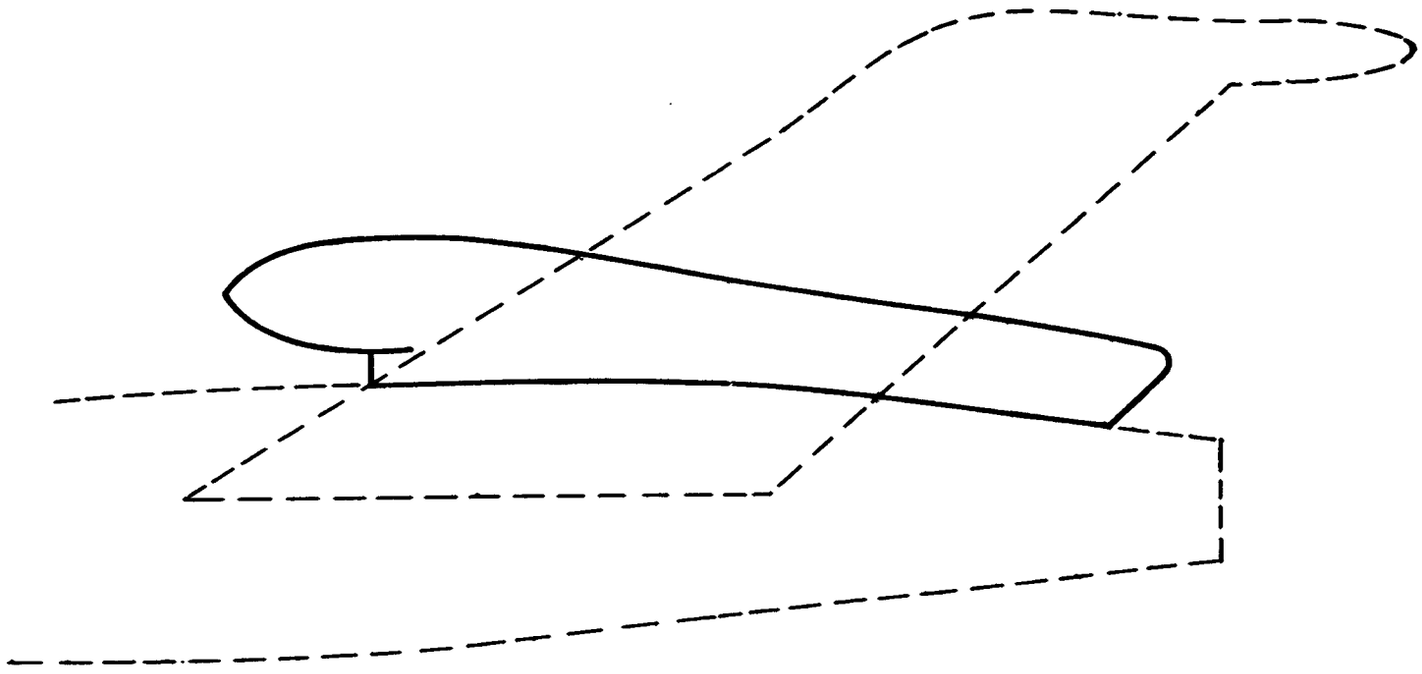

(c) Concluded. Details of vertical-tail-mounted nacelle.

Figure 2.- Continued.

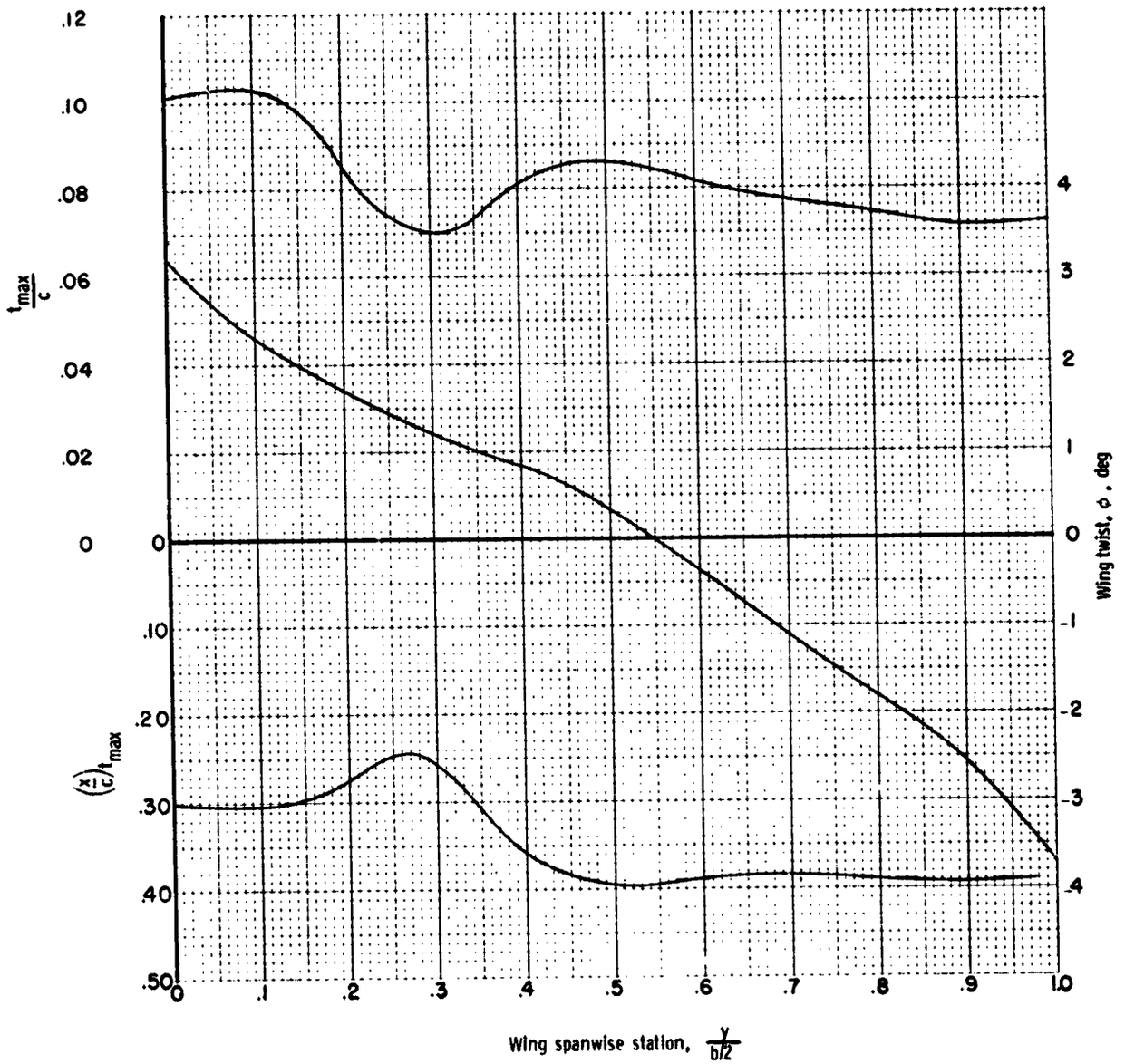

(d) Wing spanwise details.

Figure 2.- Concluded.

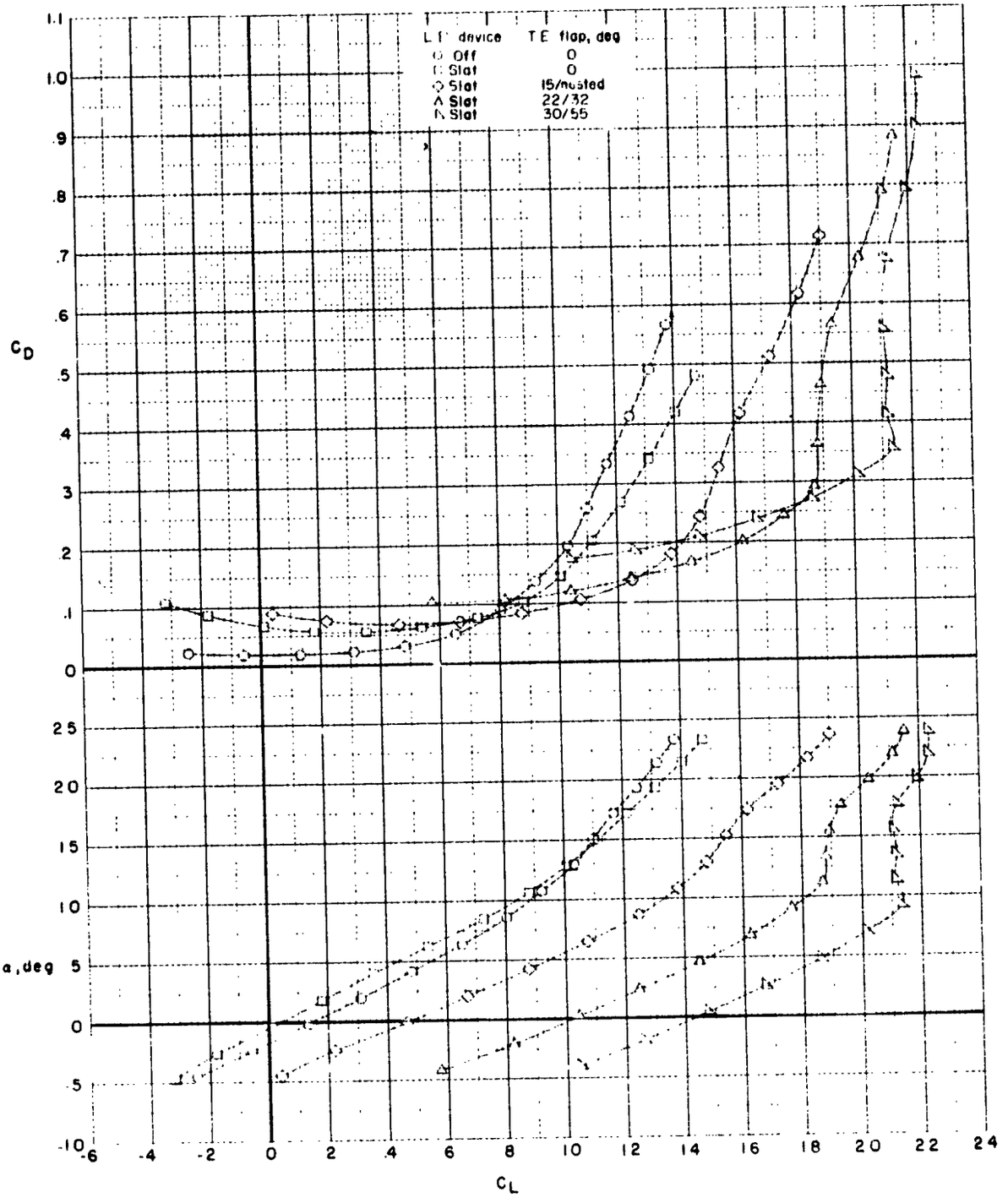

Figure 3.- Effect of leading-edge slat and several trailing-edge flap deflections. Horizontal tail off; no transition strips.

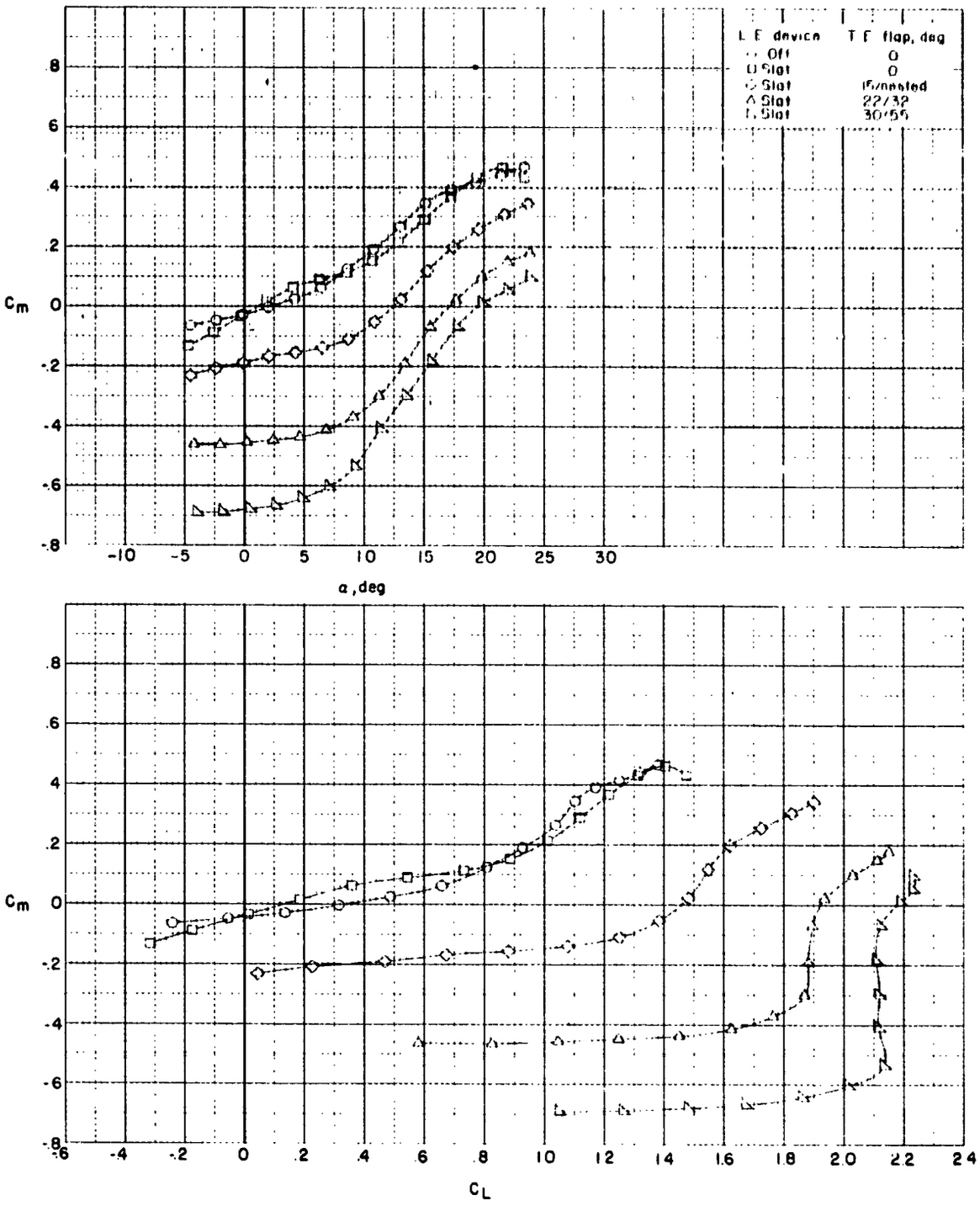

Figure 3.- Concluded.

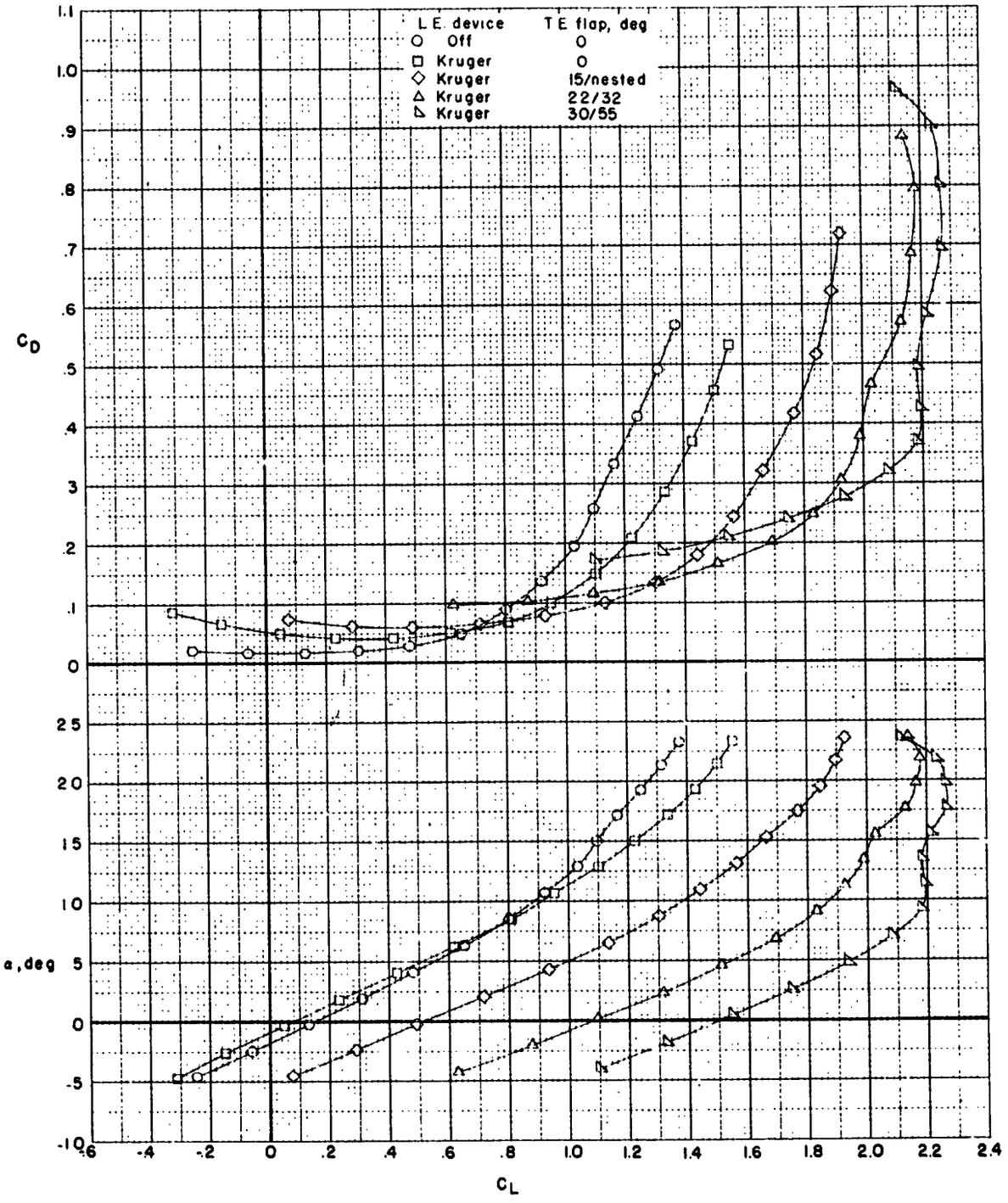

Figure 4.- Effect of leading-edge Kruger flap and several trailing-edge flap deflections. Horizontal tail off; no transition strips.

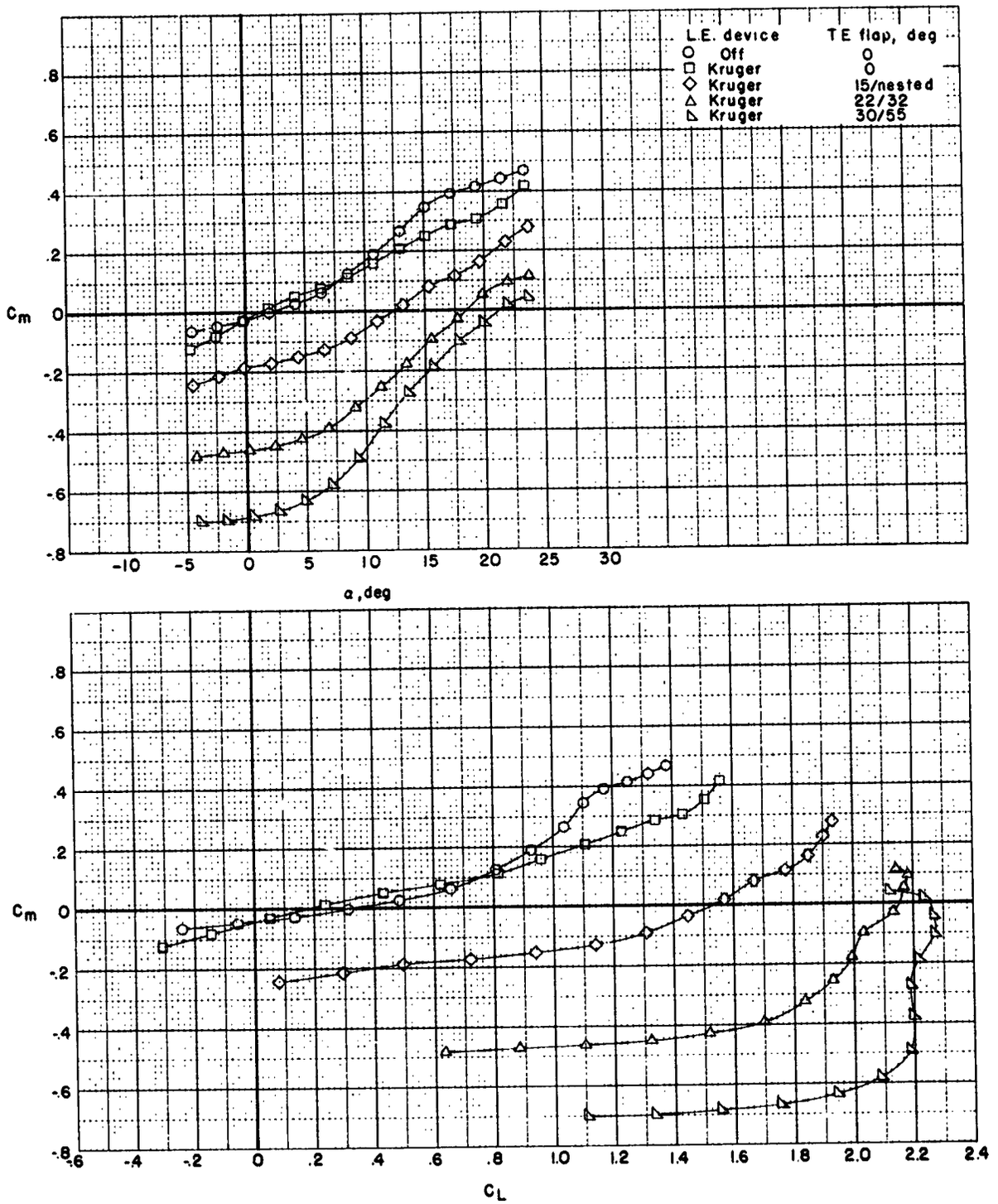

Figure 4.- Concluded.

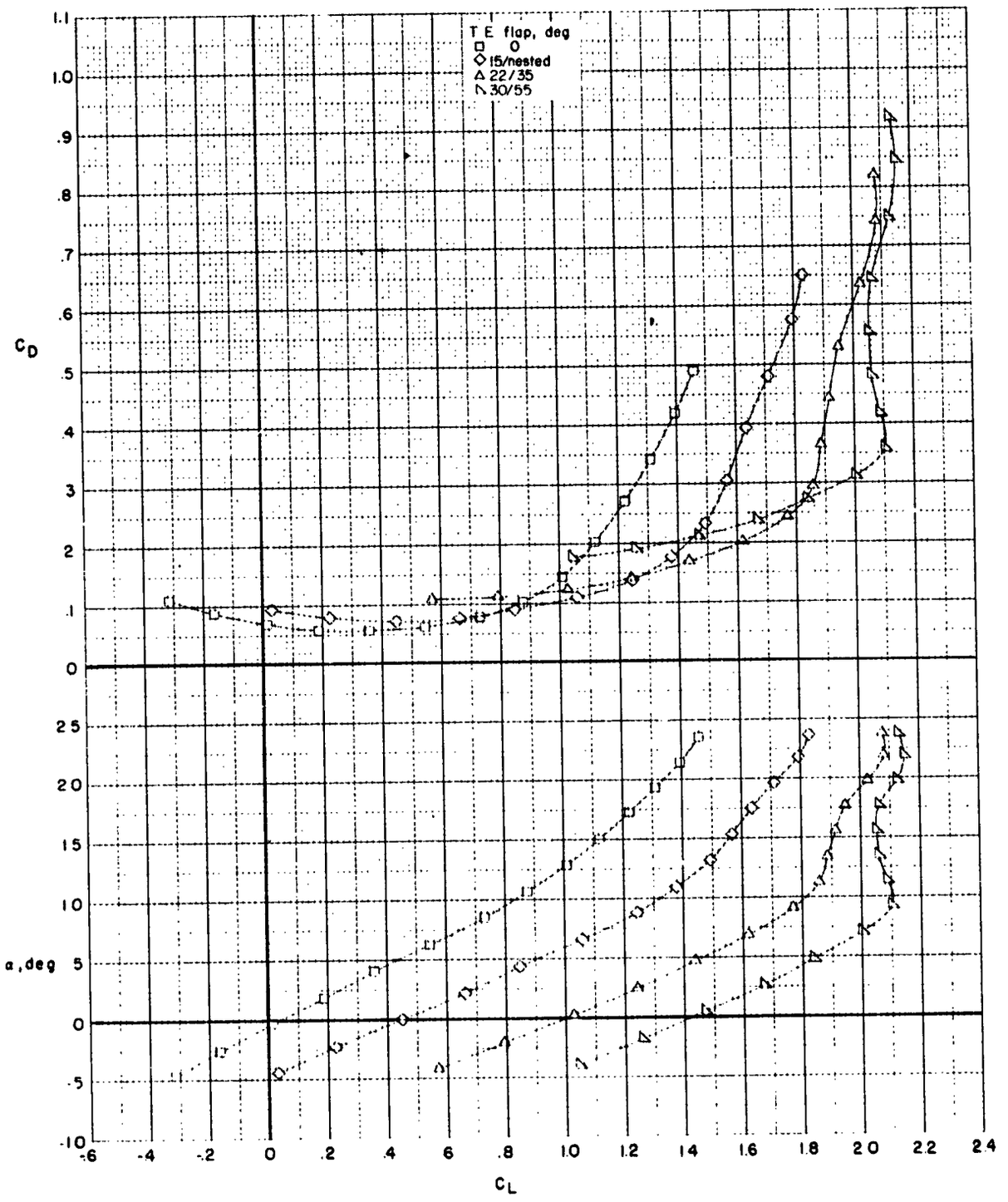

(a) $\delta_S = 45^o$.

Figure 5.- Effect of trailing-edge flap deflection with several leading-edge devices. Horizontal tail off.

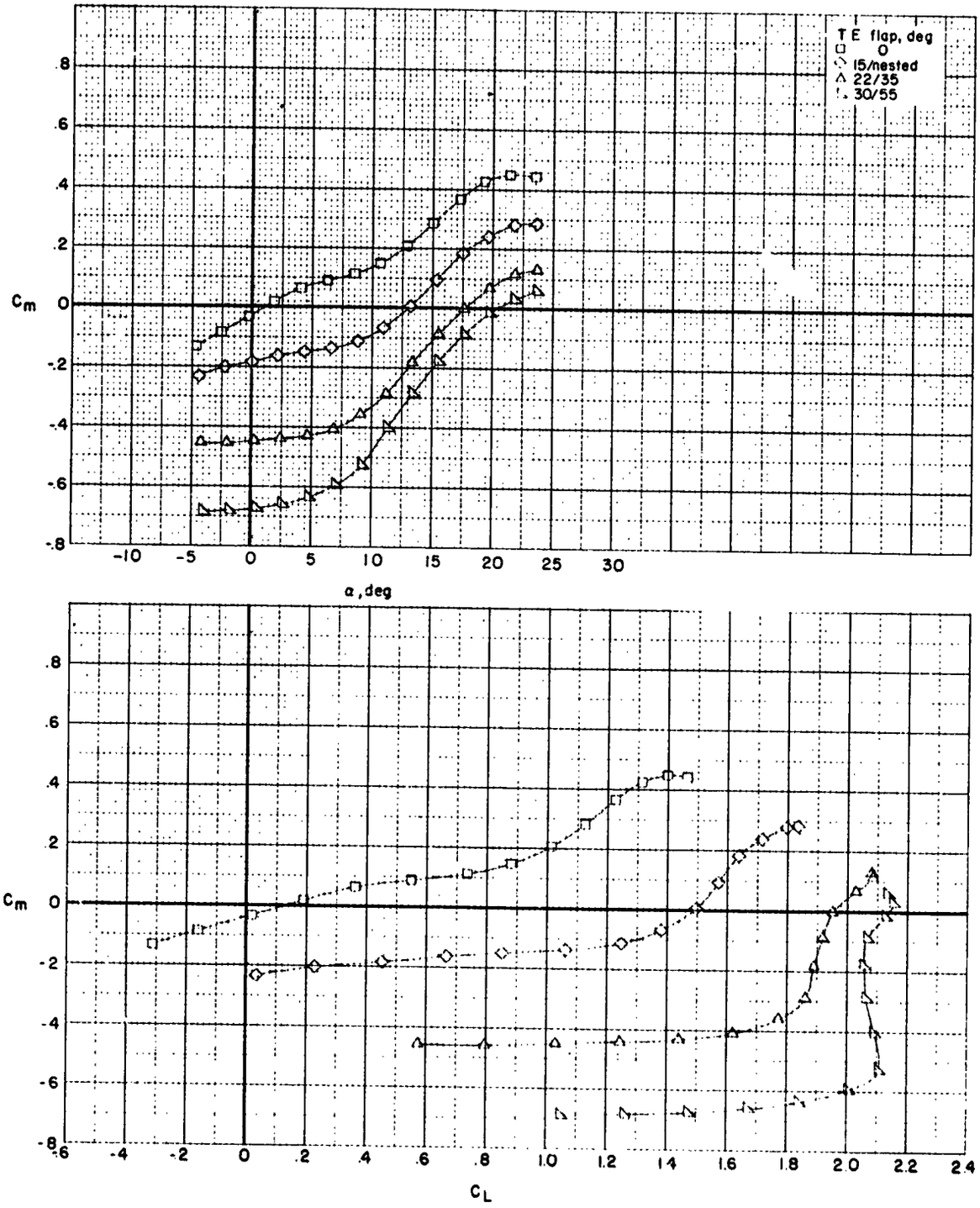

(a) Concluded.

Figure 5.- Continued.

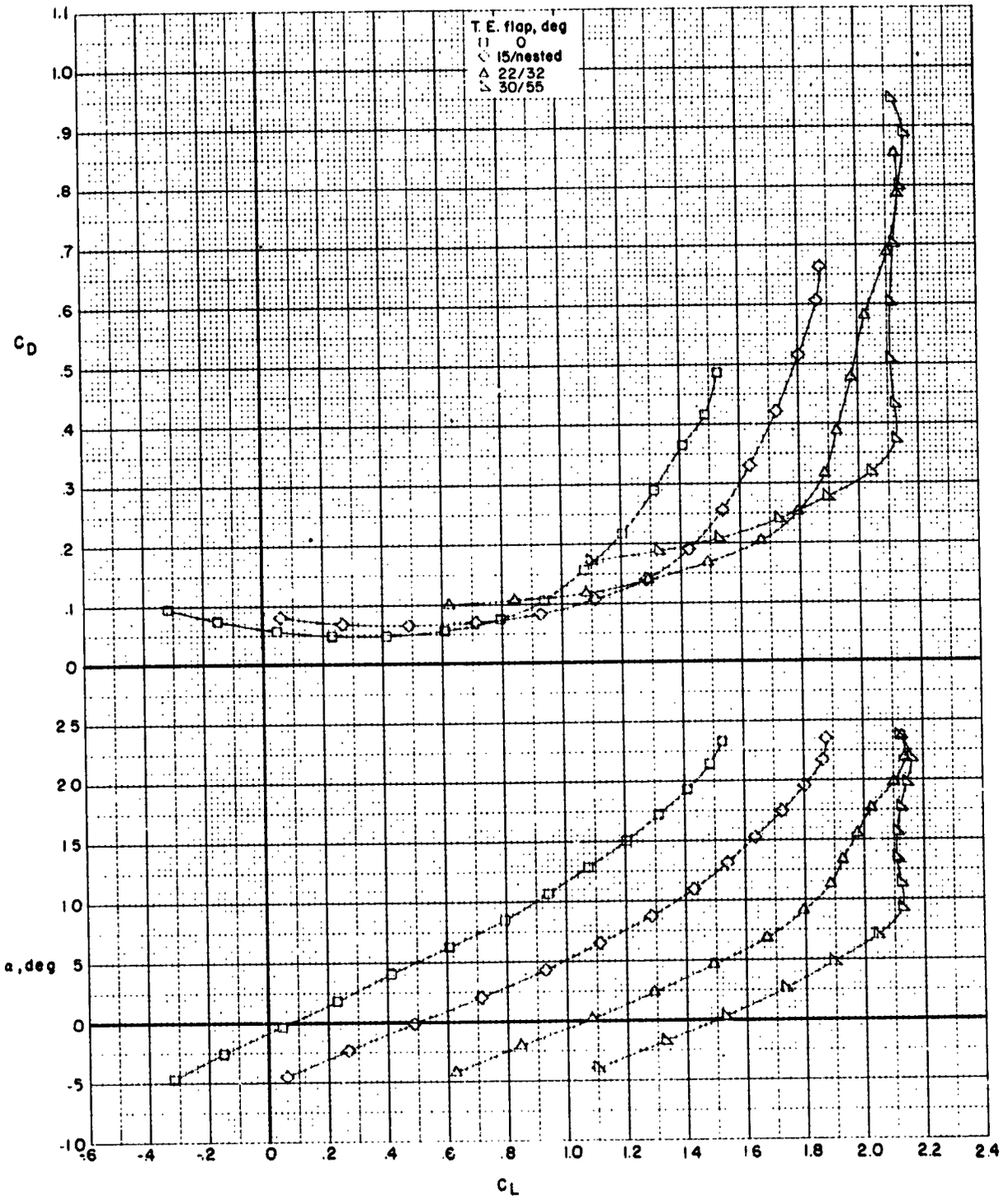

(b) $\delta_K = 45^o$.

Figure 5.- Continued.

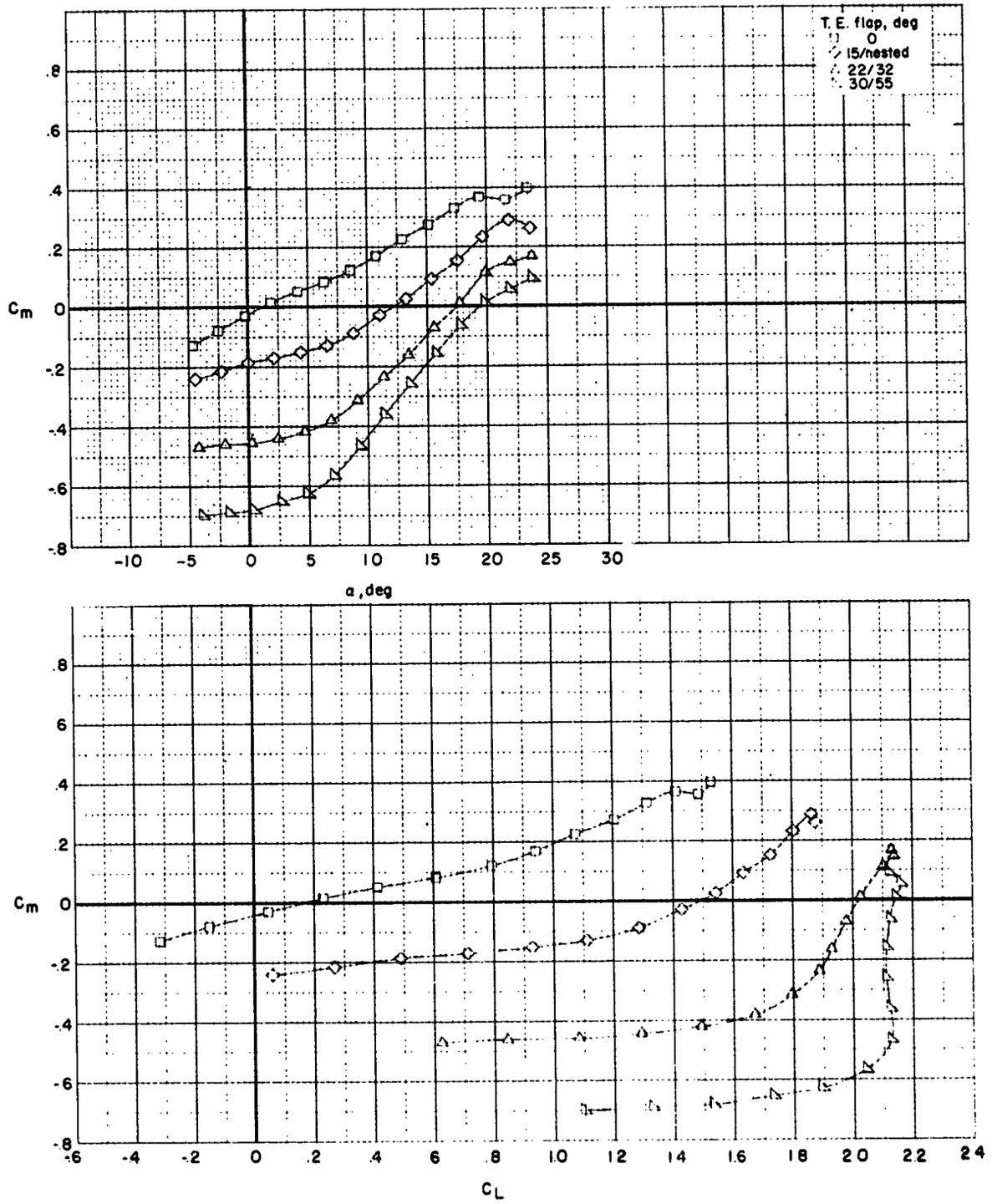

(b) Concluded.

Figure 5.- Concluded.

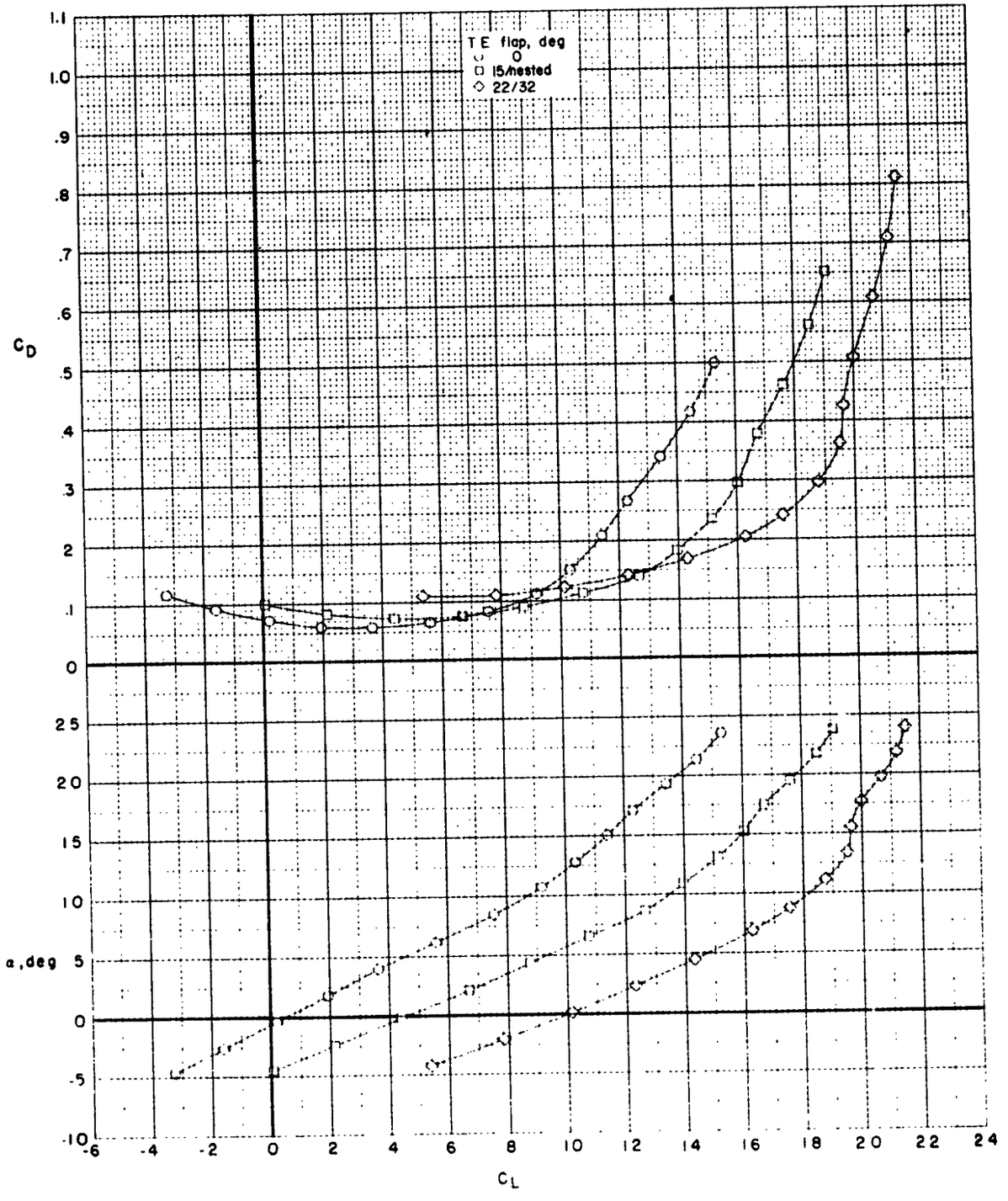

Figure 6.- Effect of trailing-edge flap deflections with $\delta_s = 45^o$ and four wing-mounted nacelles. Horizontal tail off; no flap cutout.

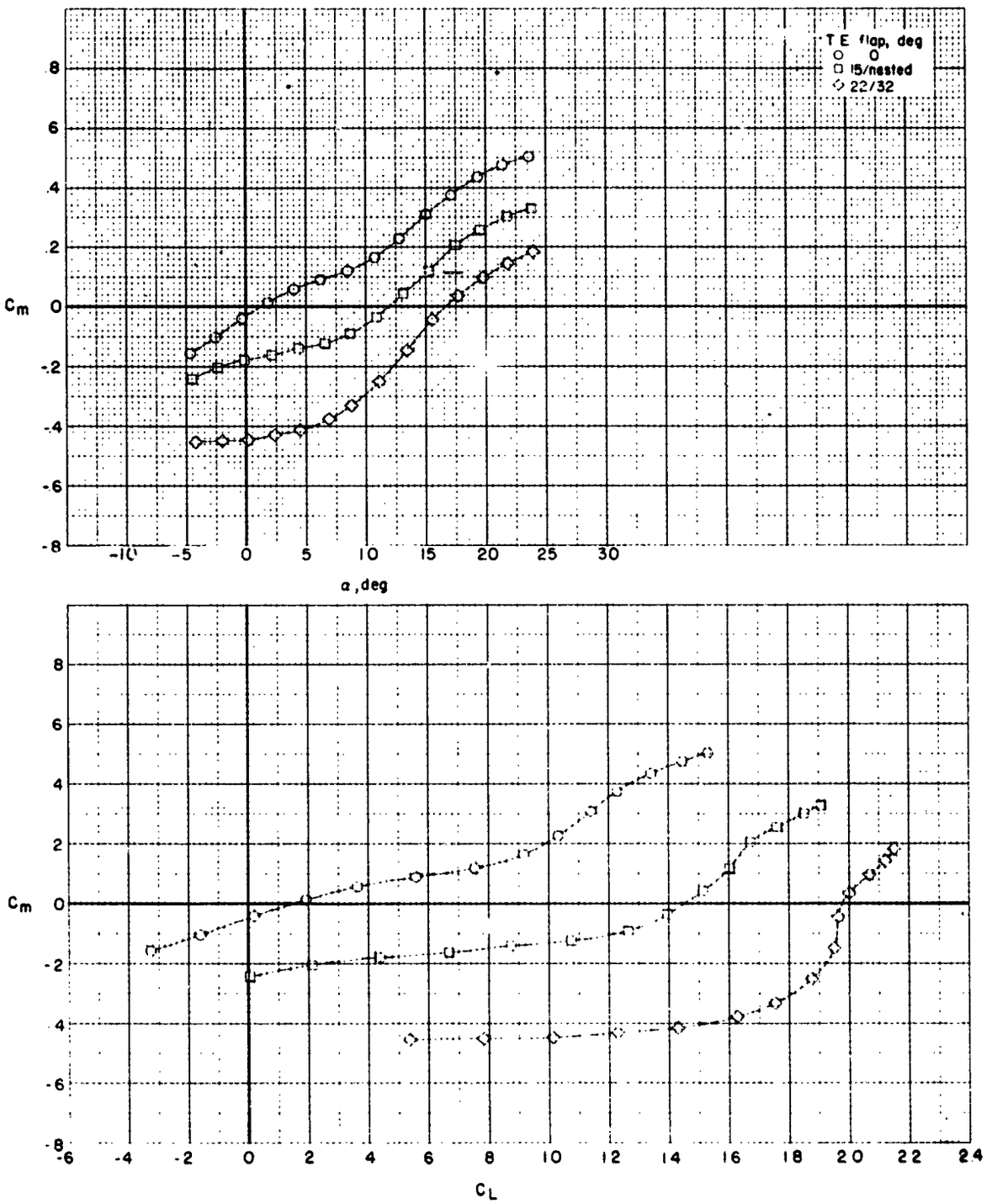

Figure 6.- Concluded.

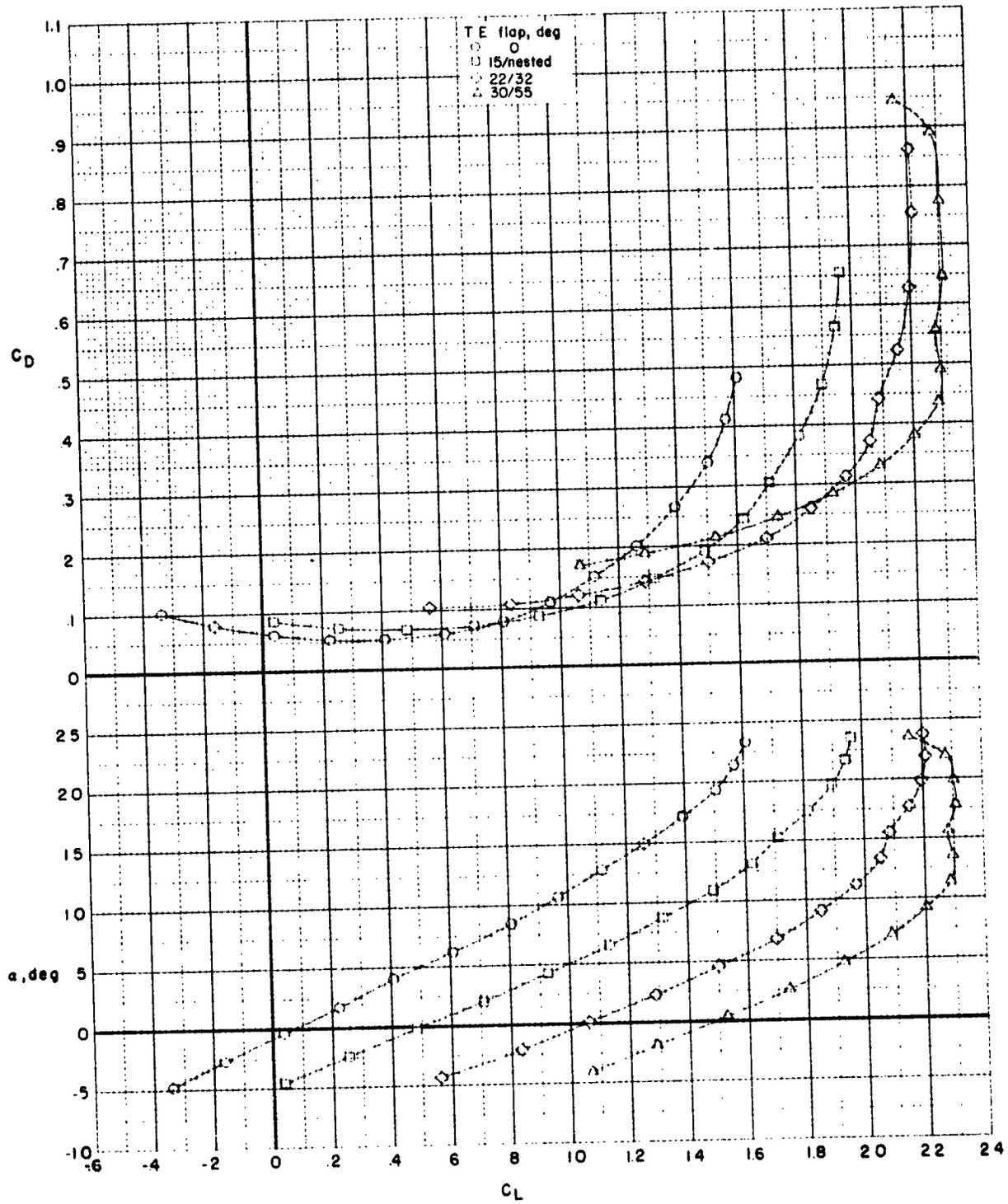

Figure 7.- Effect of trailing-edge flap deflections with $\delta_K = 45^o$ and four wing-mounted nacelles. Horizontal tail off; no flap cutout.

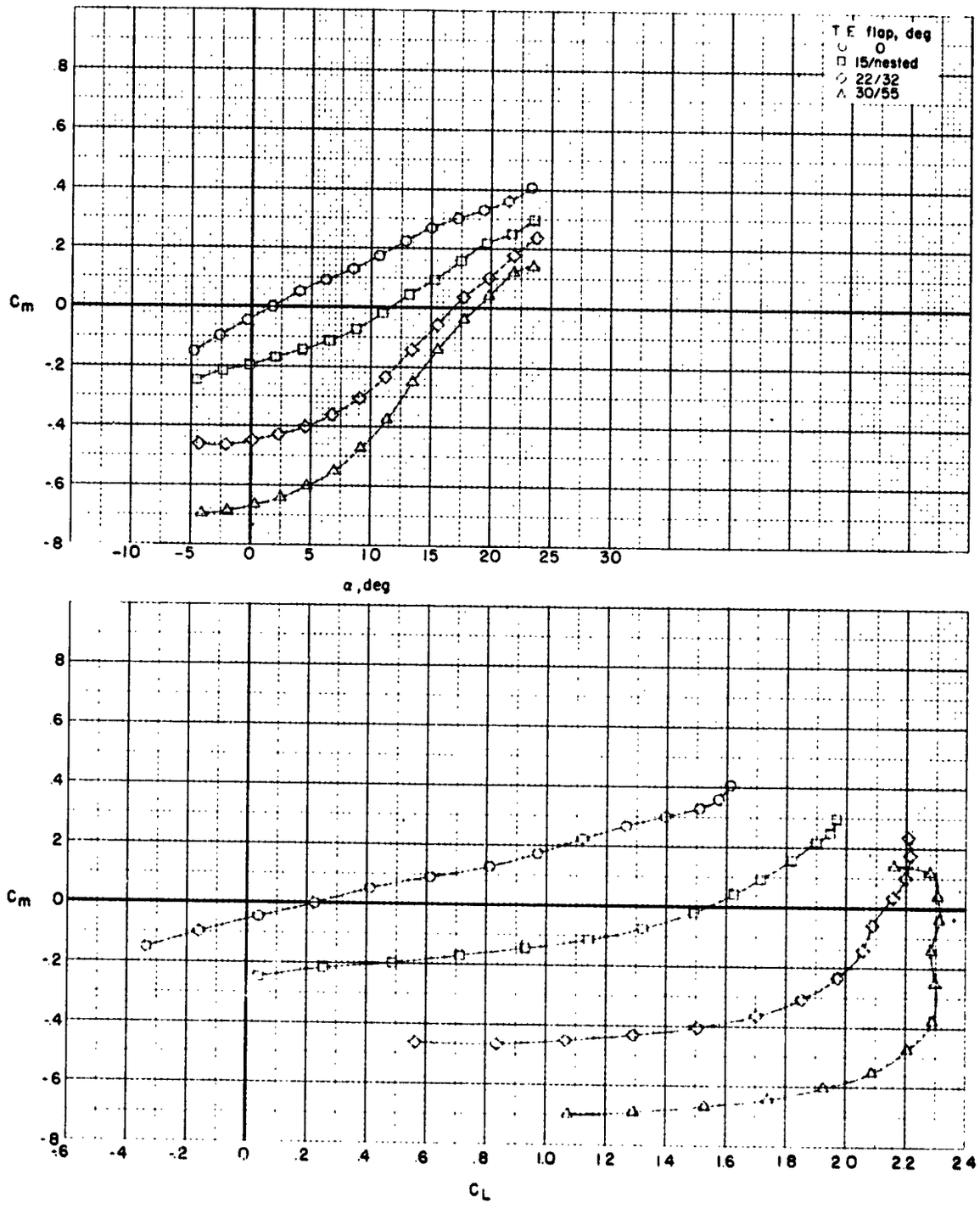

Figure 7.- Concluded.

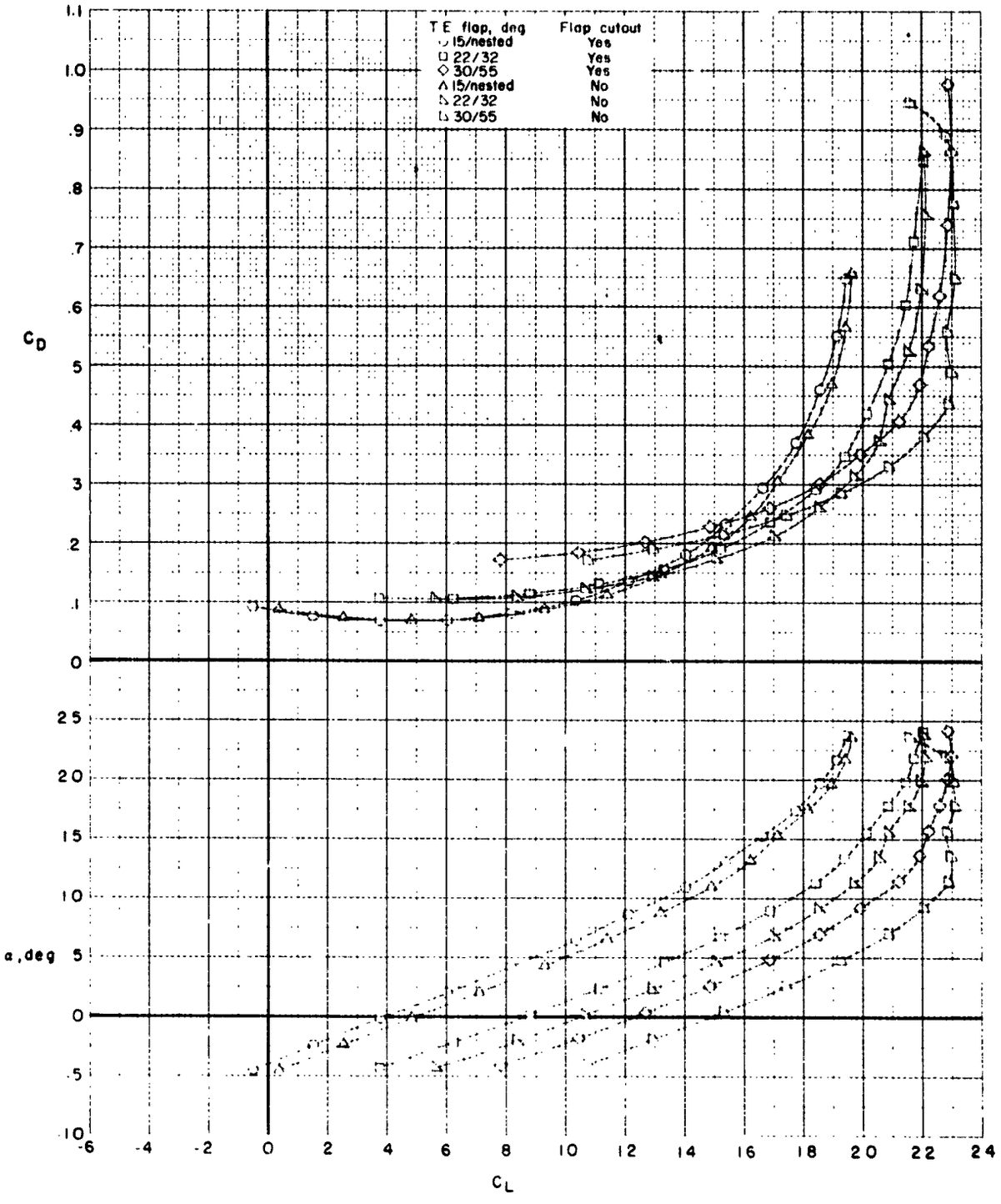

Figure 8.- Effect of flap cutout behind inboard wing nacelle of a four wing-mounted nacelle configuration with several trailing-edge flap deflections. Horizontal tail off; $\delta_K = 45^o$.

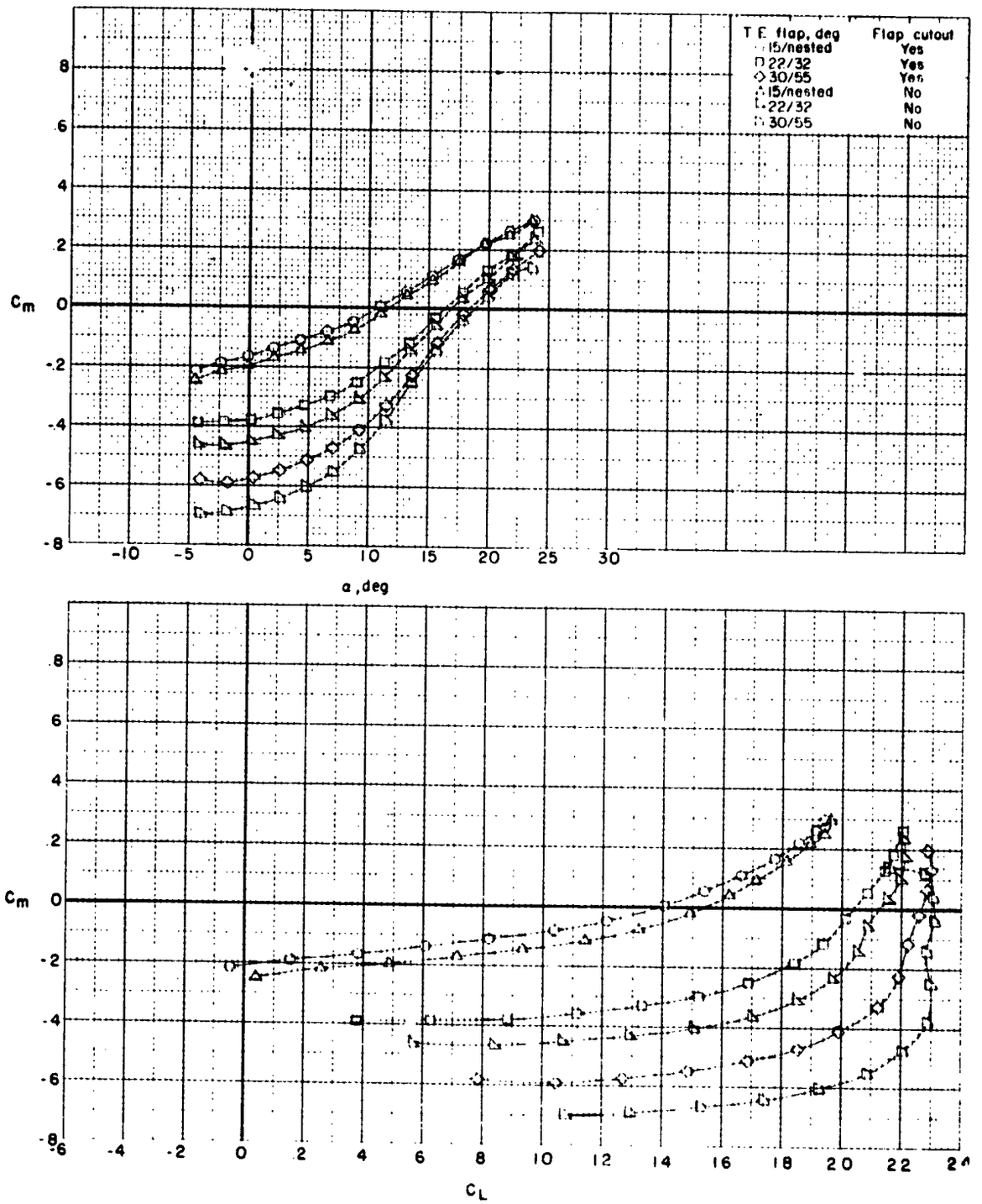

Figure 8.- Concluded.

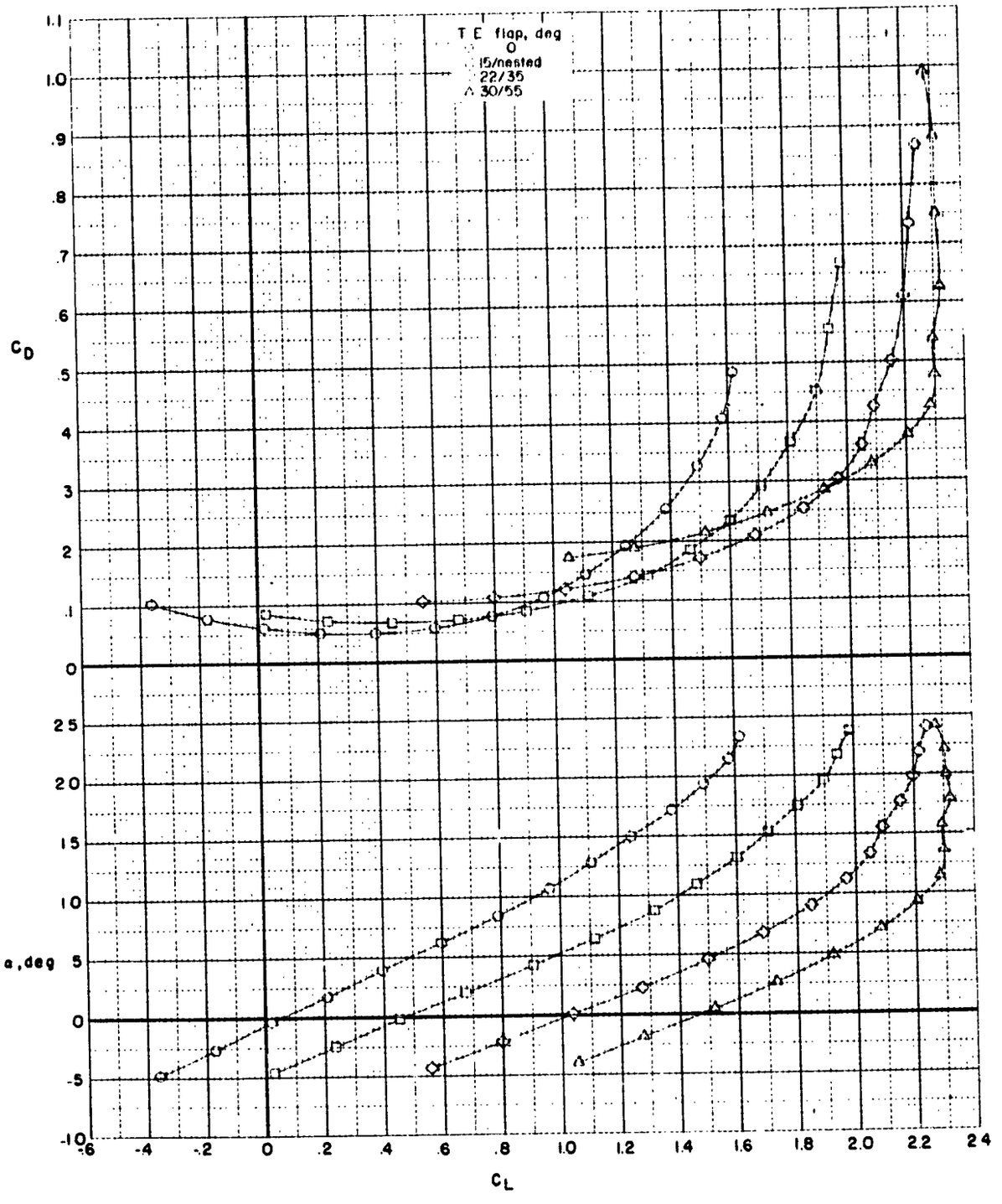

Figure 9.- Effect of trailing-edge flap deflections with $\delta_K = 45^o$ and two wing-mounted nacelles and one on the vertical tail (three engine). Horizontal tail off; no flap cutout.

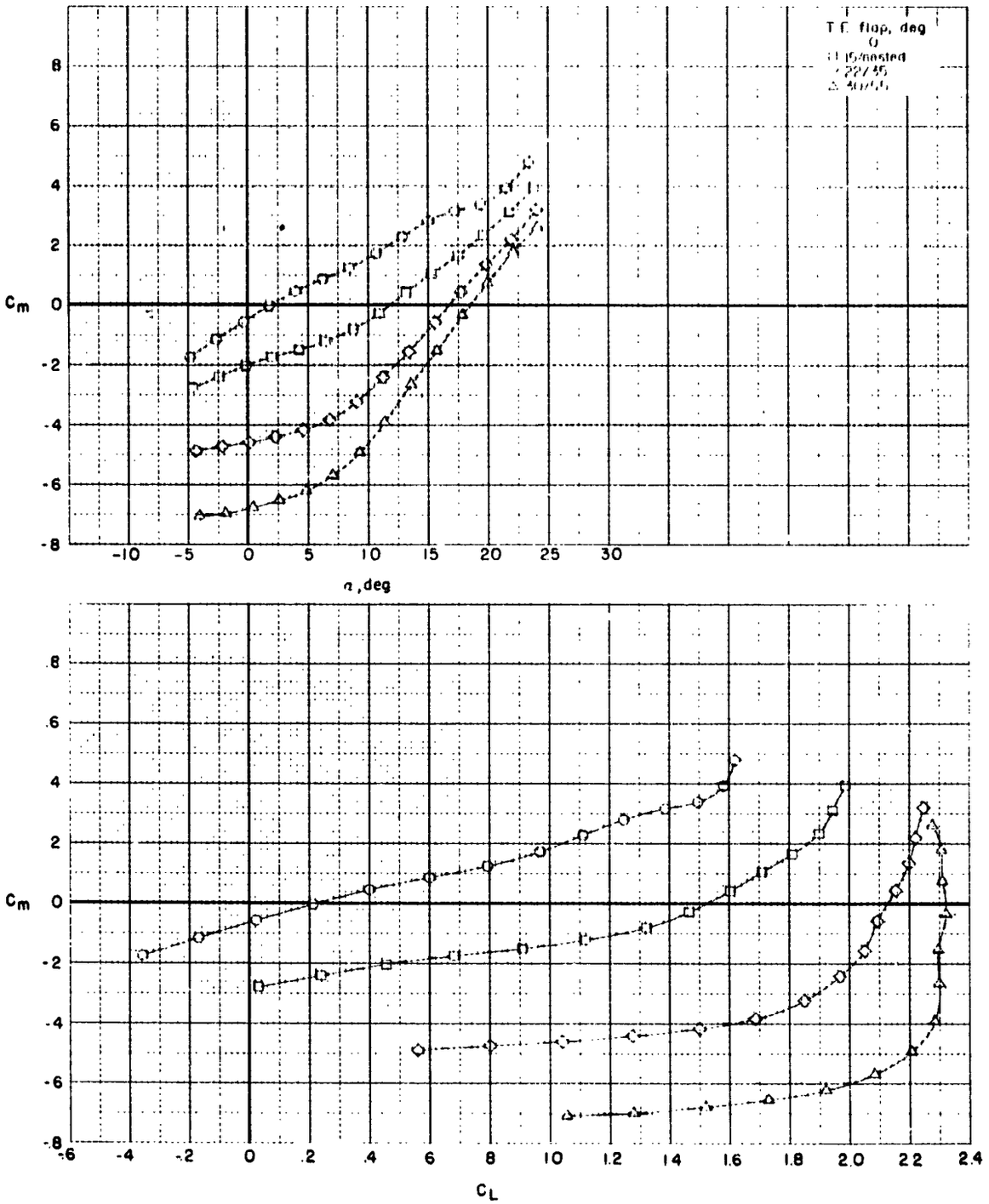

Figure 9.- Concluded.

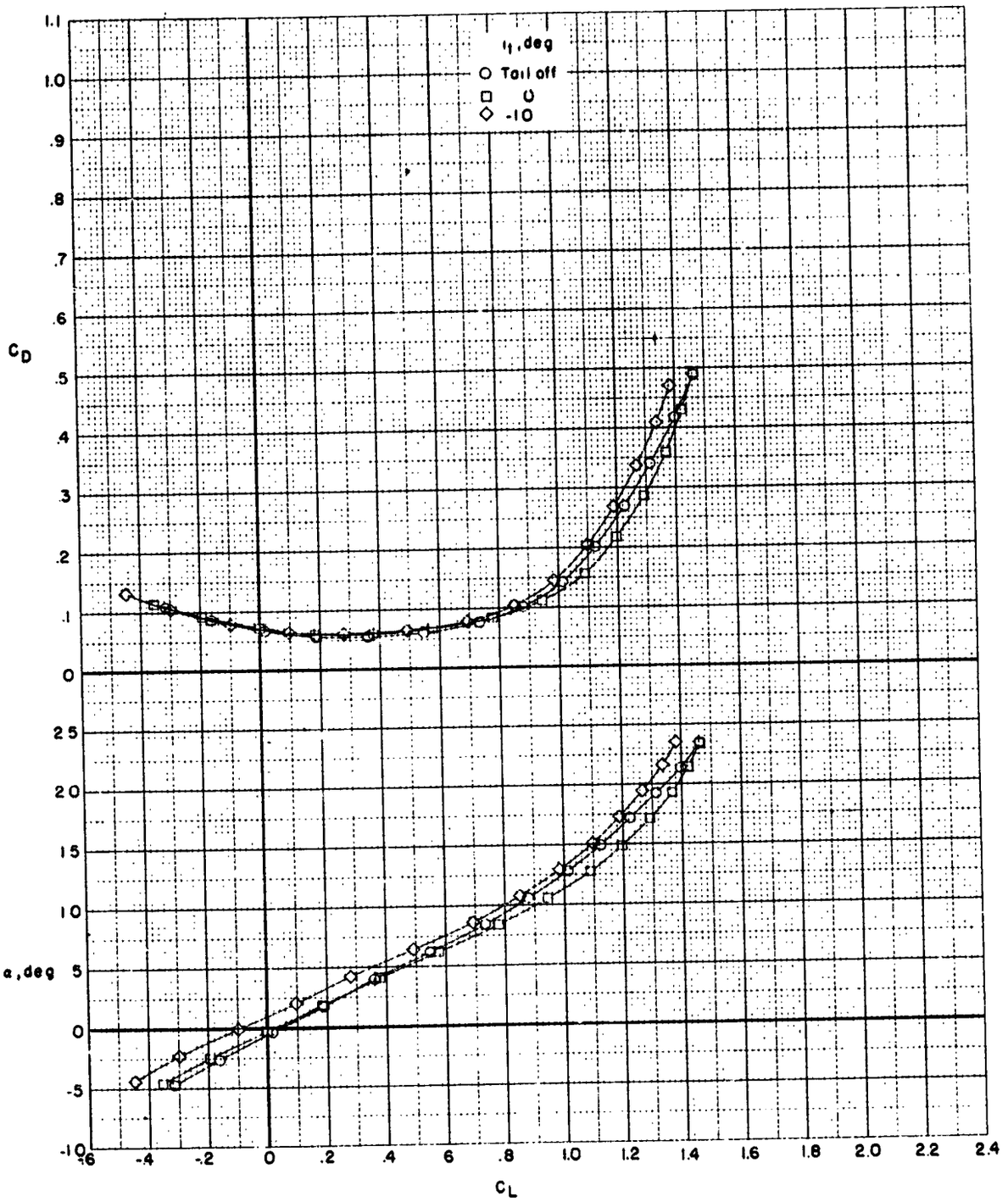

(a) $\delta_f = 0^o$.

Figure 10.- Effect of horizontal-tail deflection on longitudinal aerodynamic characteristics with various trailing-edge flap deflections and $\delta_s = 45^o$. T-tail.

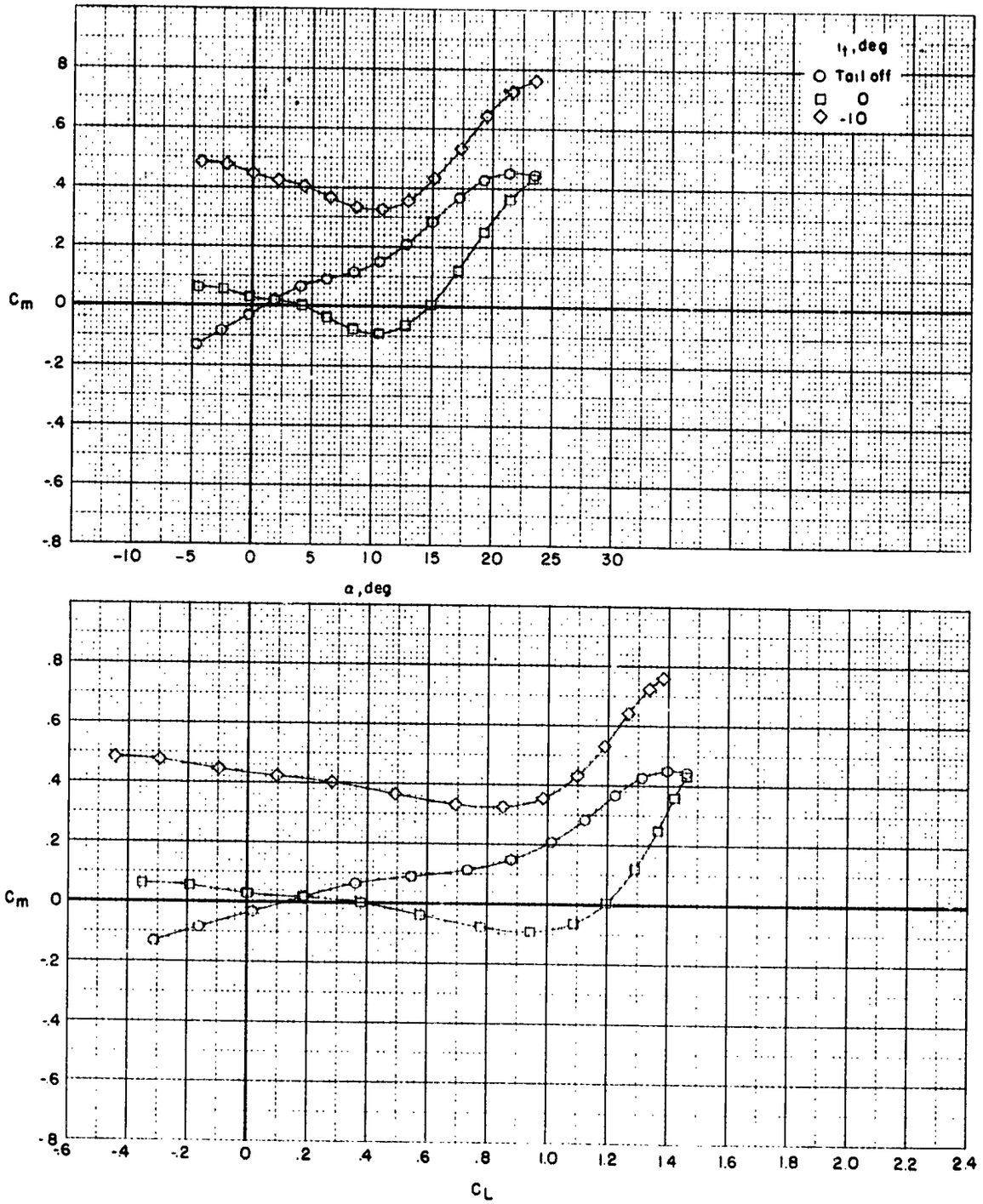

(a) Concluded.

Figure 10.- Continued.

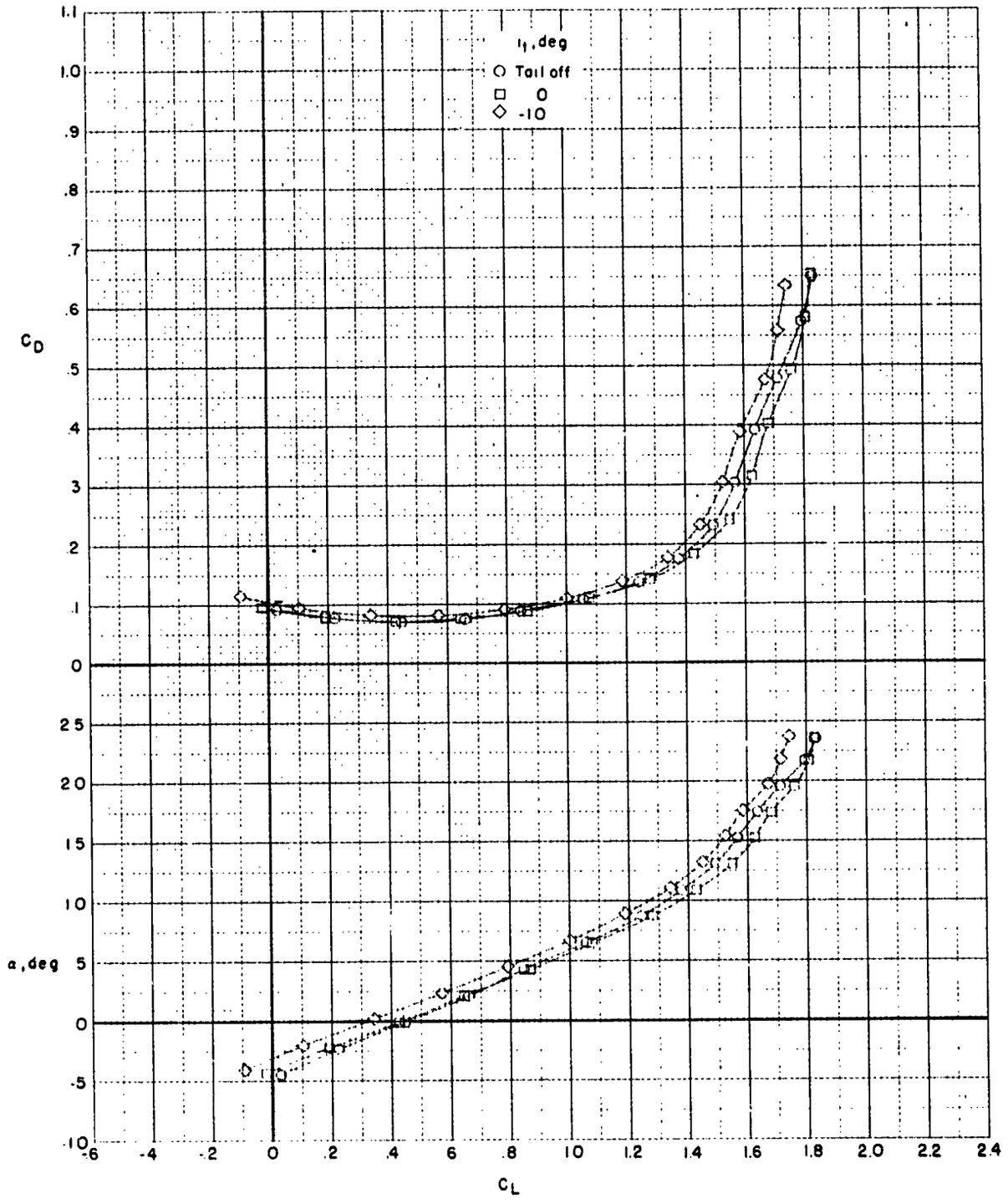

(b) $\delta_f = 15^o$/nested.

Figure 10.- Continued.

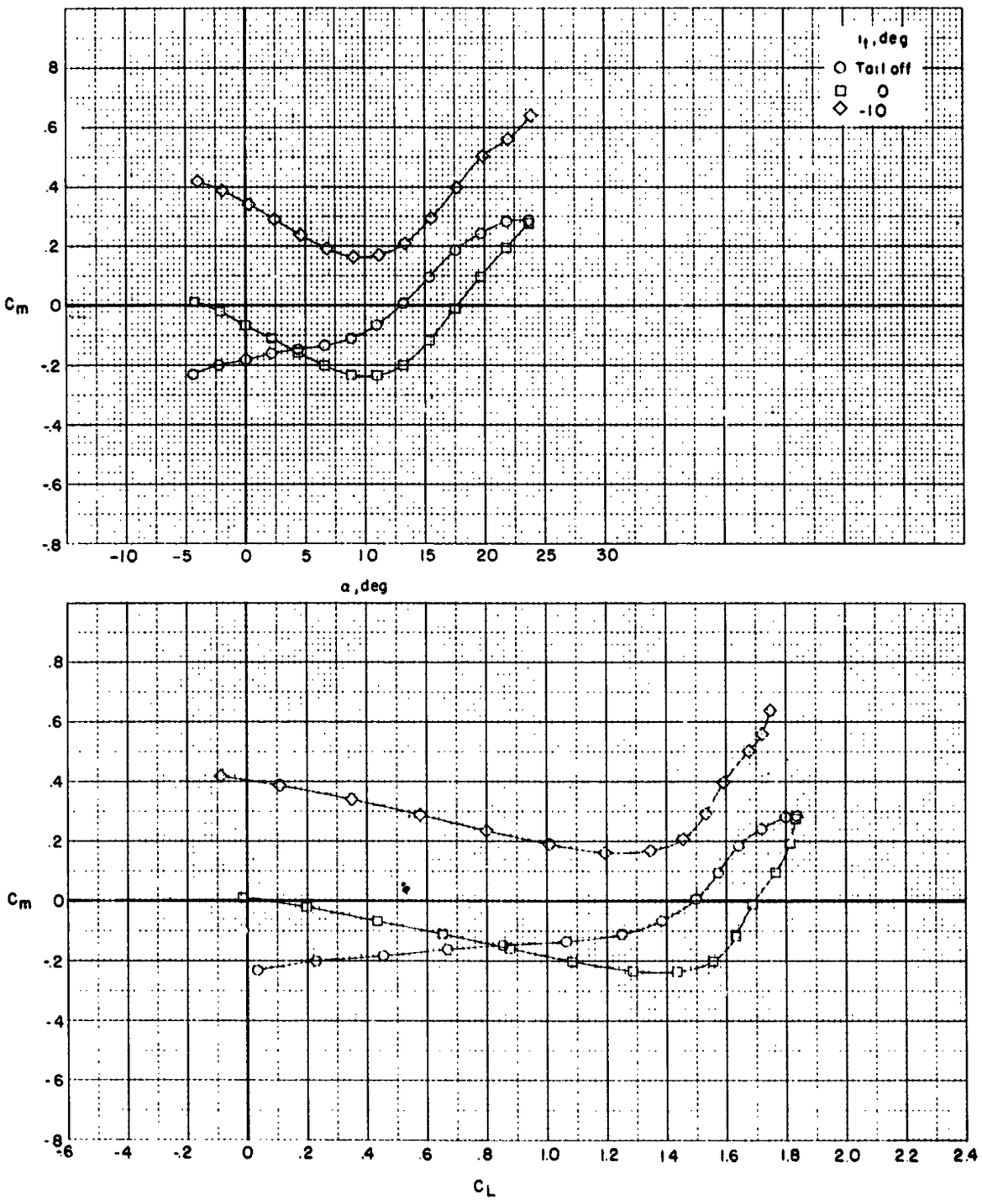

(b) Concluded.

Figure 10.- Continued.

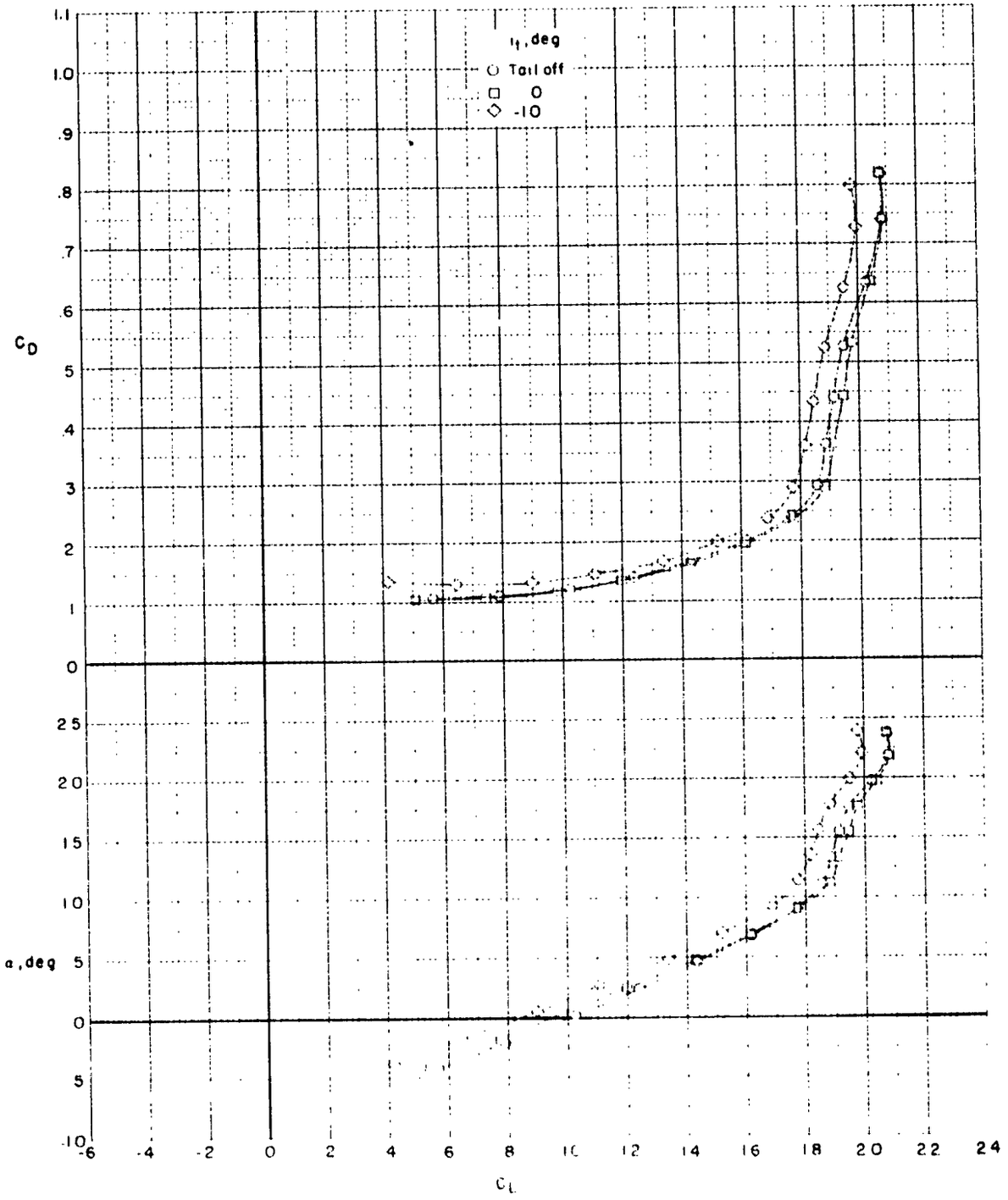

(c) $\delta_f = 22^\circ/32^\circ$.

Figure 10.- Continued.

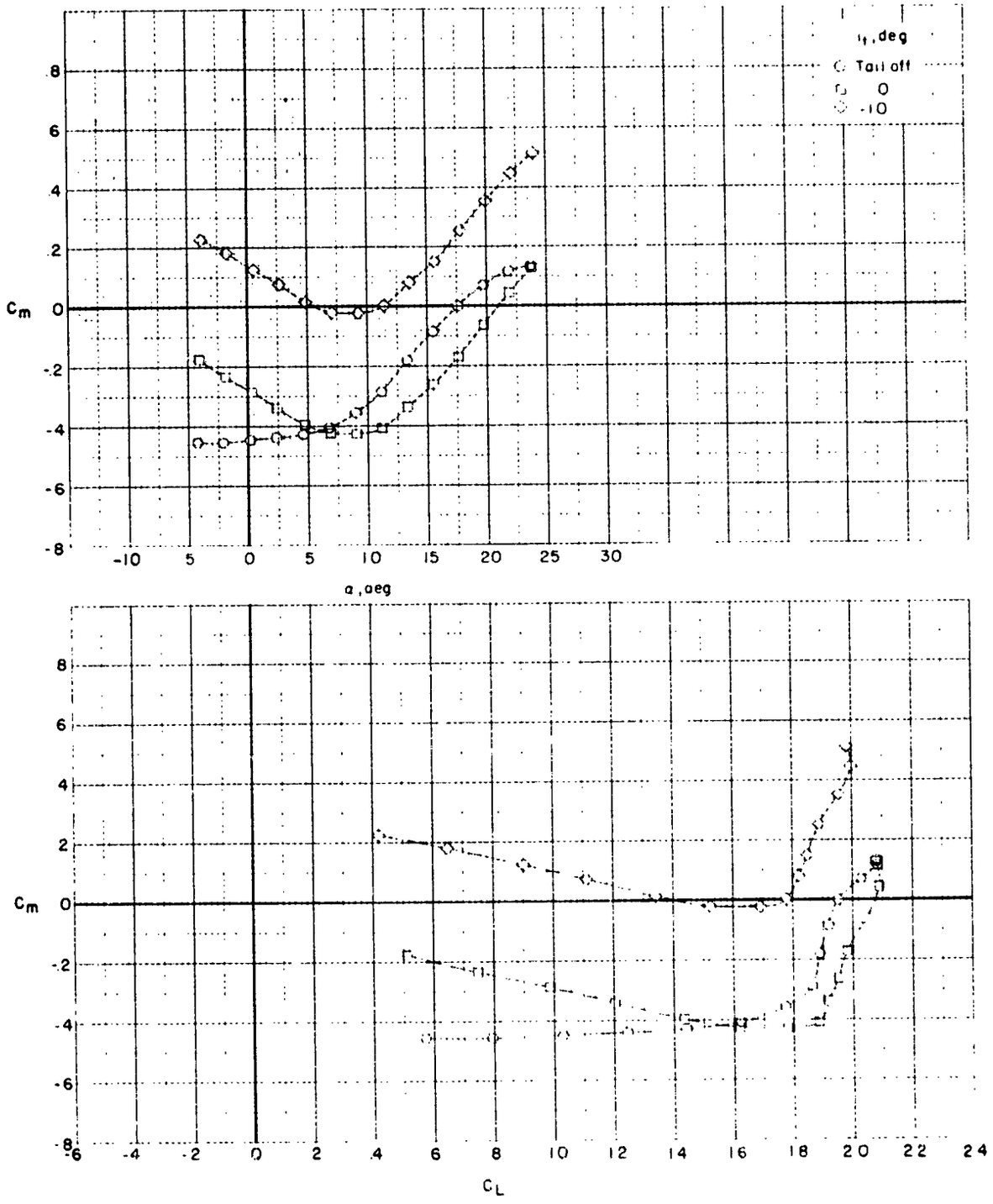

(c) Concluded.

Figure 10.- Continued.

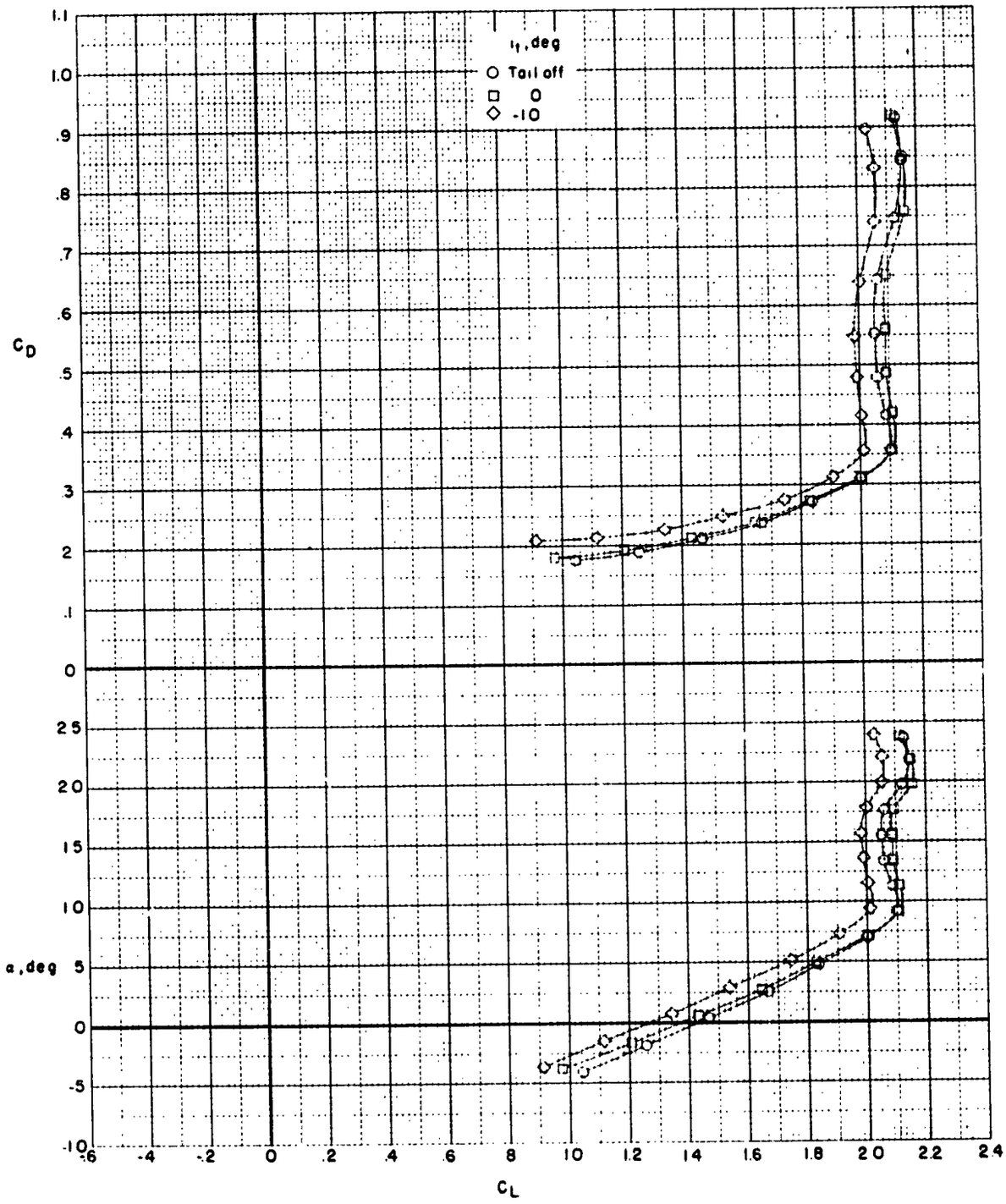

(d) $\delta_f = 30^o/55^o$

Figure 10.- Continued.

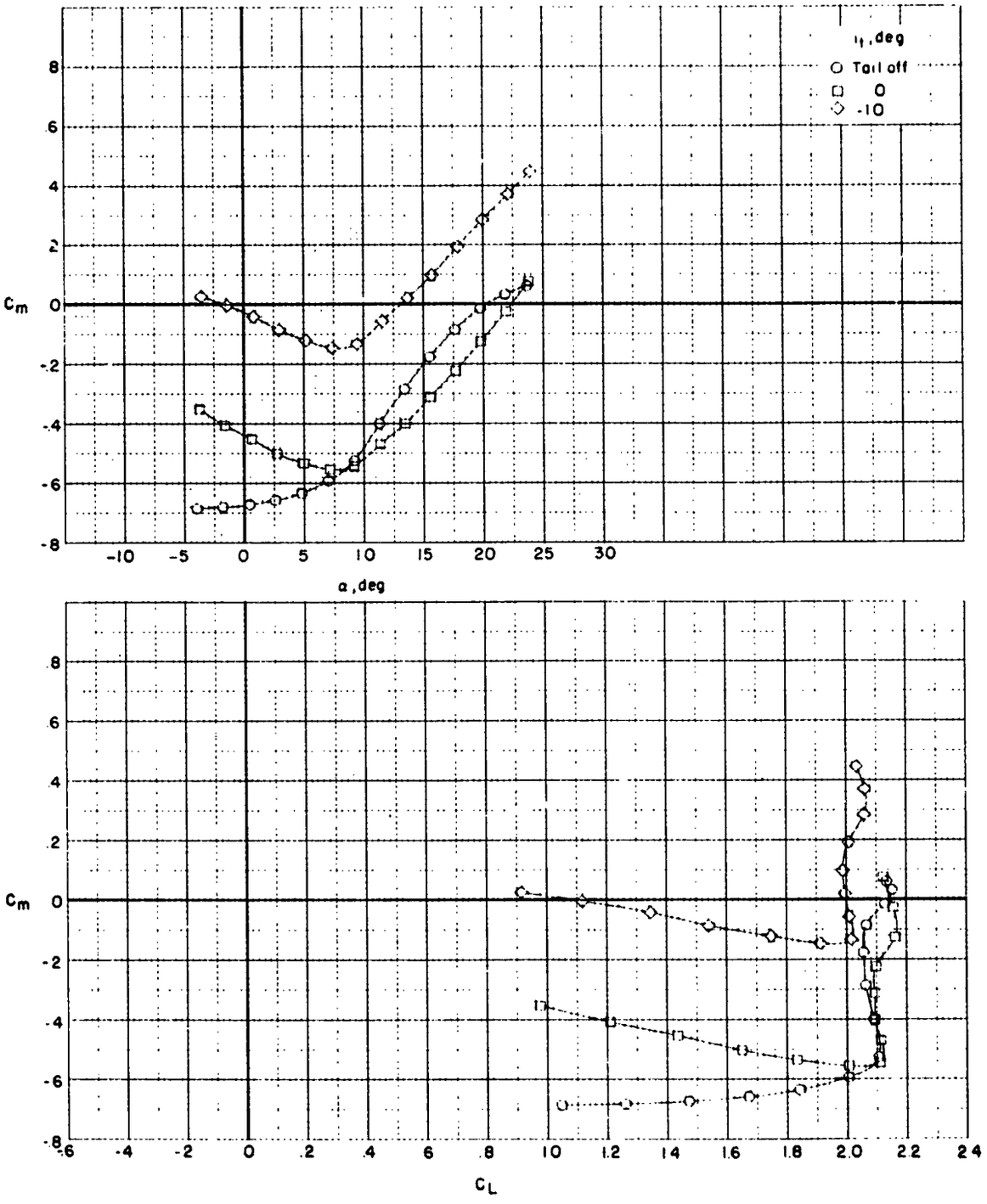

(d) Concluded.

Figure 10.- Concluded.

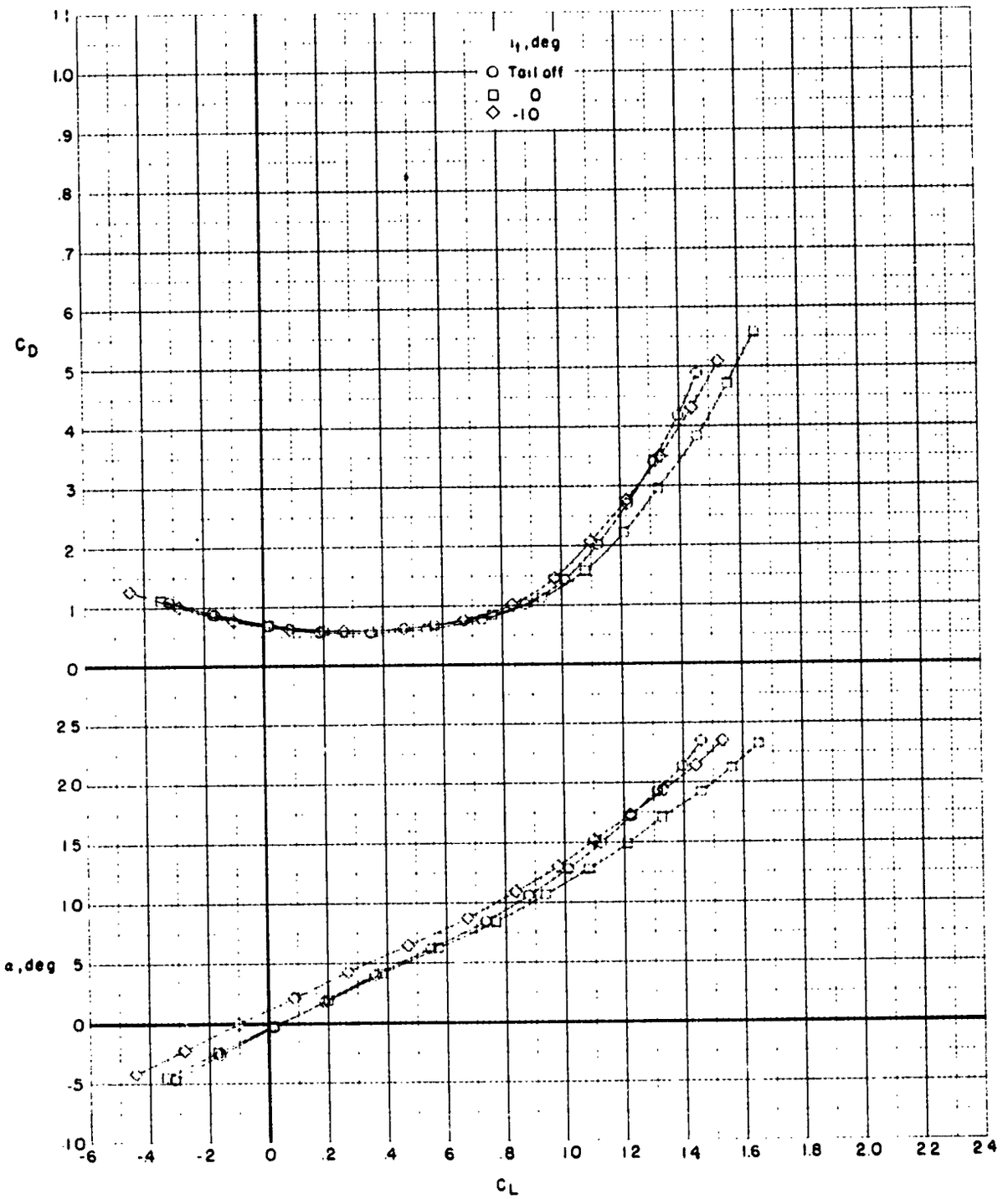

(a) $\delta_f = 0^o$.

Figure 11.- Effect of horizontal-tail deflection on longitudinal aerodynamic characteristics with various trailing-edge flap deflections and $\delta_s = 45^o$. Low tail.

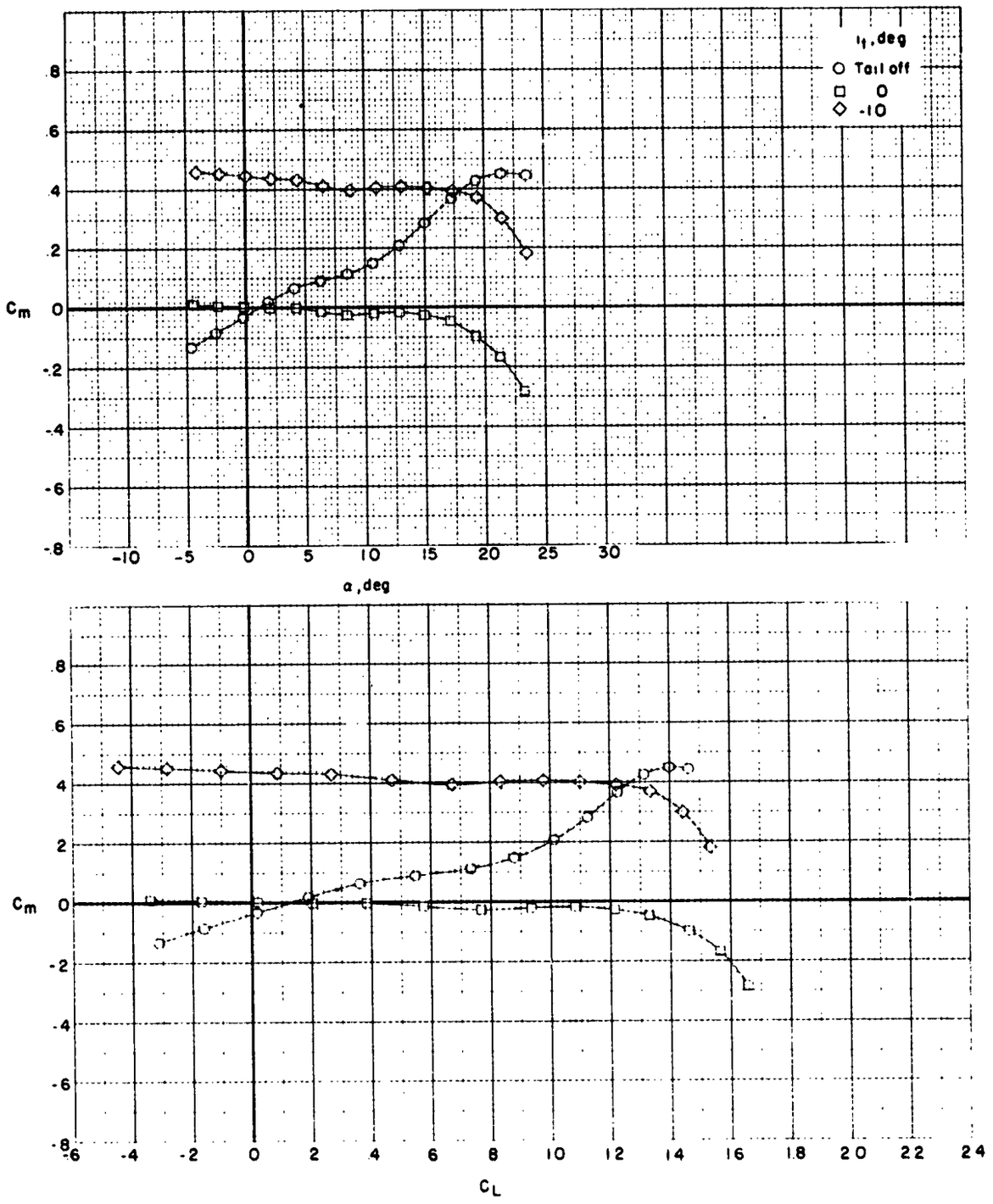

(a) Concluded.

Figure 11.- Continued.

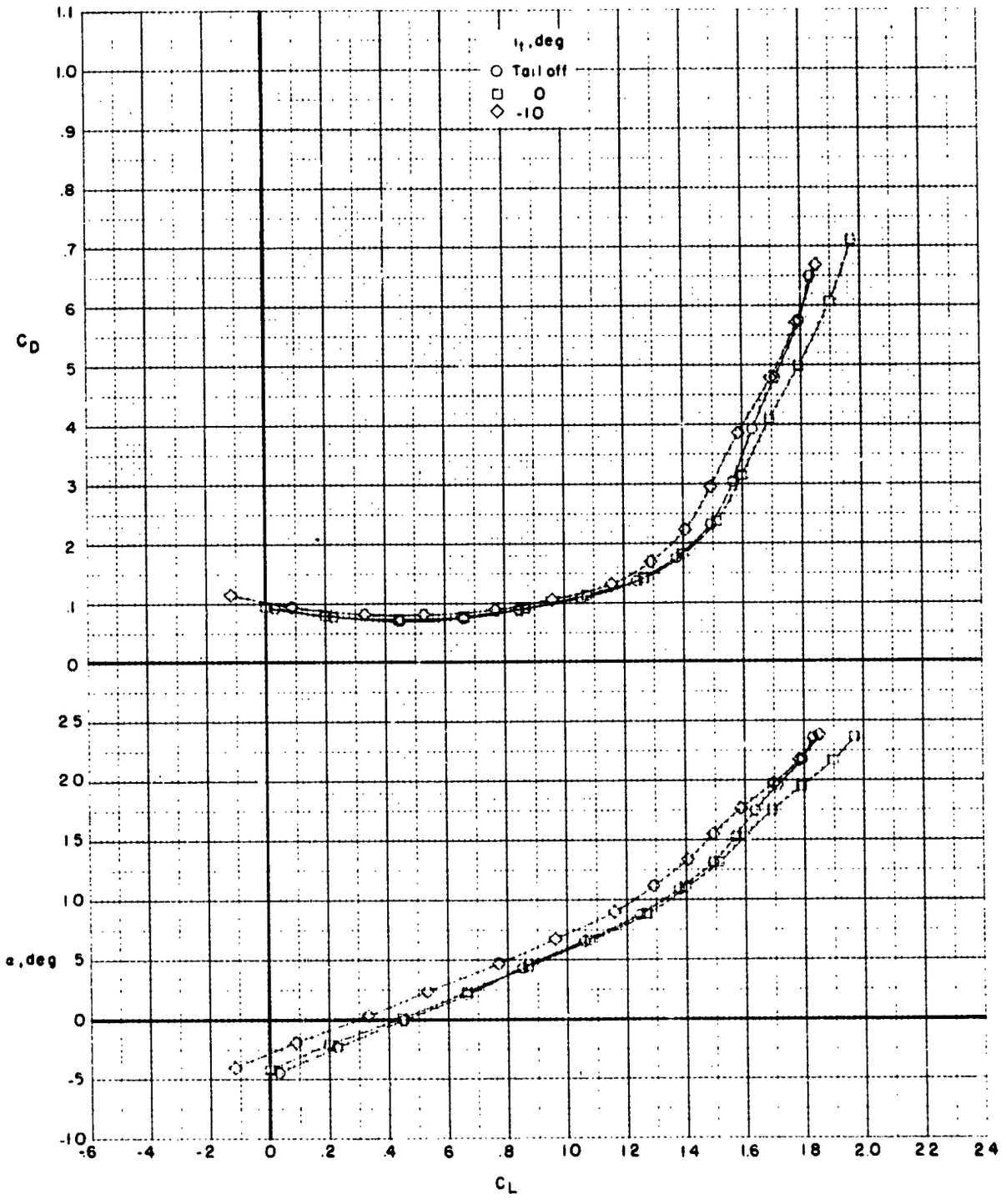

(b) δ_f = 15°/nested.

Figure 11.- Continued.

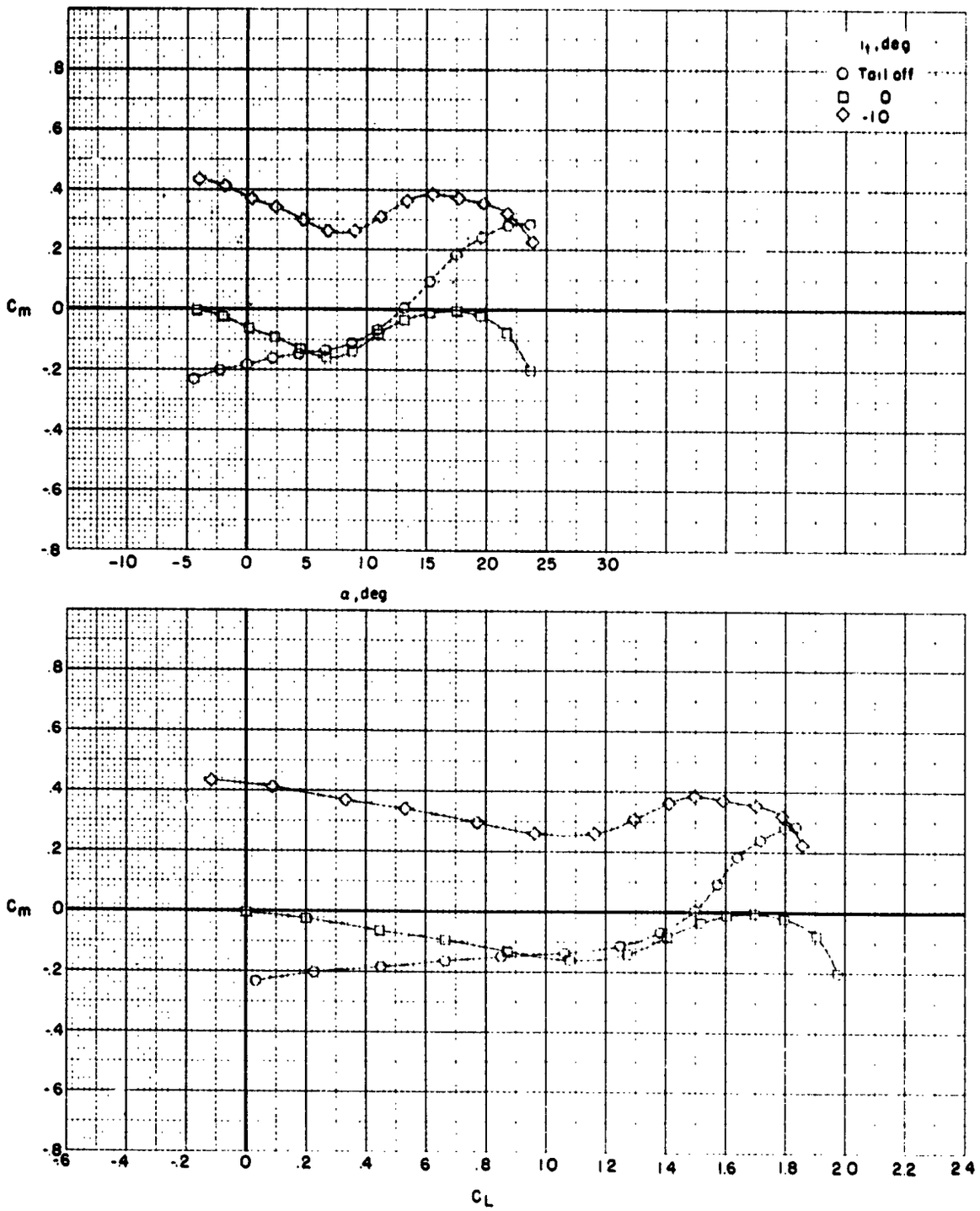

(b) C ncluded.

Figure 11.- Continued.

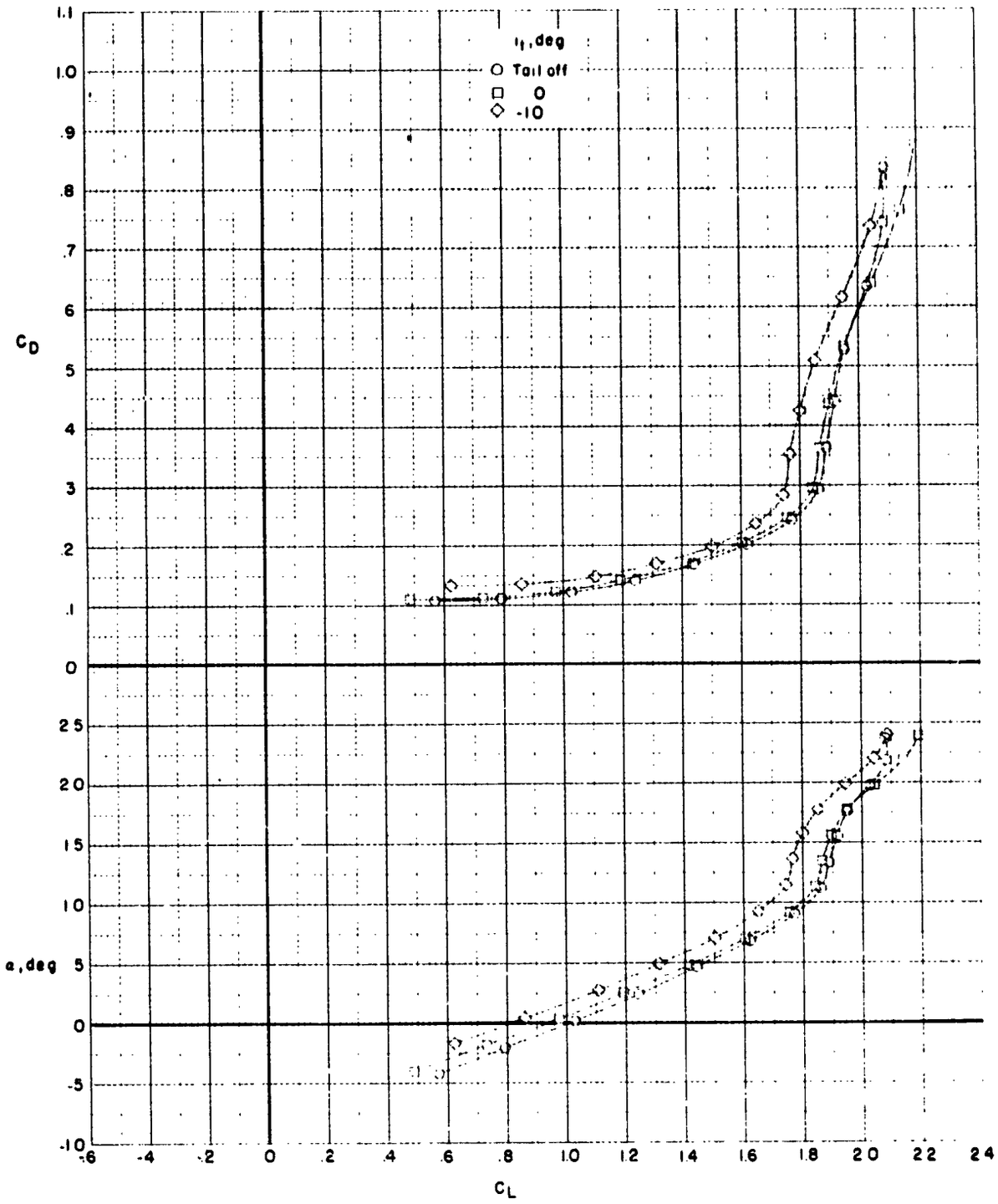

(c) $\delta_f = 22^o/32^o$.

Figure 11.- Continued.

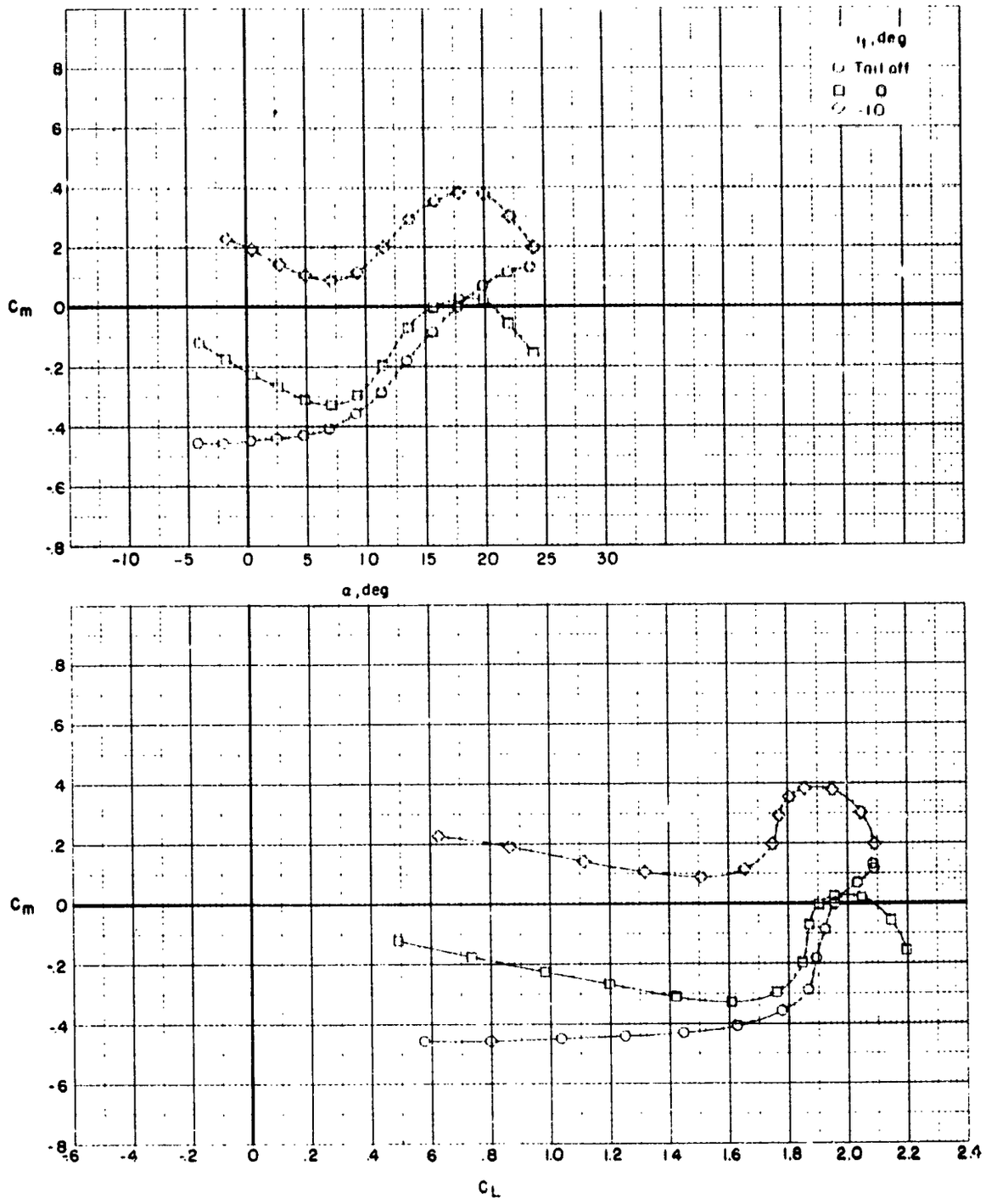

(c) Concluded.

Figure 11.- Continued.

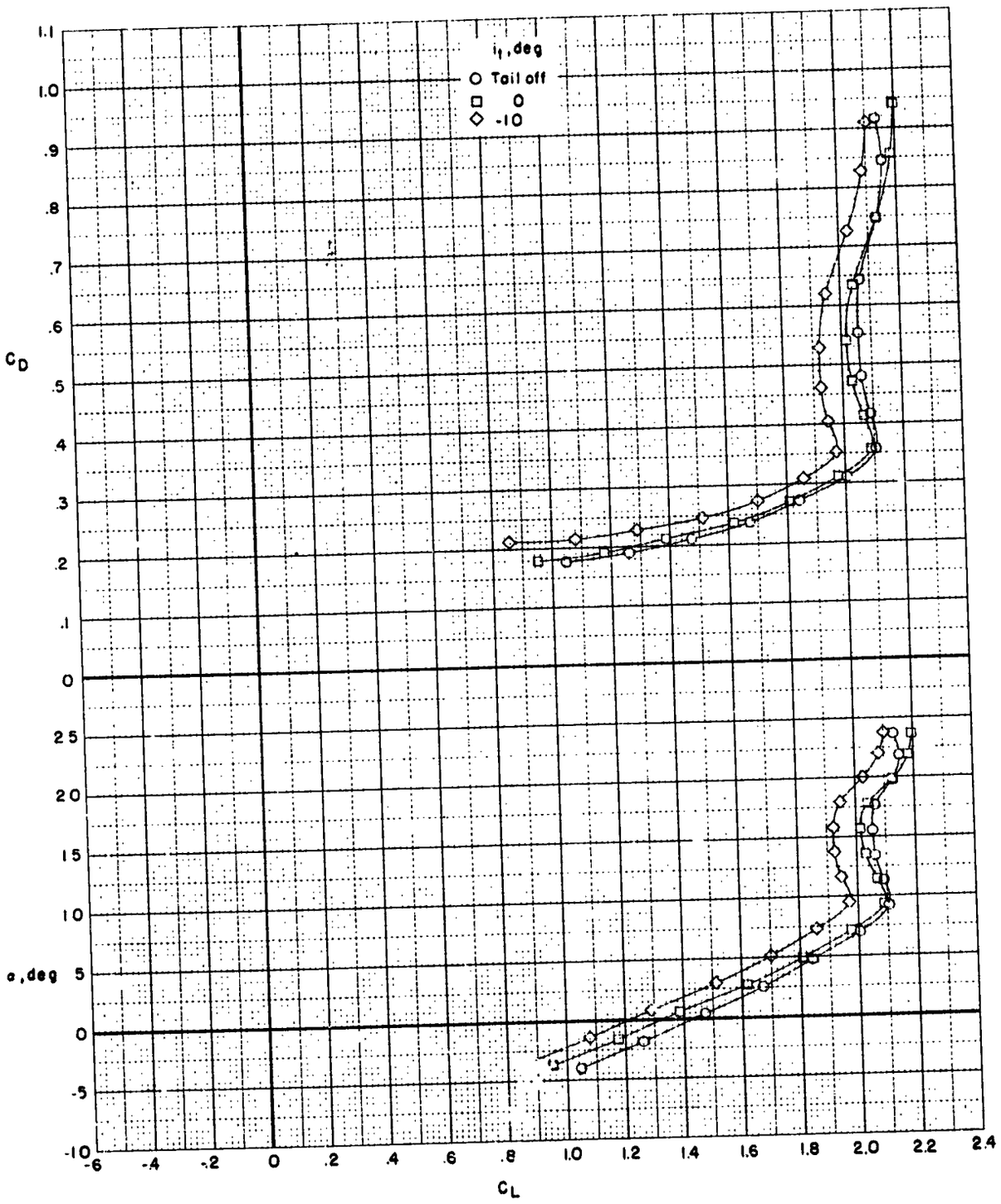

(d) $\delta_f = 30^o/55^o$.

Figure 11.- Continued.

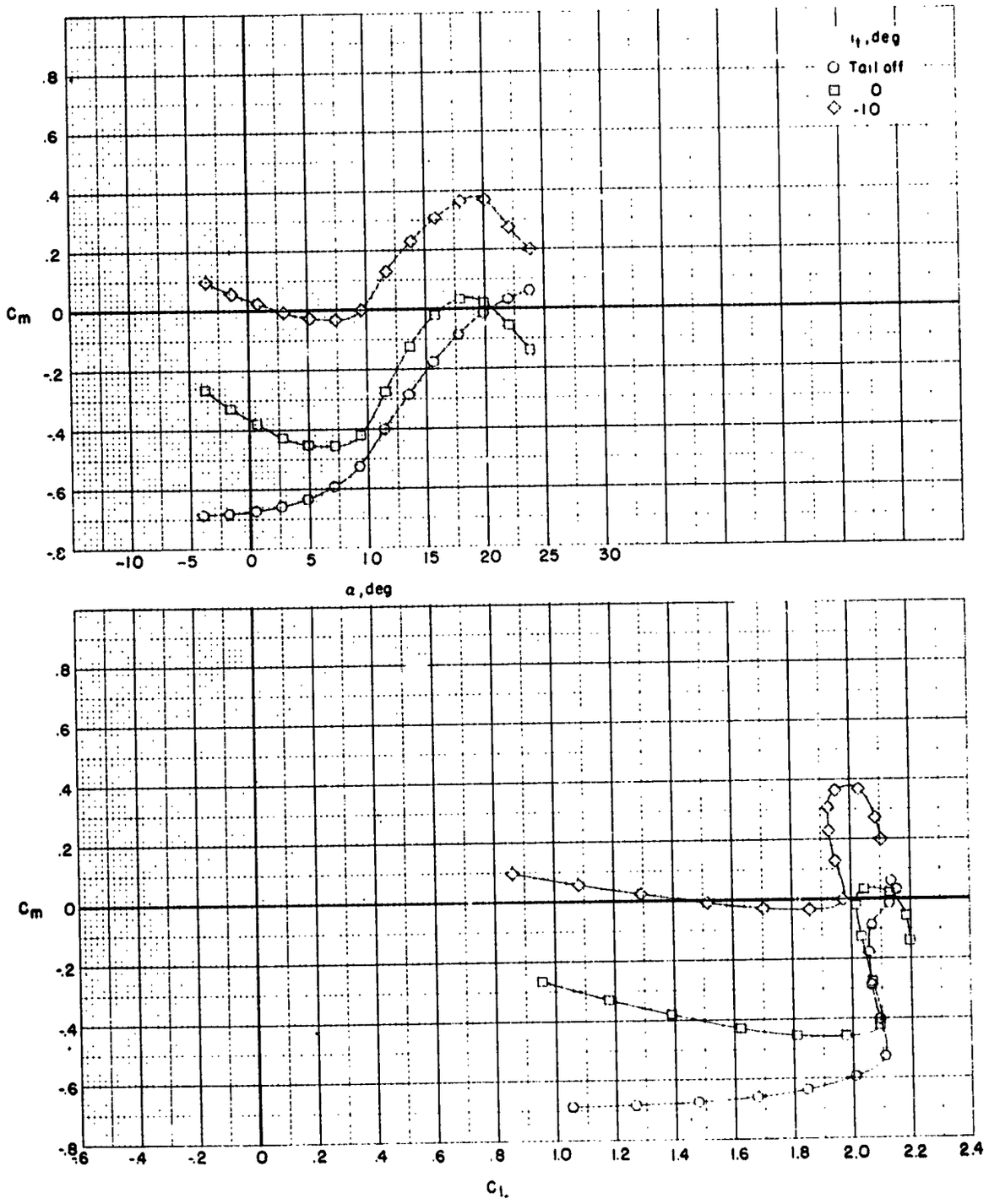

(d) Concluded.

Figure 11.- Concluded.

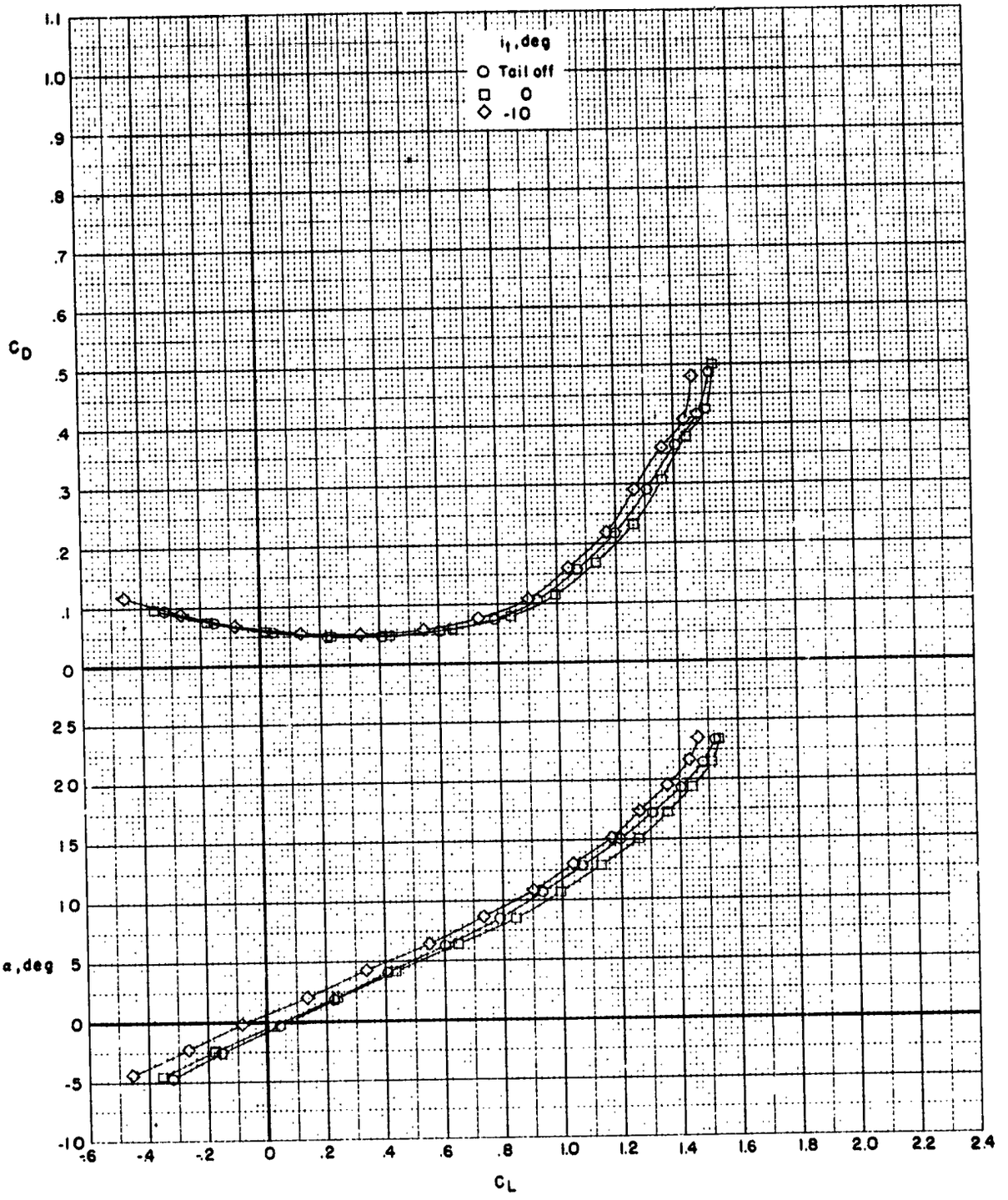

(a) $\delta_f = 0^o$.

Figure 12.- Effect of horizontal-tail deflection on longitudinal aerodynamic characteristics with various trailing-edge flap deflections and $\delta_K = 45^o$. T-tail.

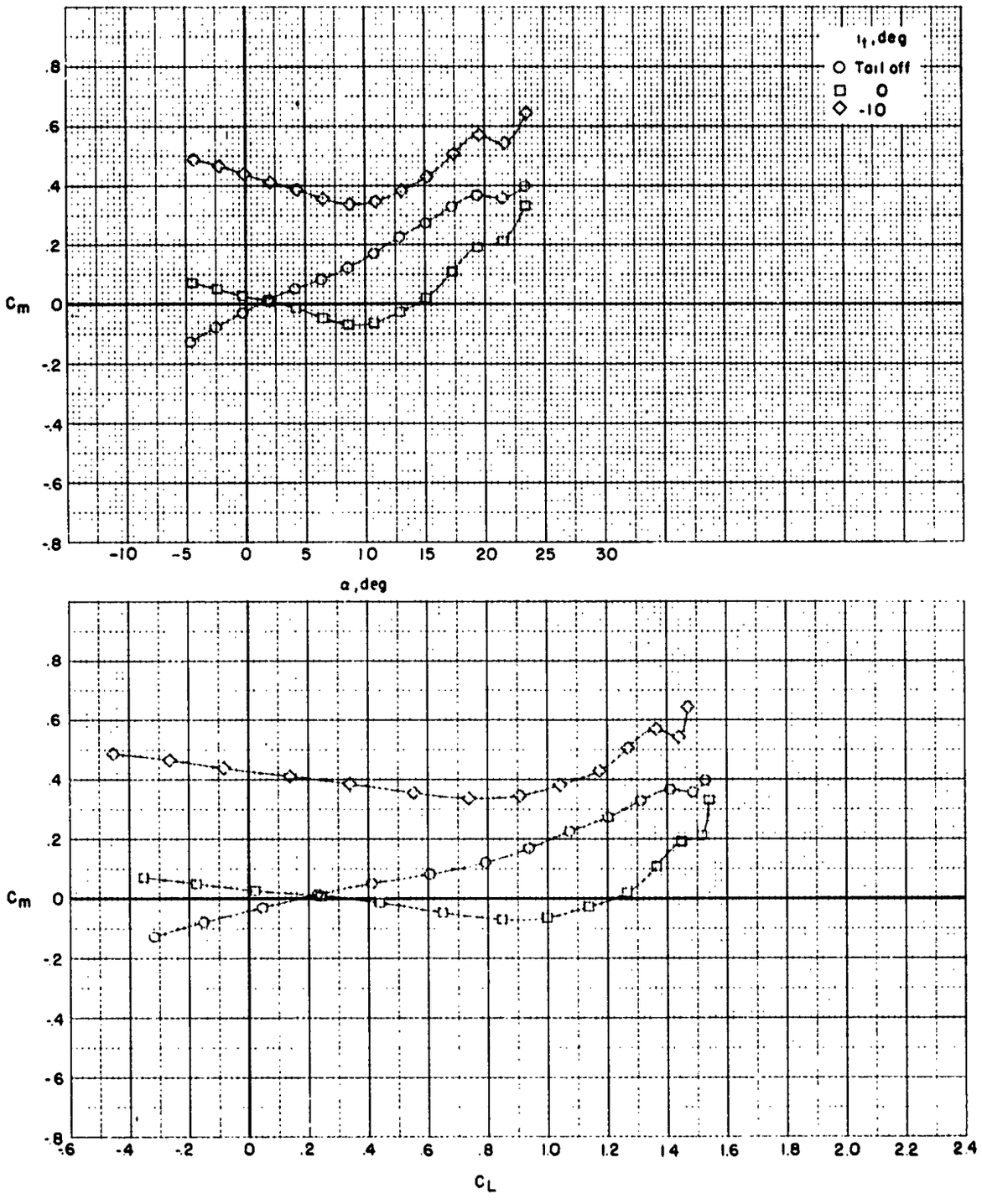

(a) Concluded.

Figure 12.- Continued.

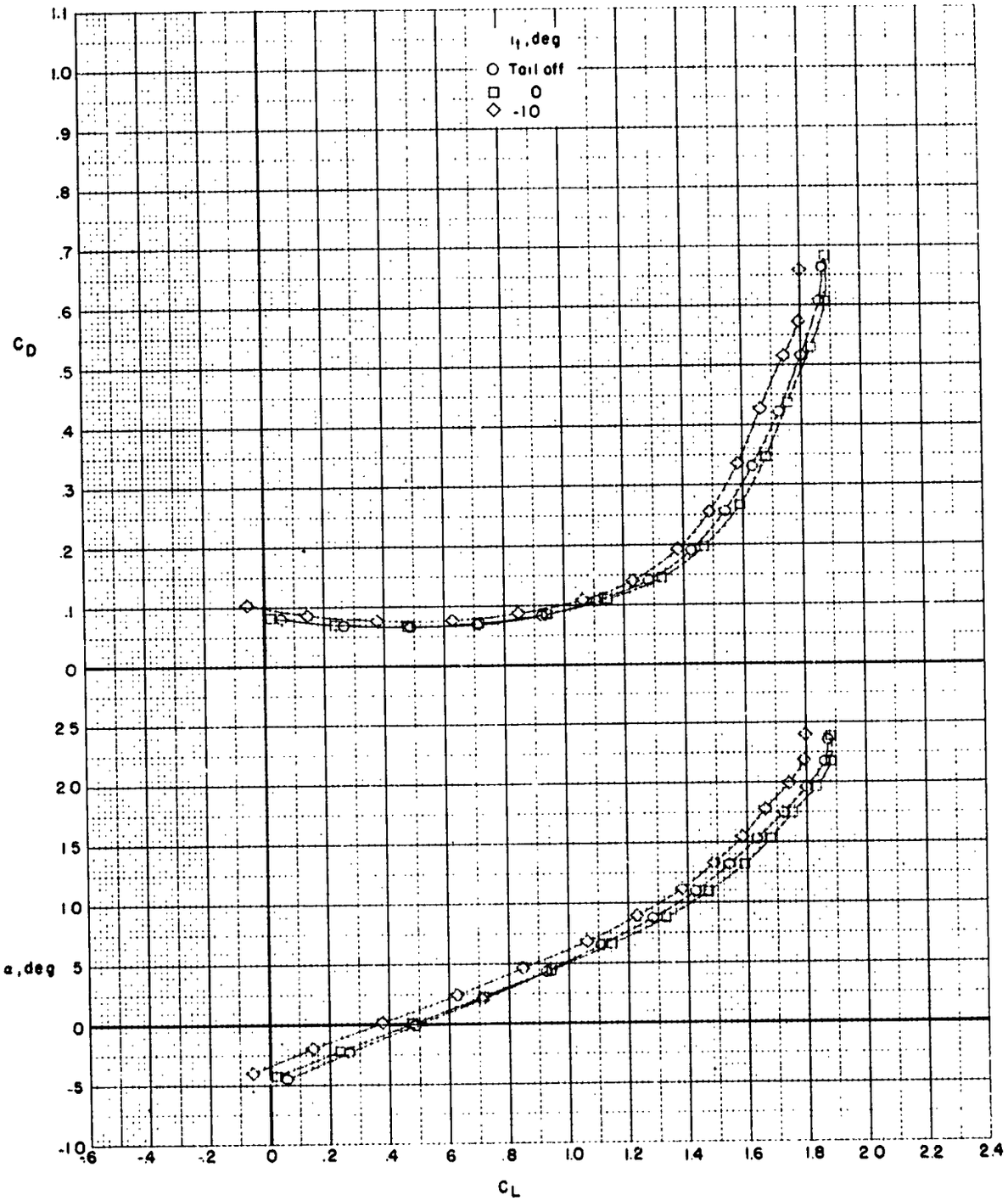

(b) $\delta_f = 15^o$/nested.

Figure 12.- Continued.

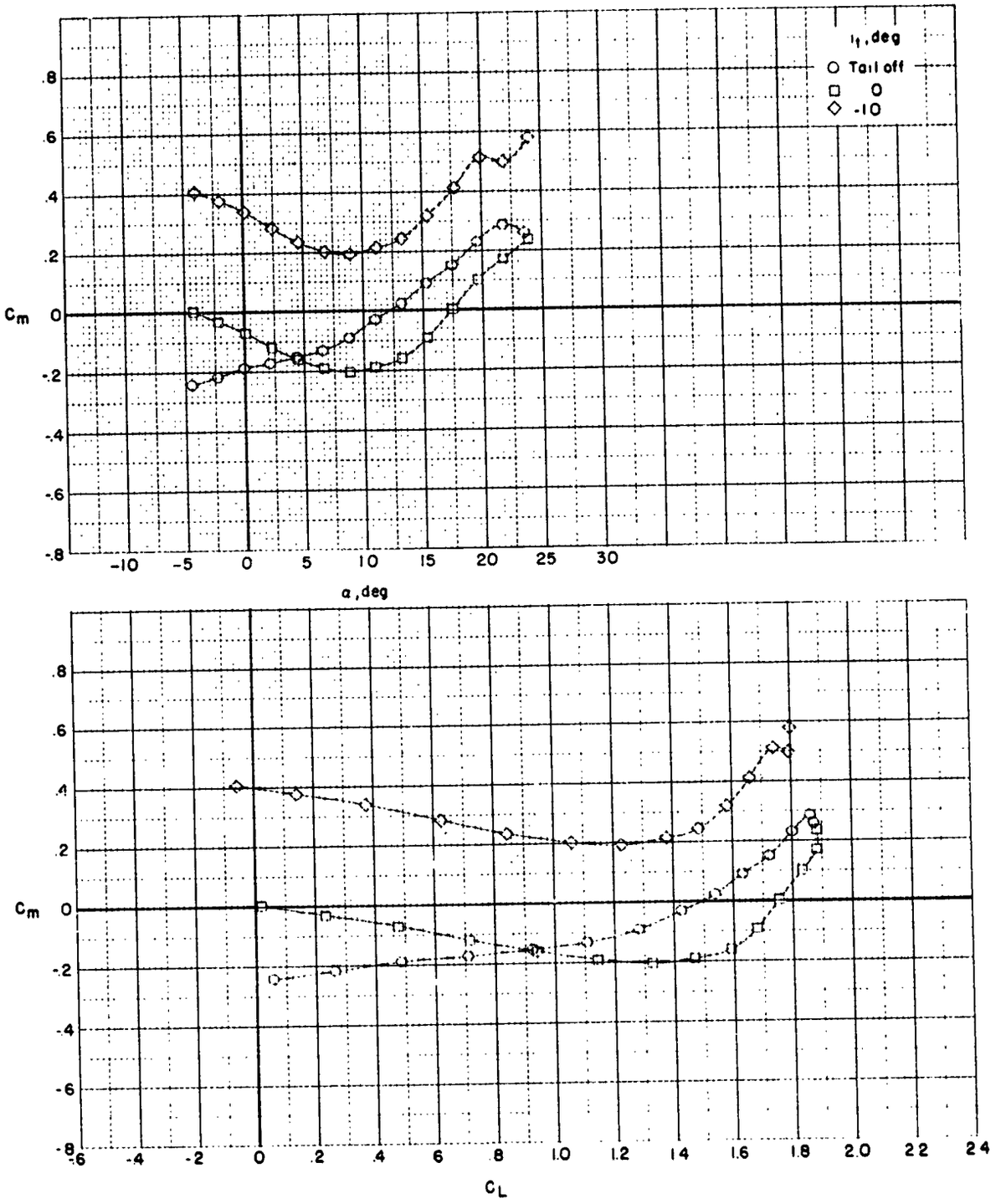

(b) Concluded.

Figure 12.- Continued.

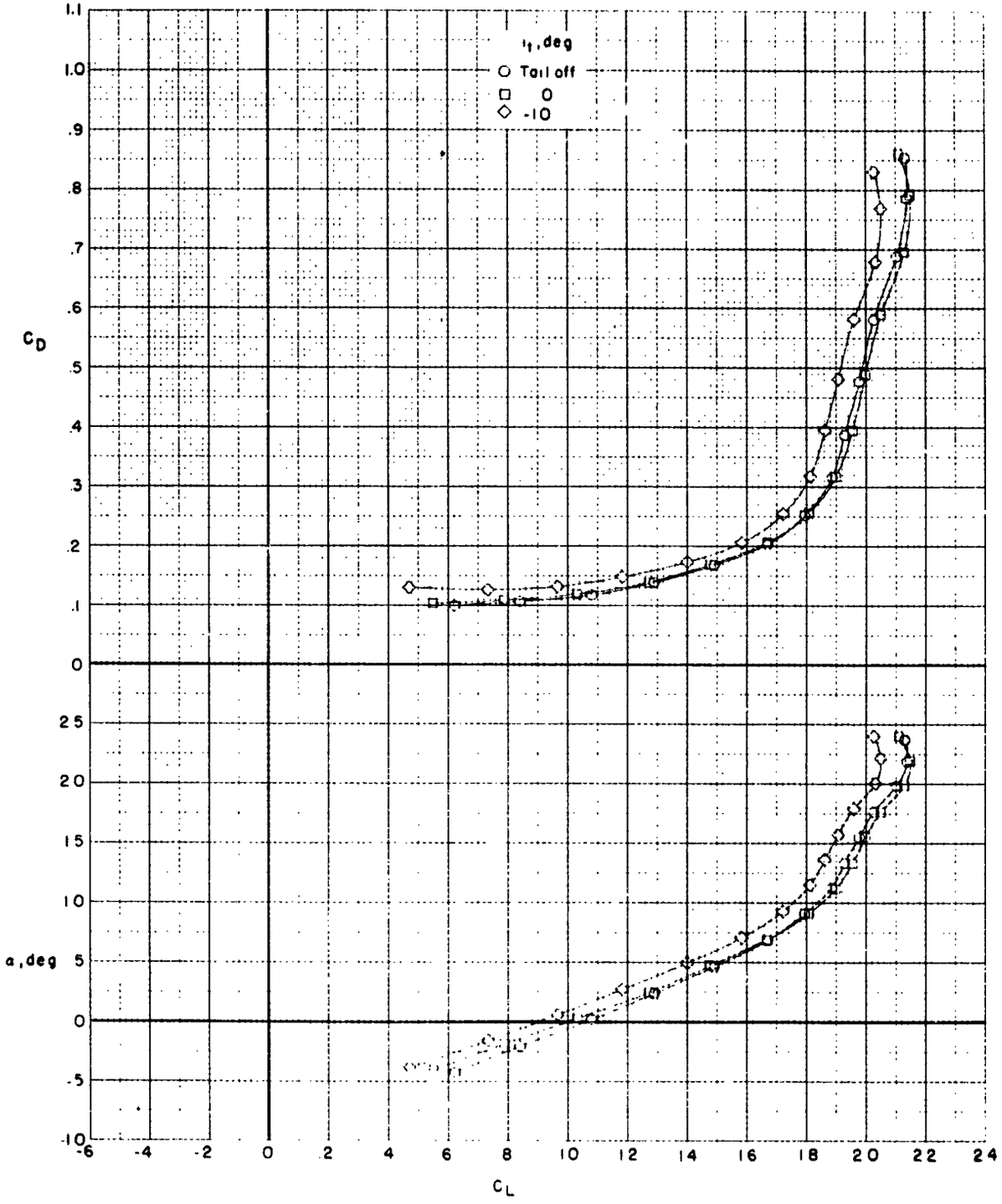

(c) $\delta_f = 22^o/32^o$.

Figure 12.- Continued.

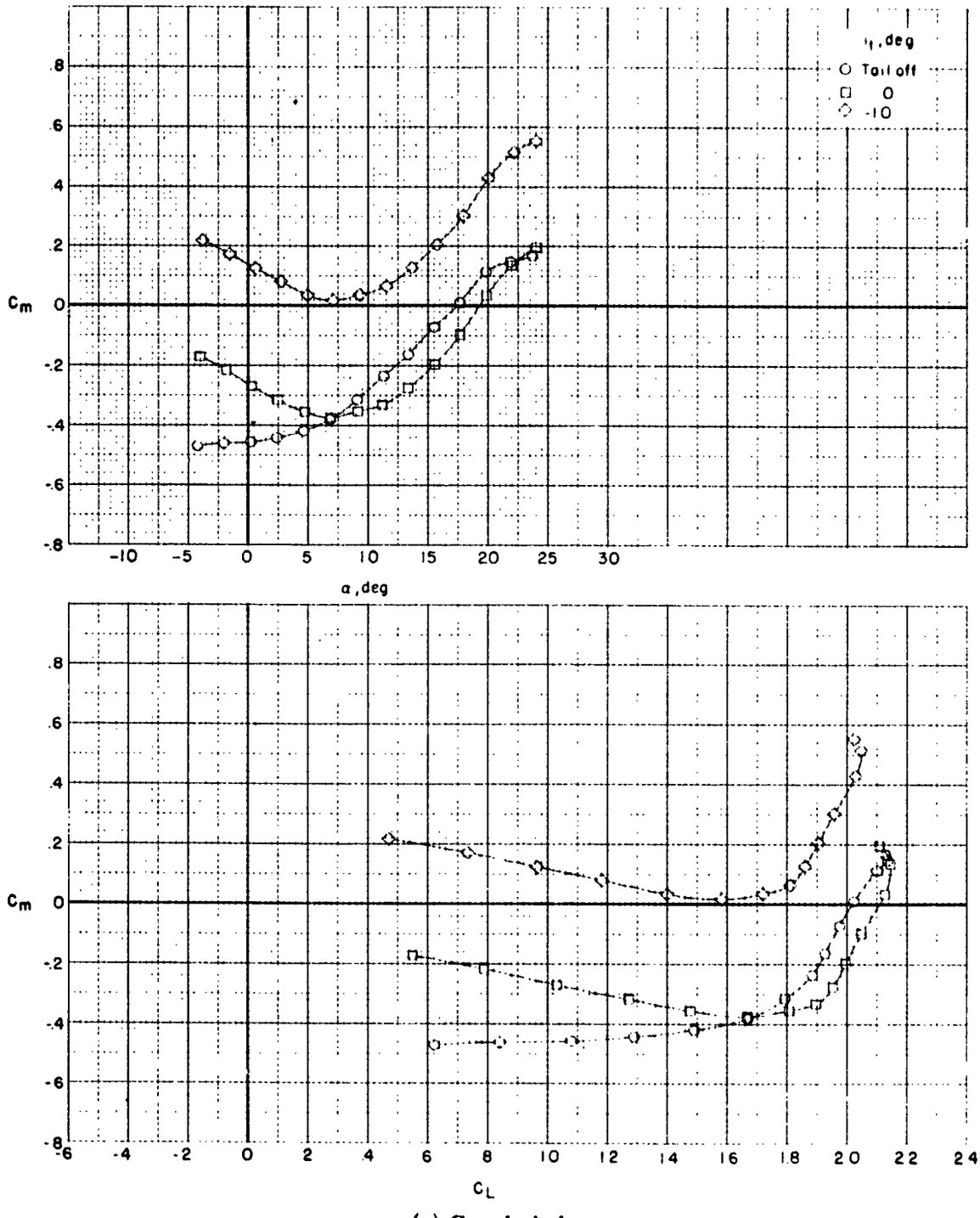

(c) Concluded.

Figure 12.- Continued.

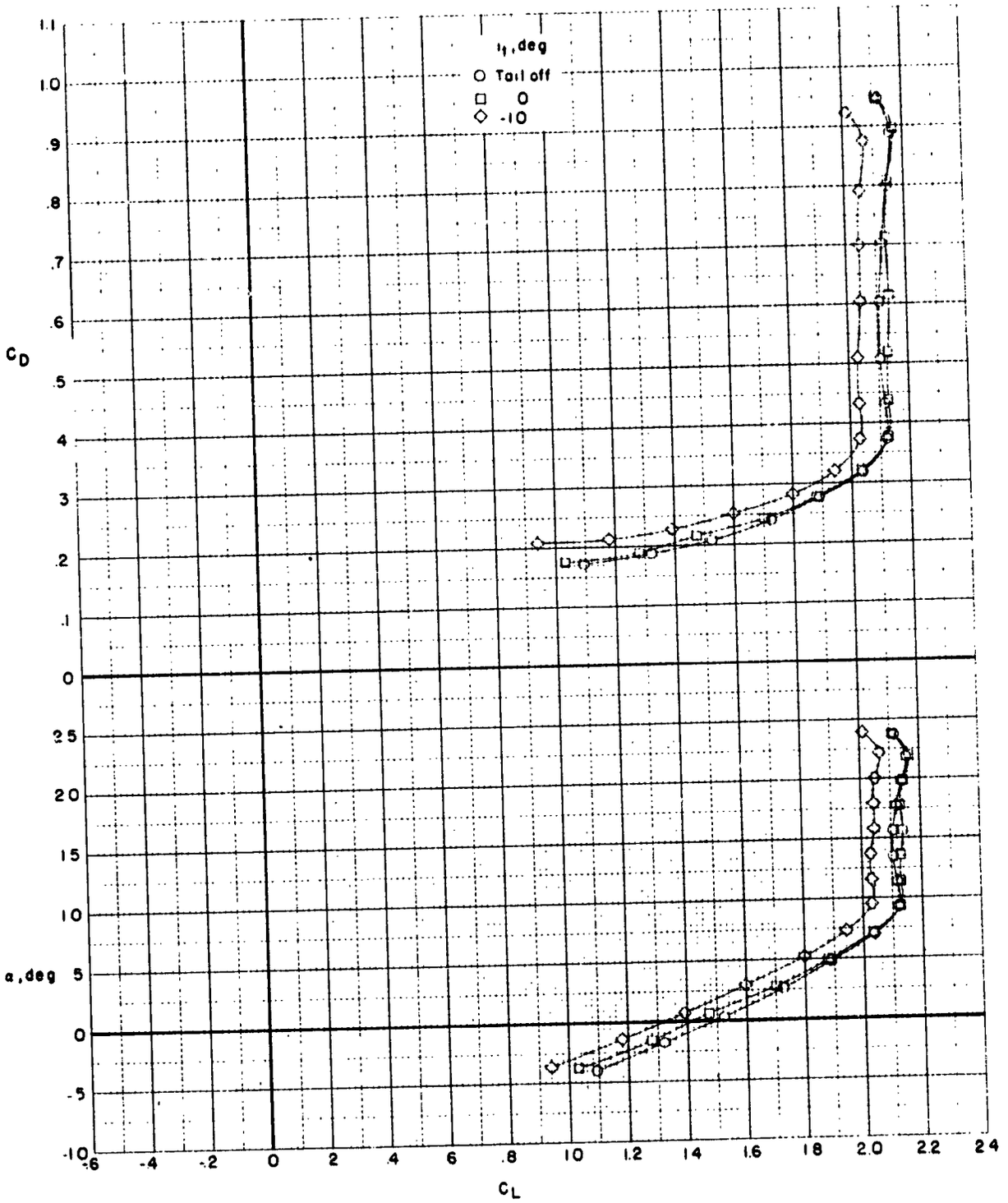

(d) $\delta_f = 30^o/55^o$.

Figure 12.- Continued.

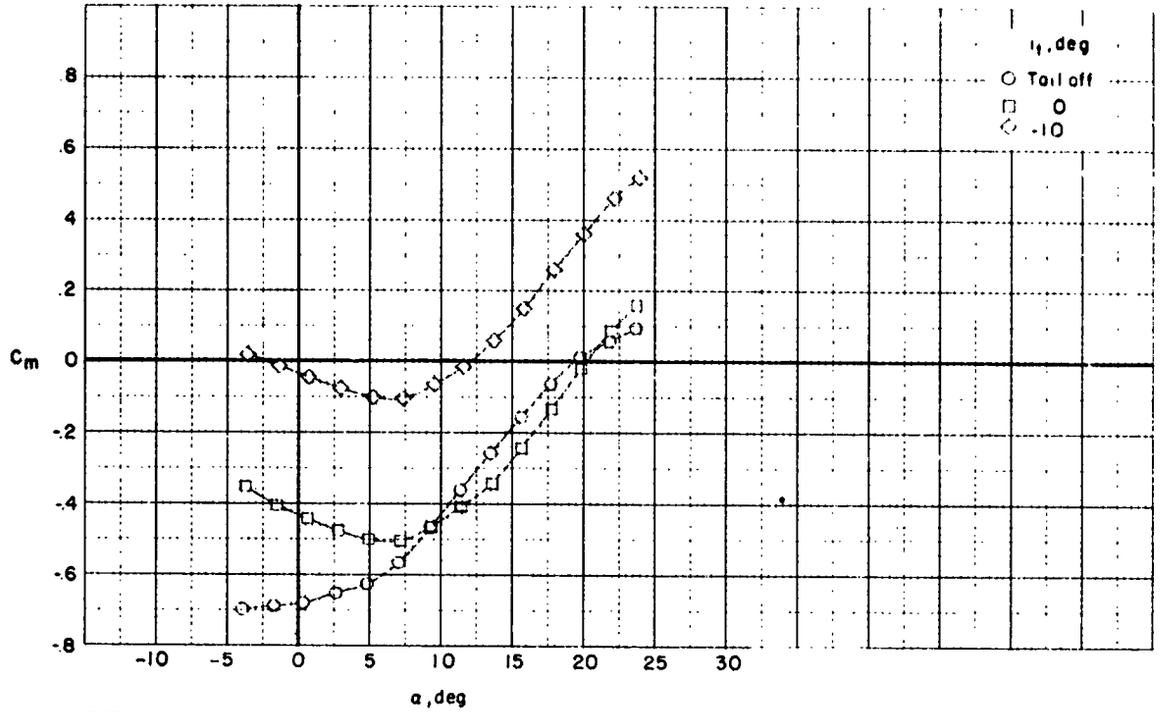

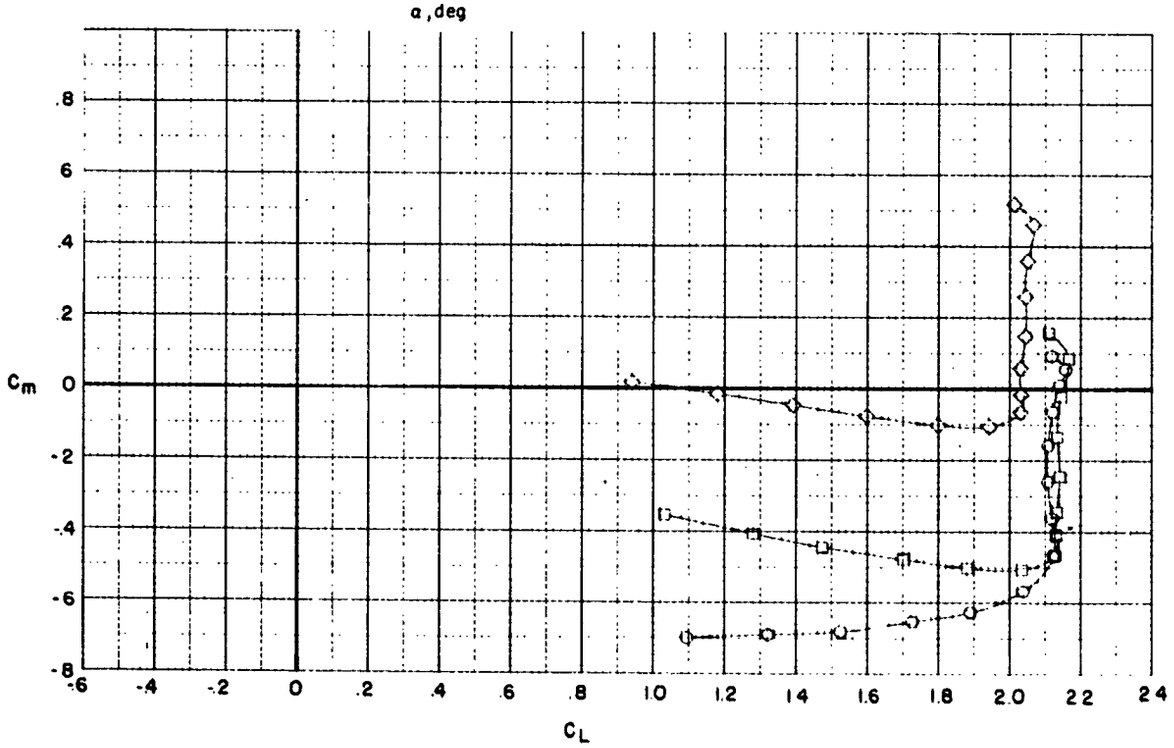

(d) Concluded.

Figure 12.- Concluded.

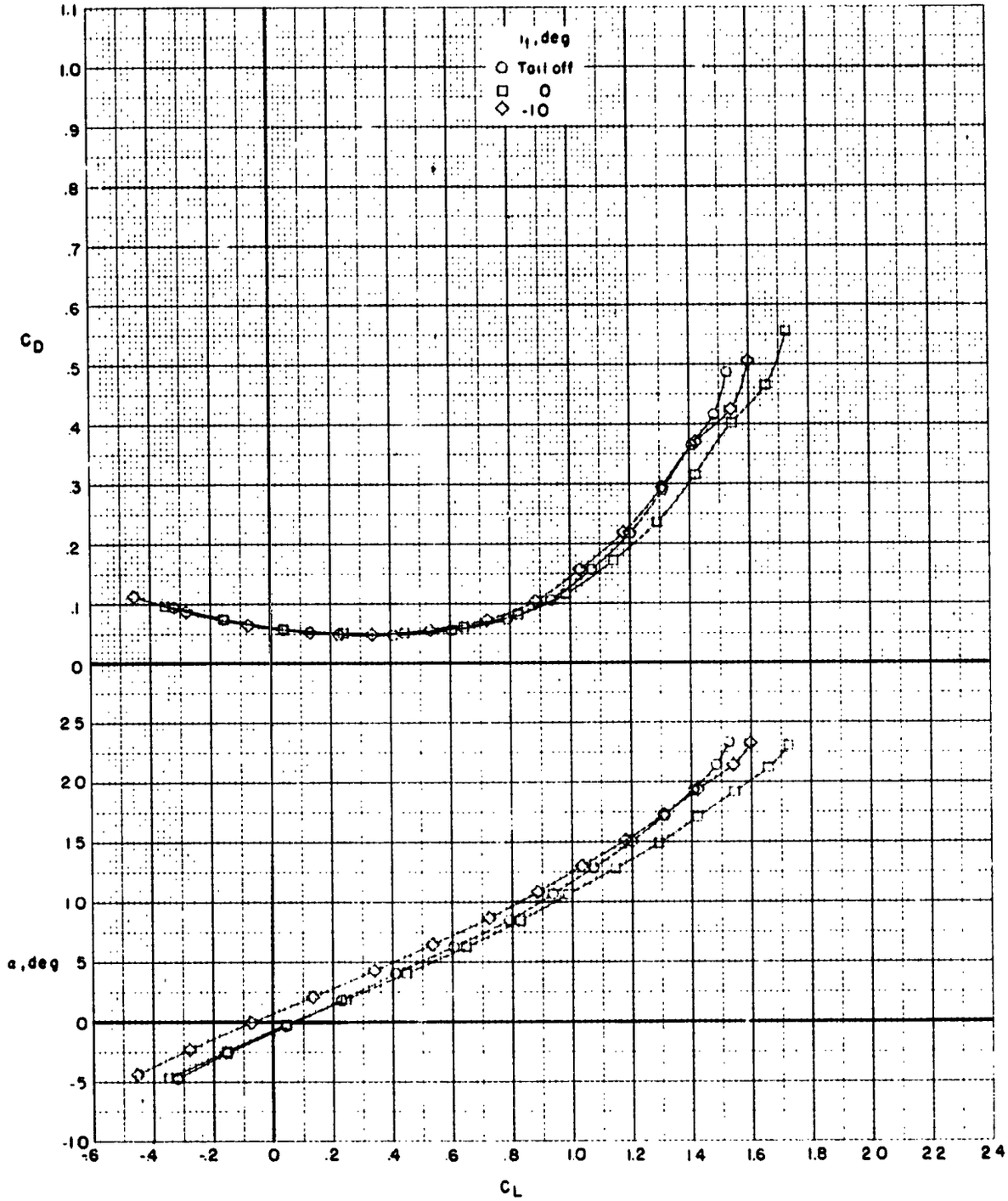

(a) $\delta_f = 0^o$.

Figure 13.- Effect of horizontal-tail deflection on longitudinal aerodynamic characteristics with various trailing-edge flap deflections and $\delta_K = 45^o$. Low tail.

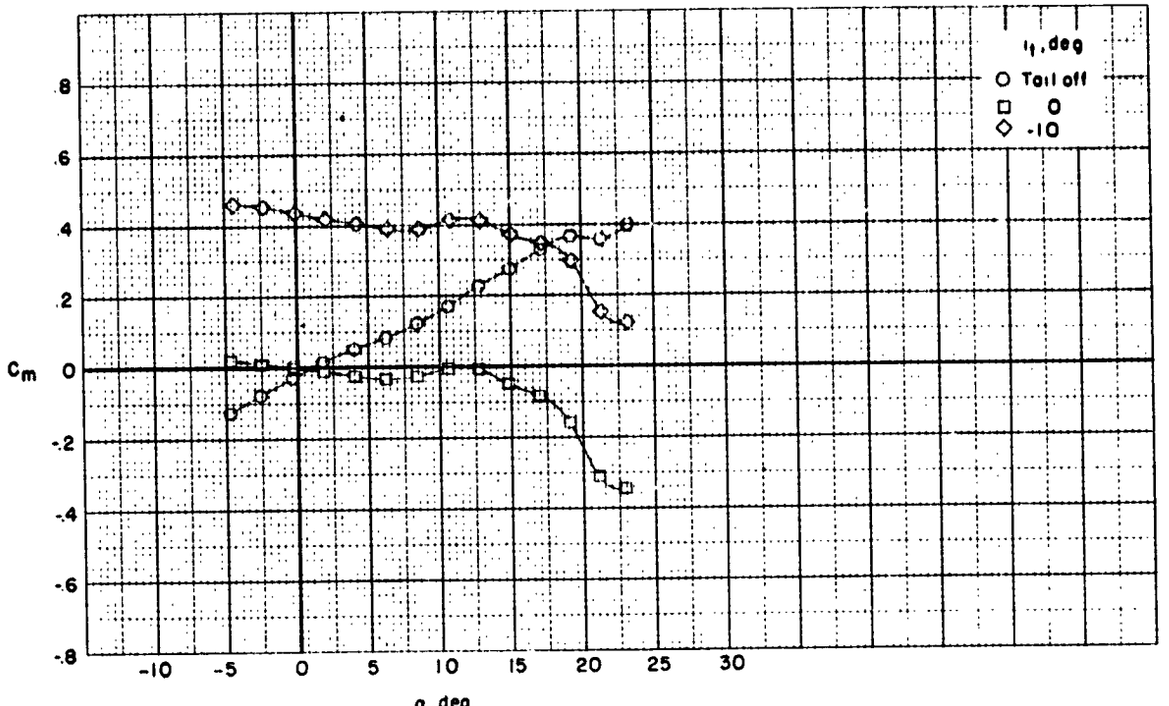

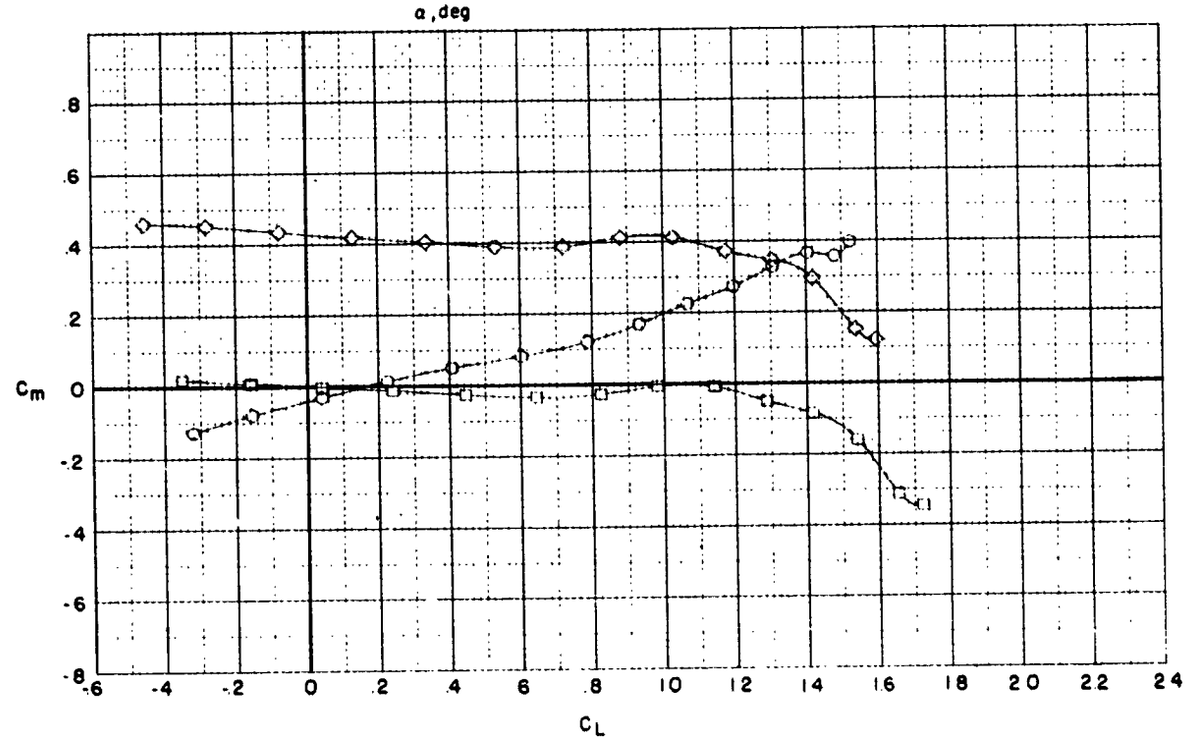

(a) Concluded.

Figure 13.- Continued.

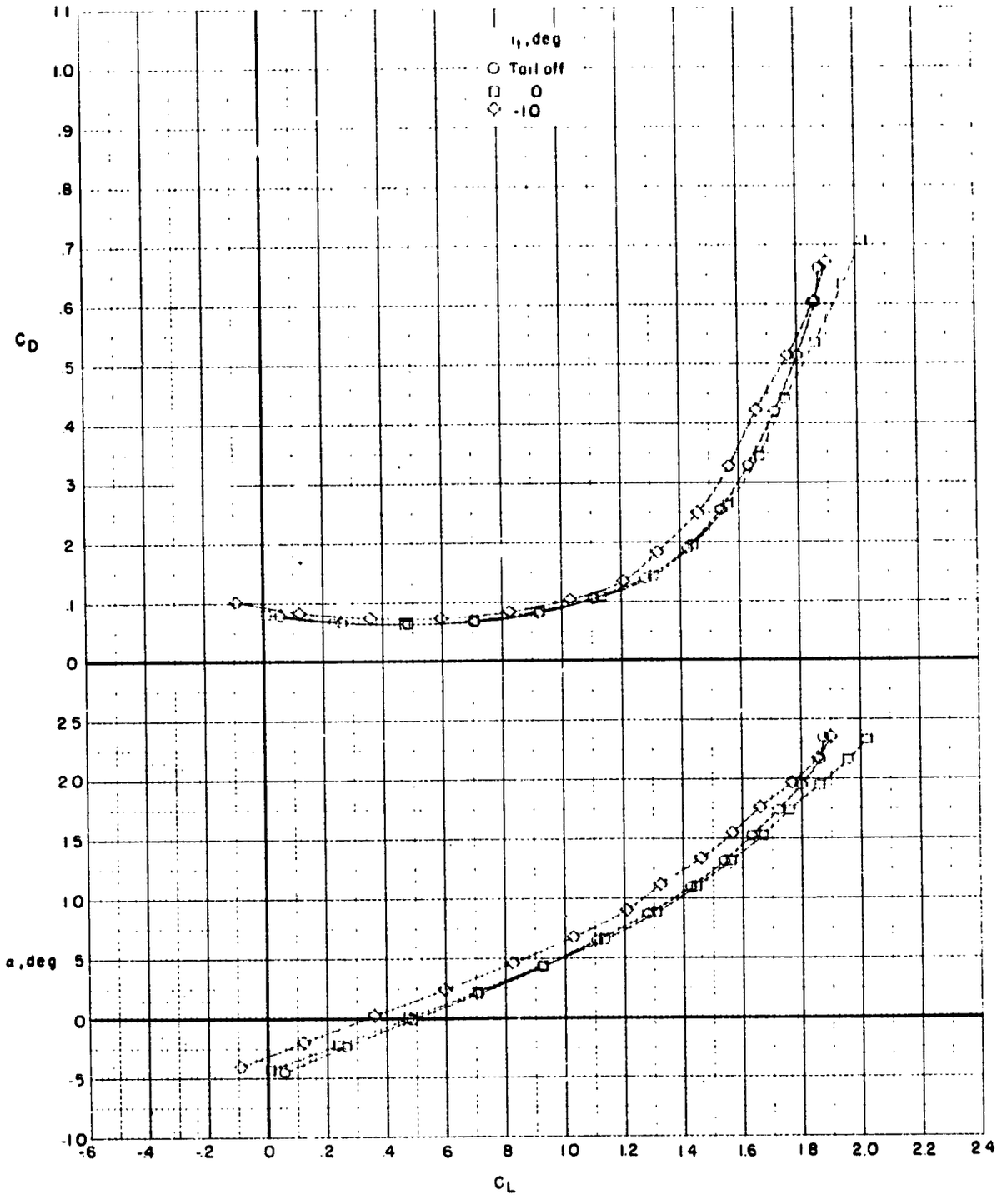

(b) $\delta_f = 15^o$/nested.

Figure 13.- Continued.

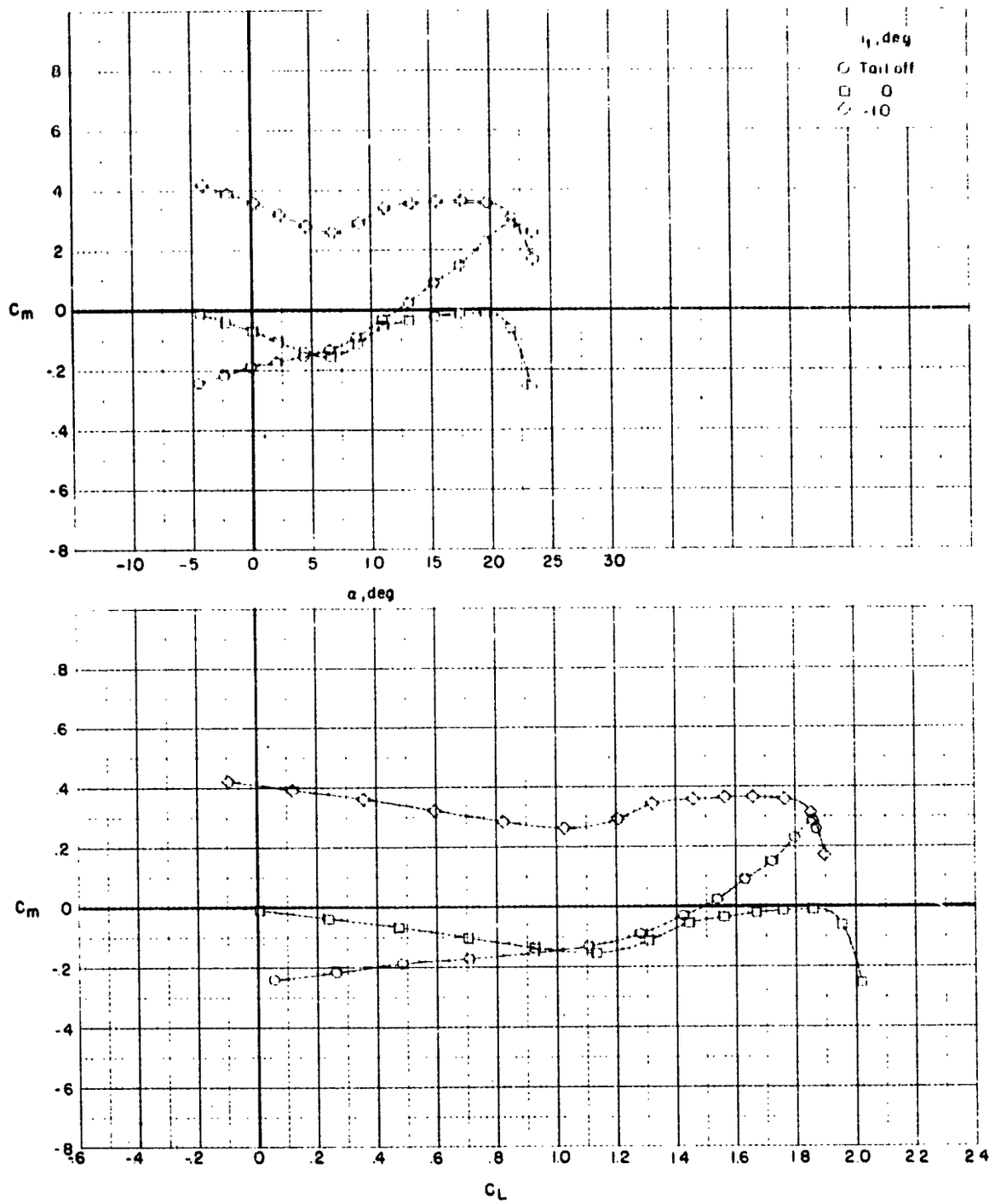

(b) Concluded.

Figure 13.- Continued.

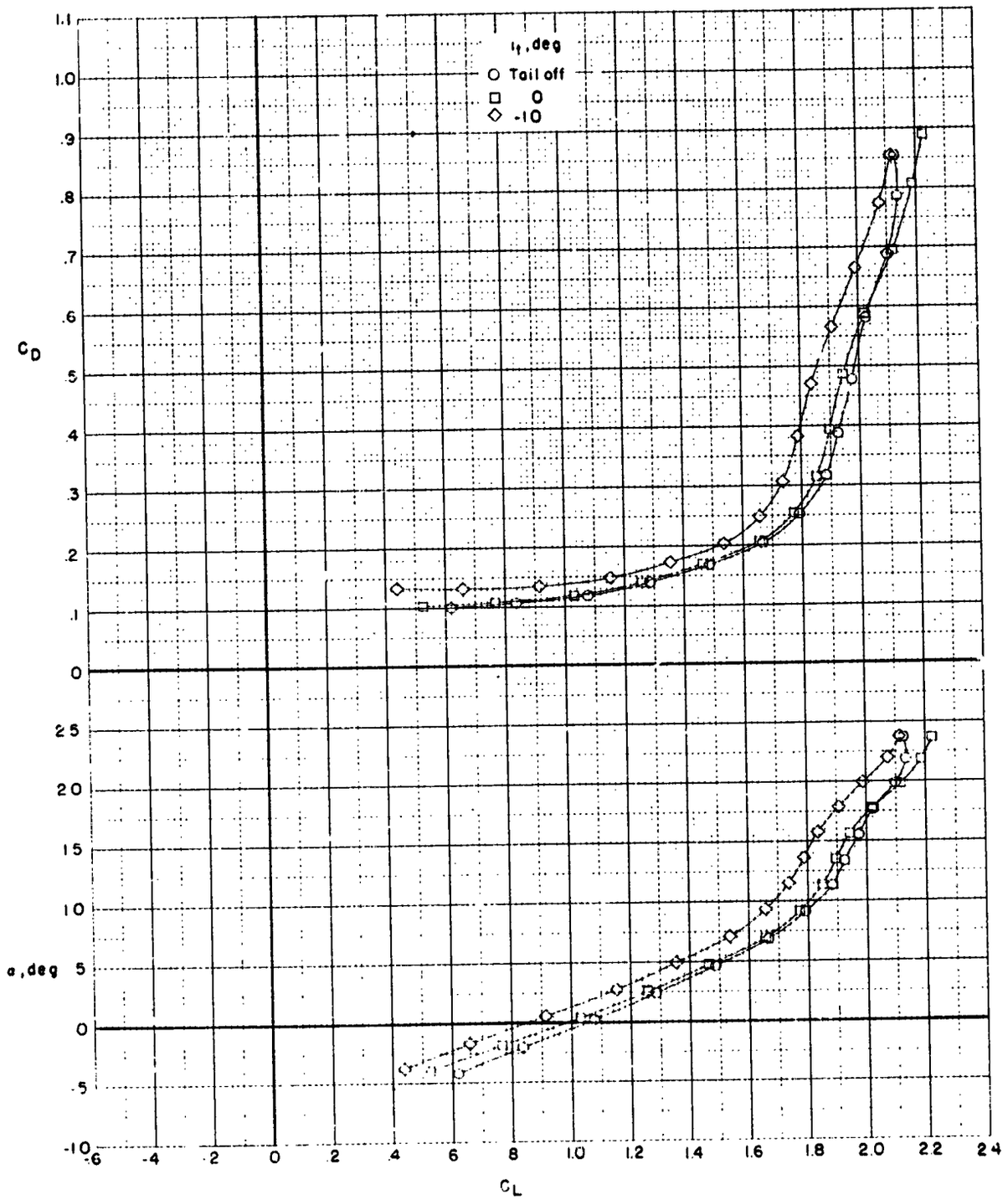

(c) $\delta_f = 22^o/32^o$.

Figure 13.- Continued.

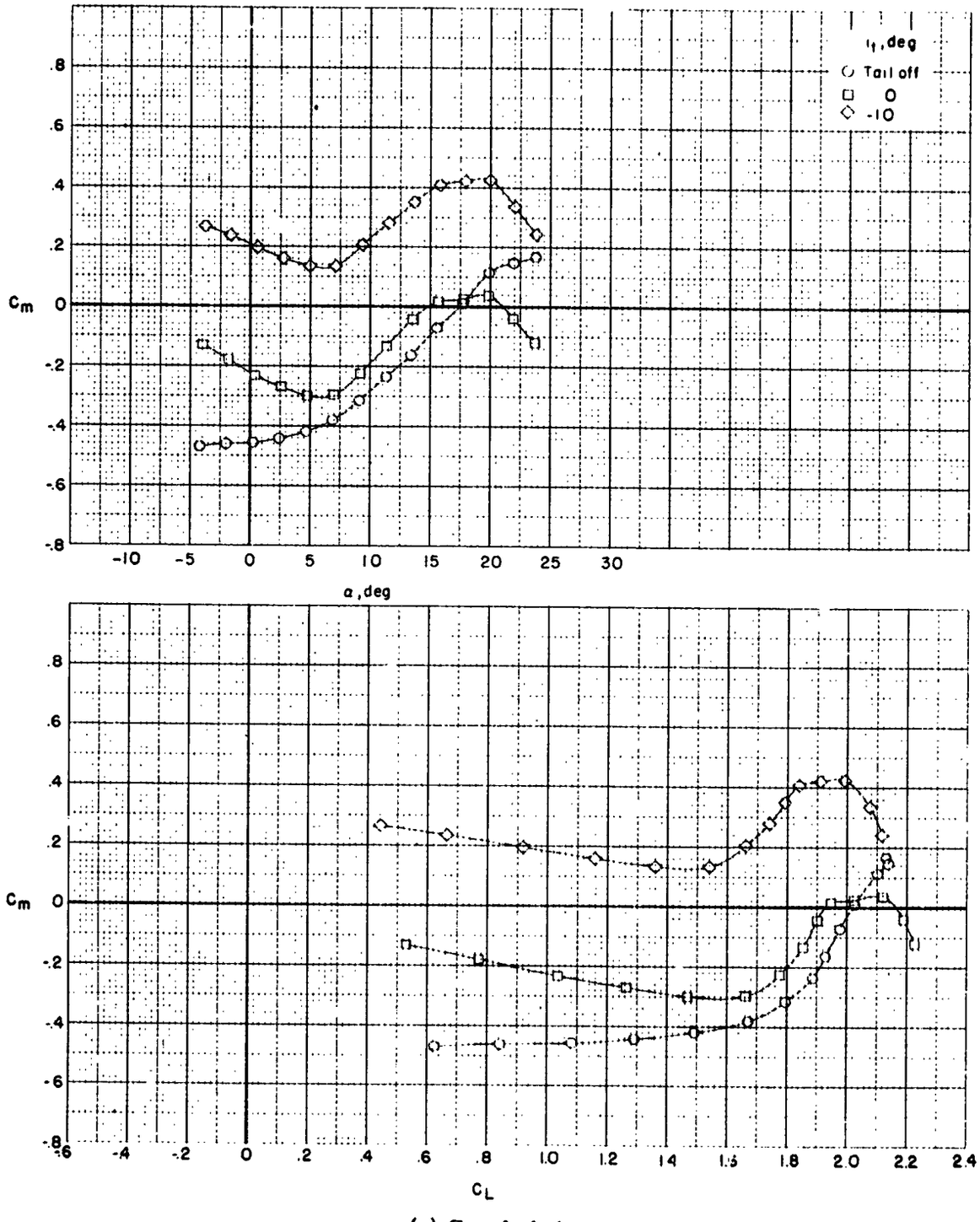

(c) Concluded.

Figure 13.- Continued.

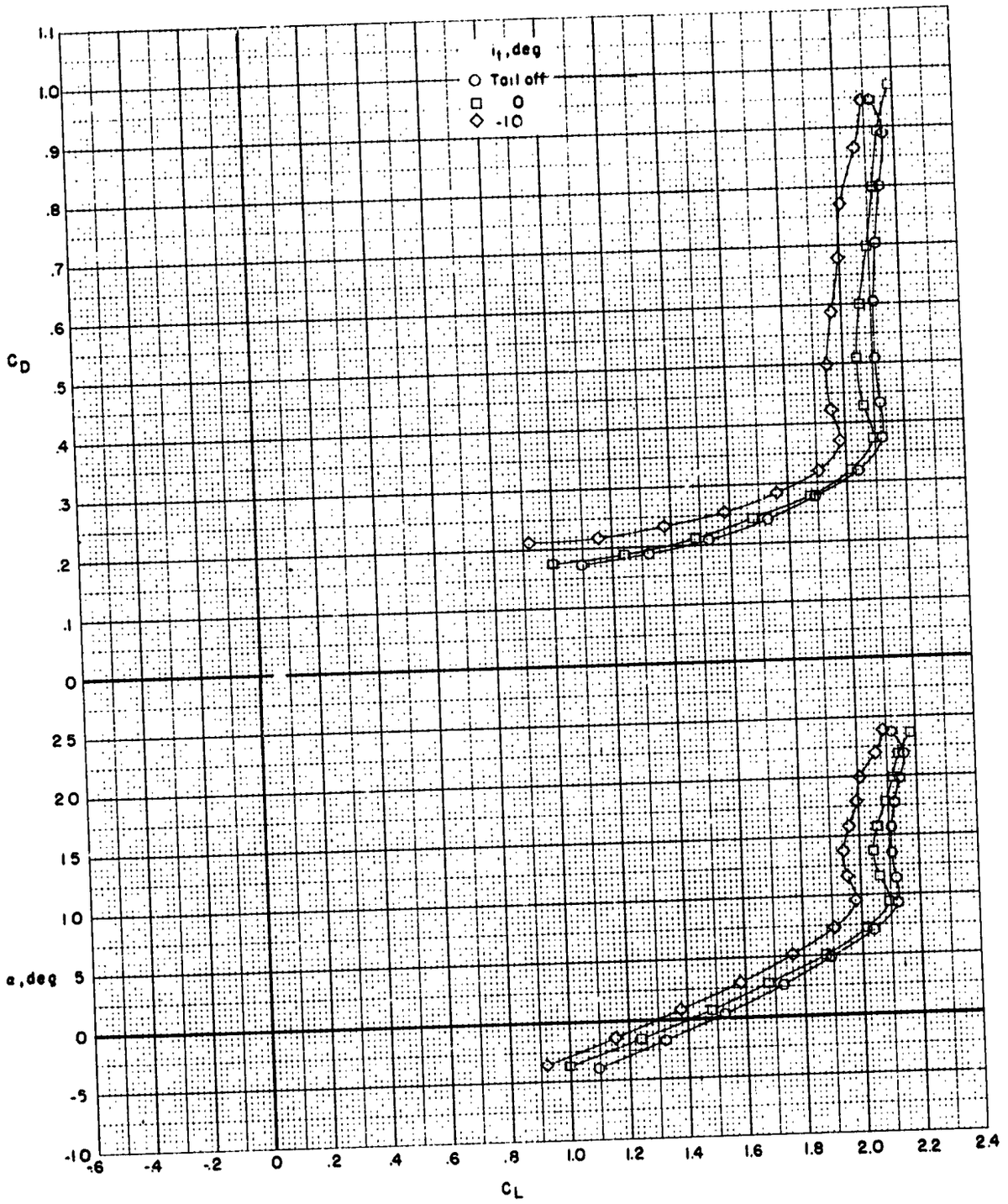

(d) $\delta_f = 30^o/55^o$.

Figure 13.- Continued.

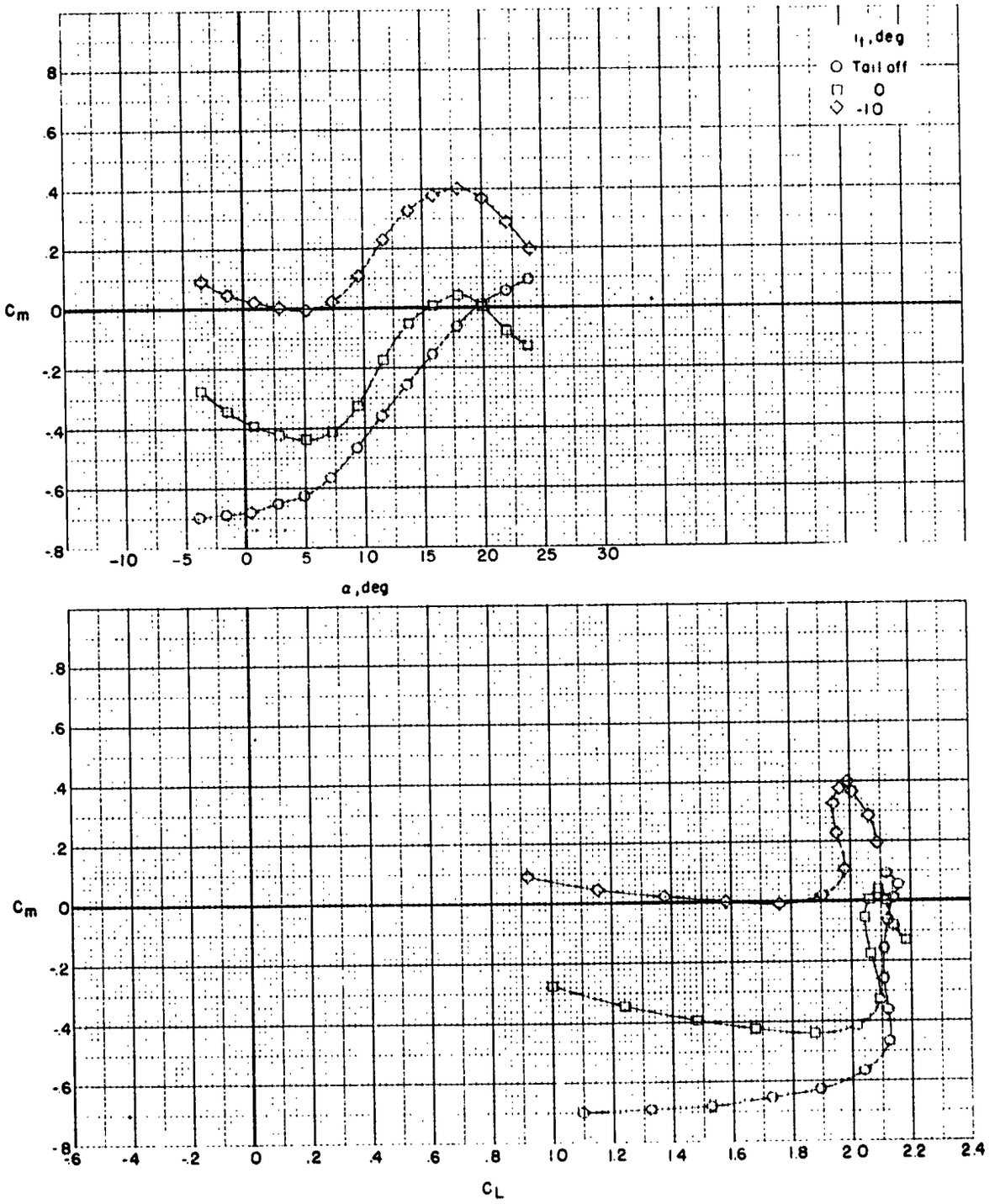

(d) Concluded.

Figure 13.- Concluded.

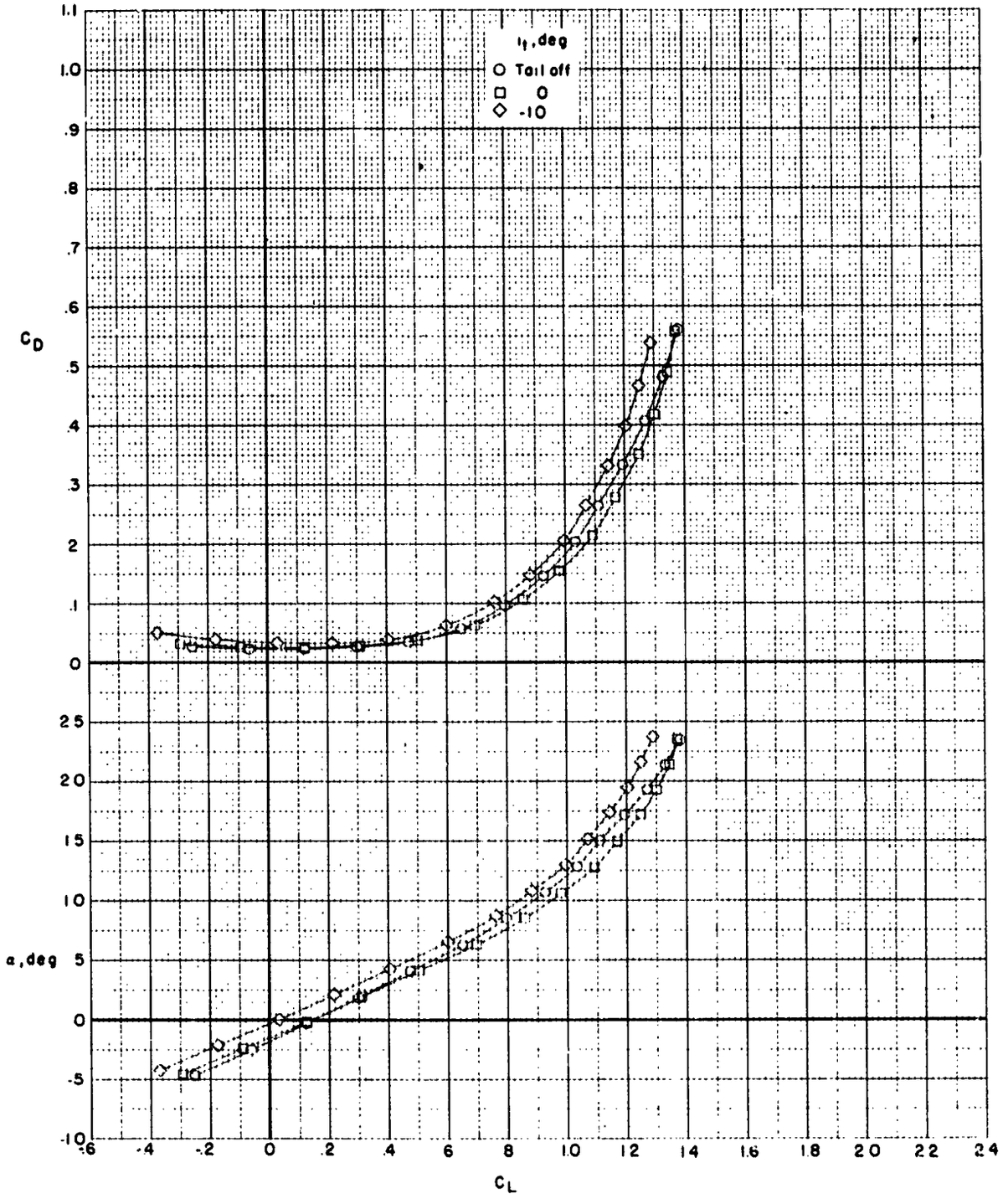

Figure 14.- Effect of horizontal-tail deflection on longitudinal aerodynamic characteristics of clean-wing configuration with T-tail.

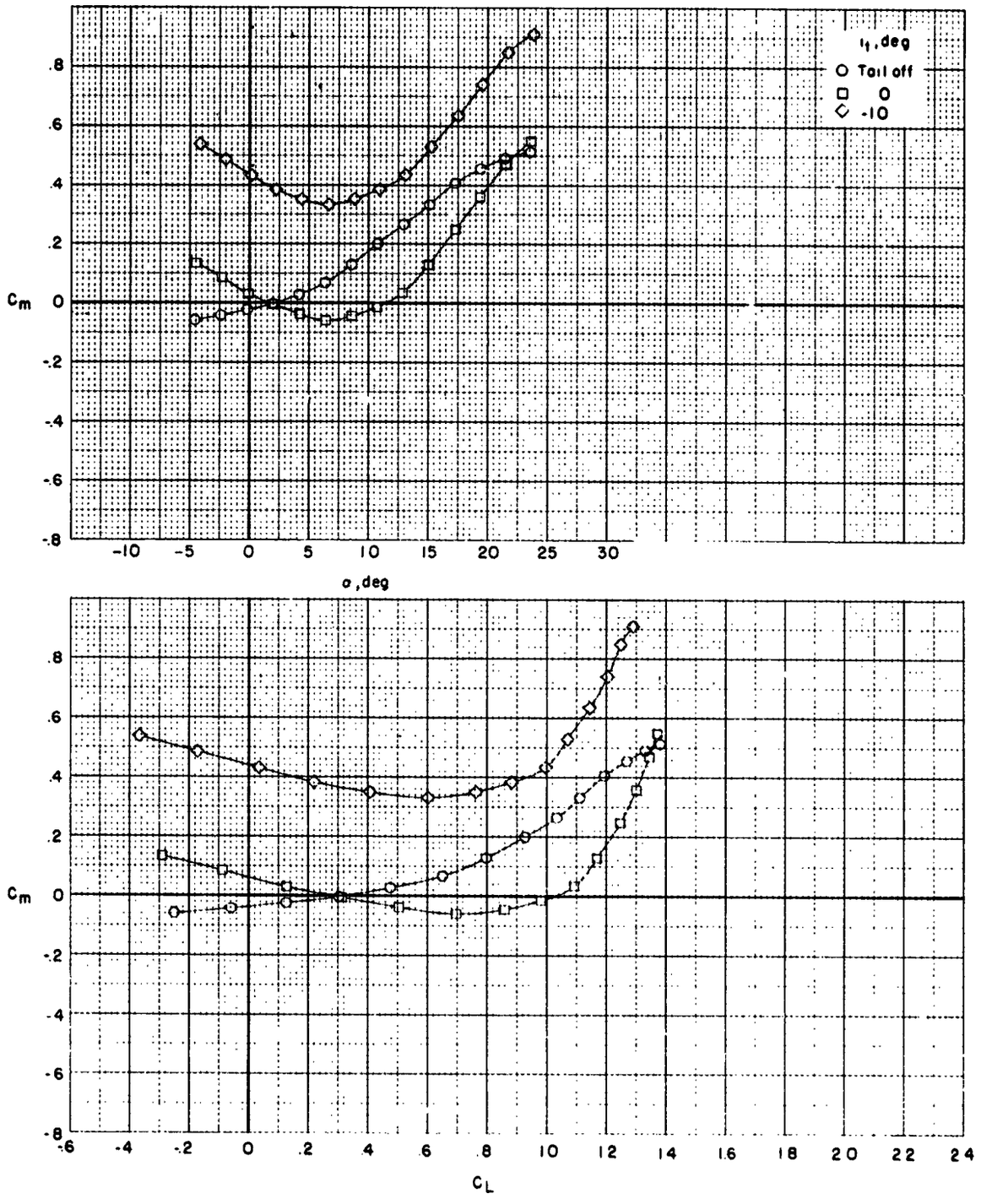

Figure 14.- Concluded.

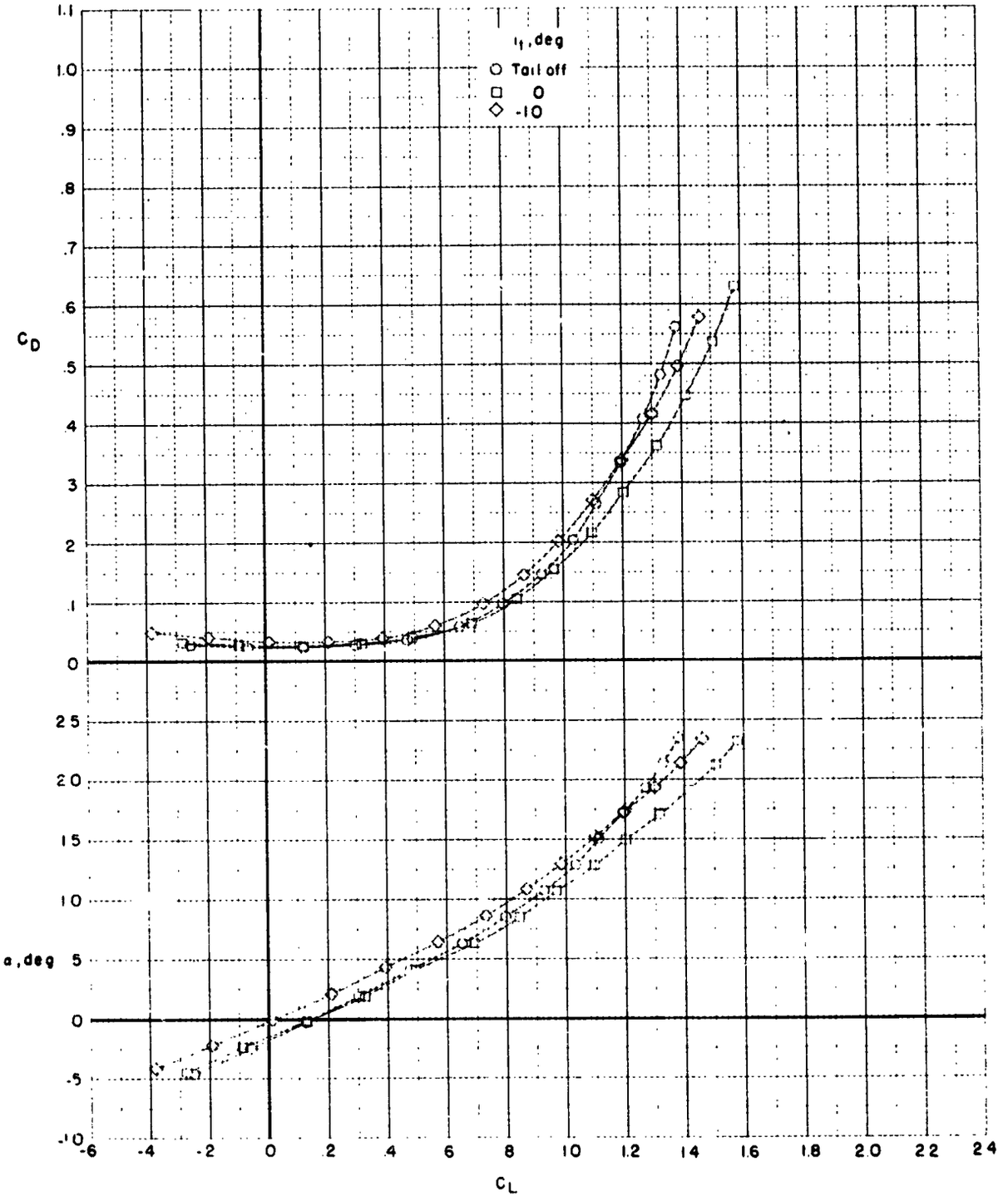

Figure 15.- Effect of horizontal-tail deflection on the longitudinal aerodynamic characteristics of clean-wing configuration with low tail.

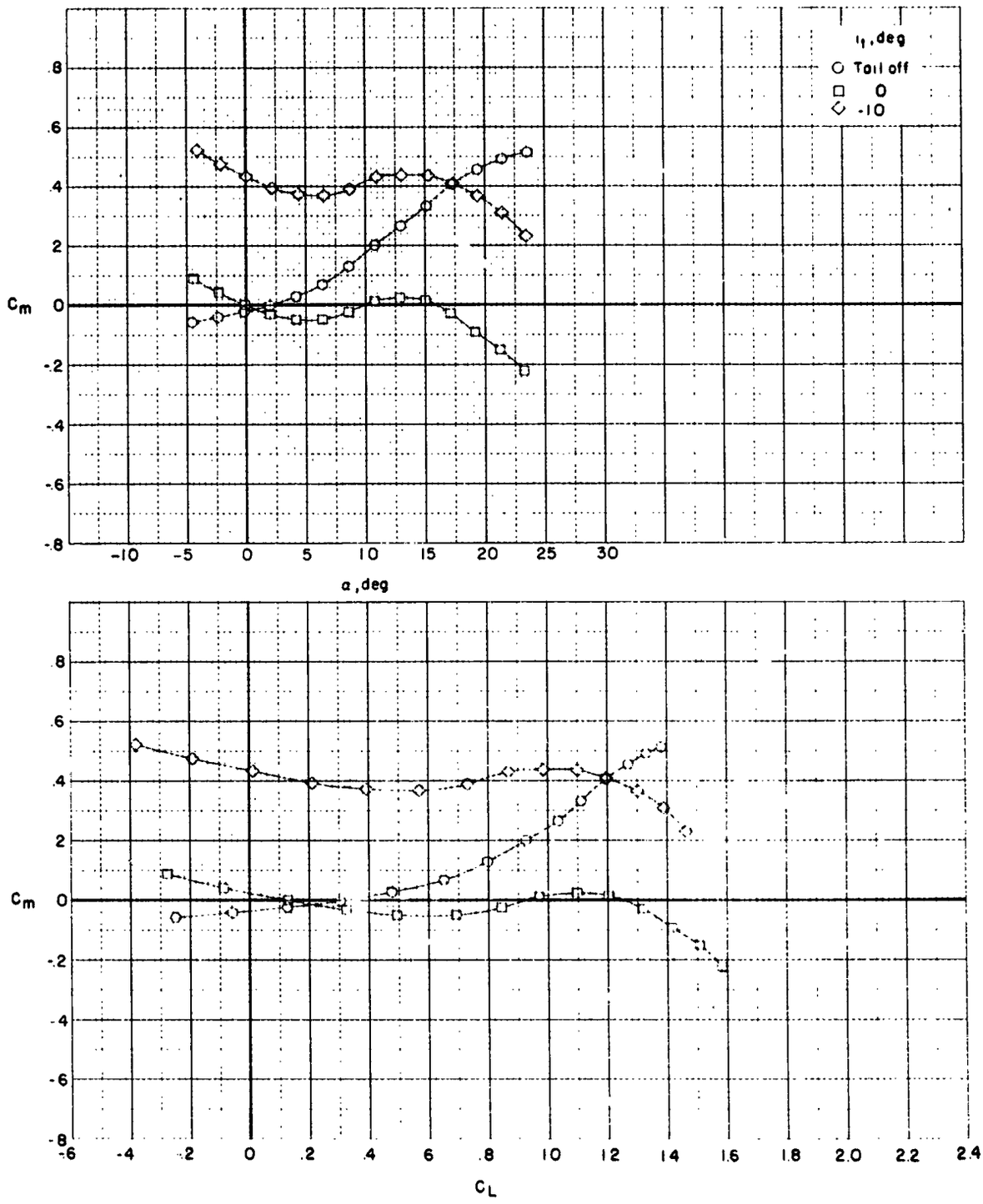

Figure 15.- Concluded.

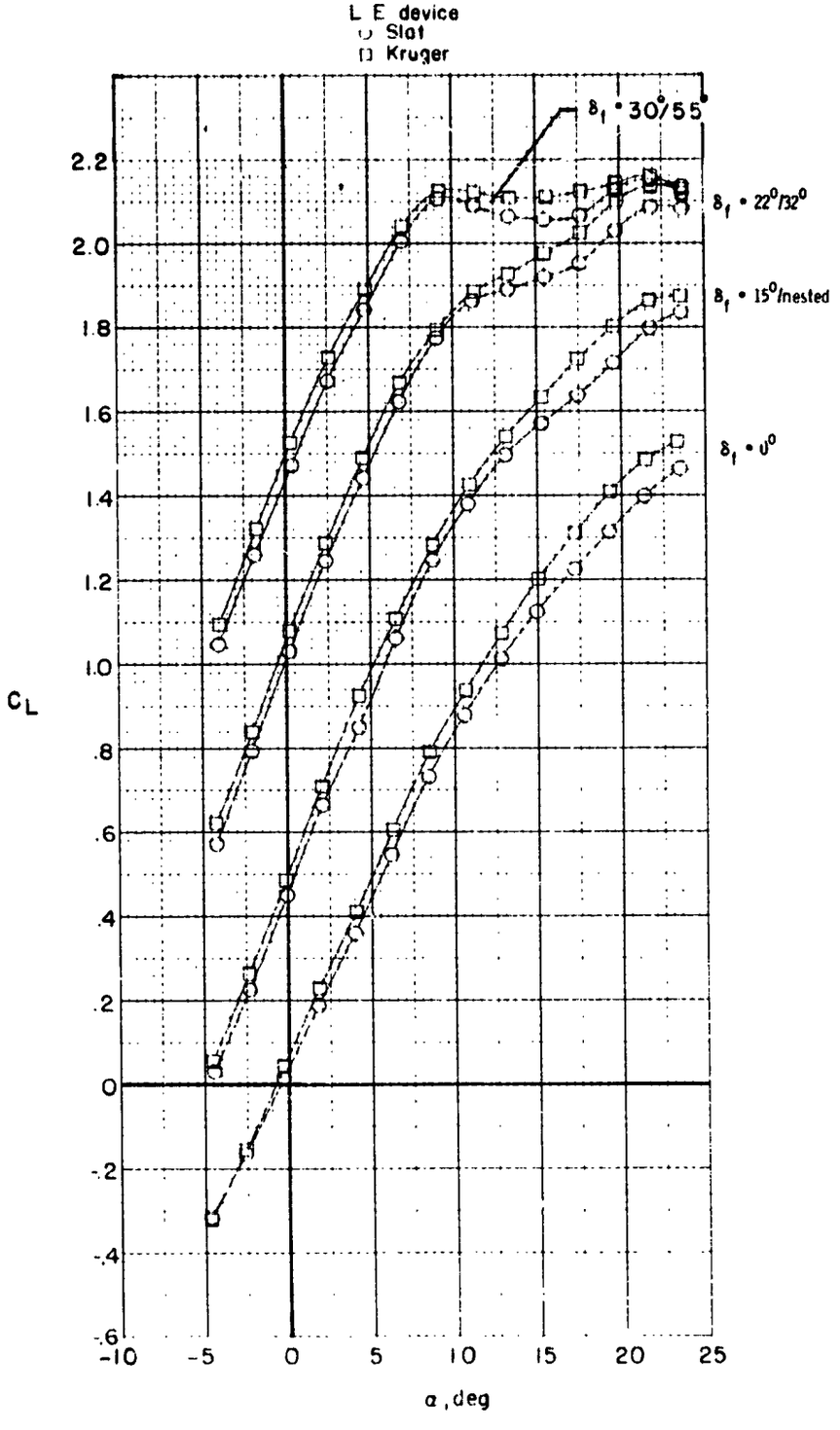

Figure 16.- Comparison of the variation of lift coefficient with angle of attack for various leading-edge devices and several trailing-edge flap deflections. $\delta_S = \delta_K = 45^\circ$; horizontal tail off.

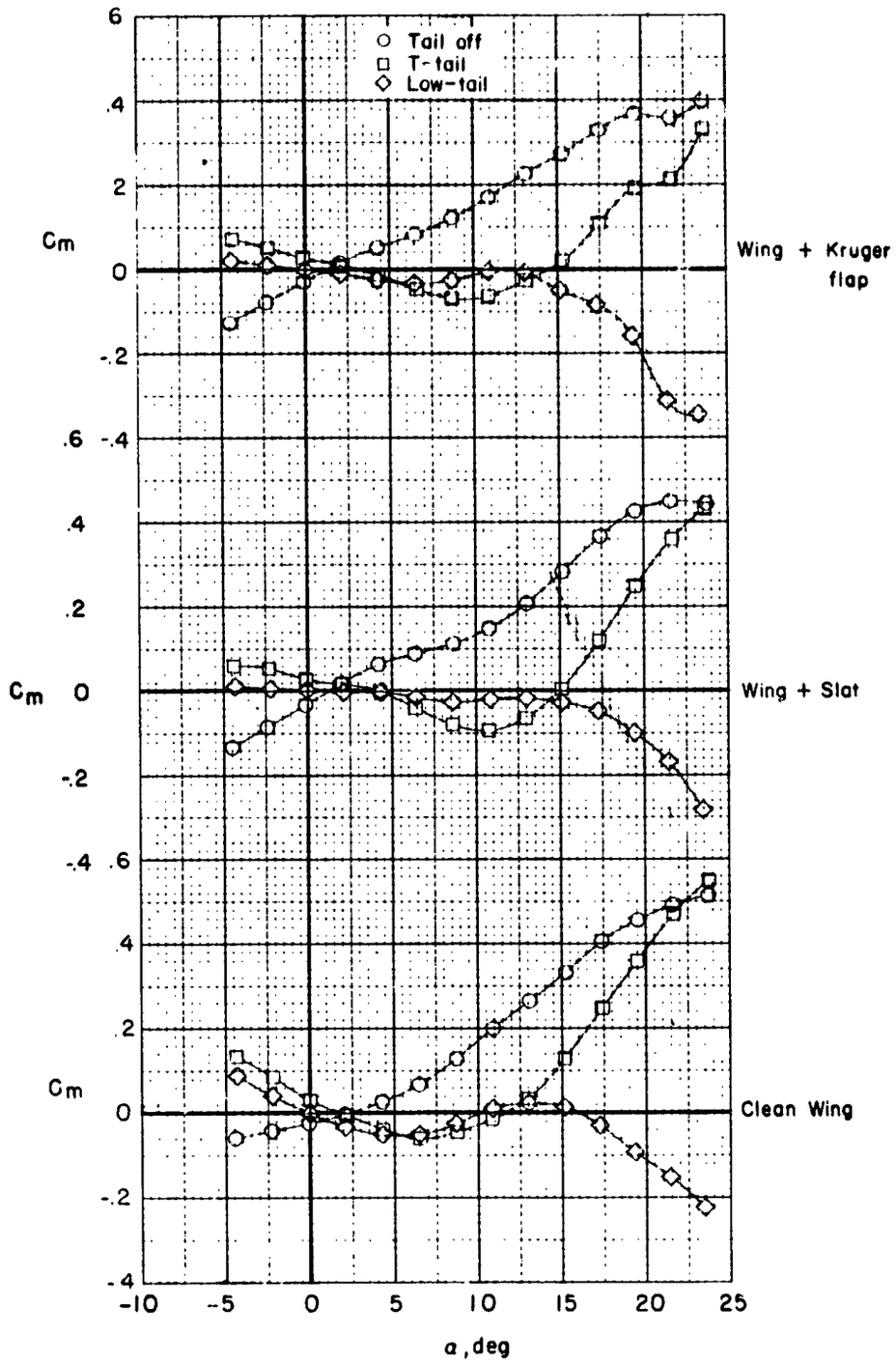

(a) Trailing-edge flap off.

Figure 17.- Comparison of the variation of longitudinal stability with angle of attack for two horizontal-tail heights and various leading-edge devices.

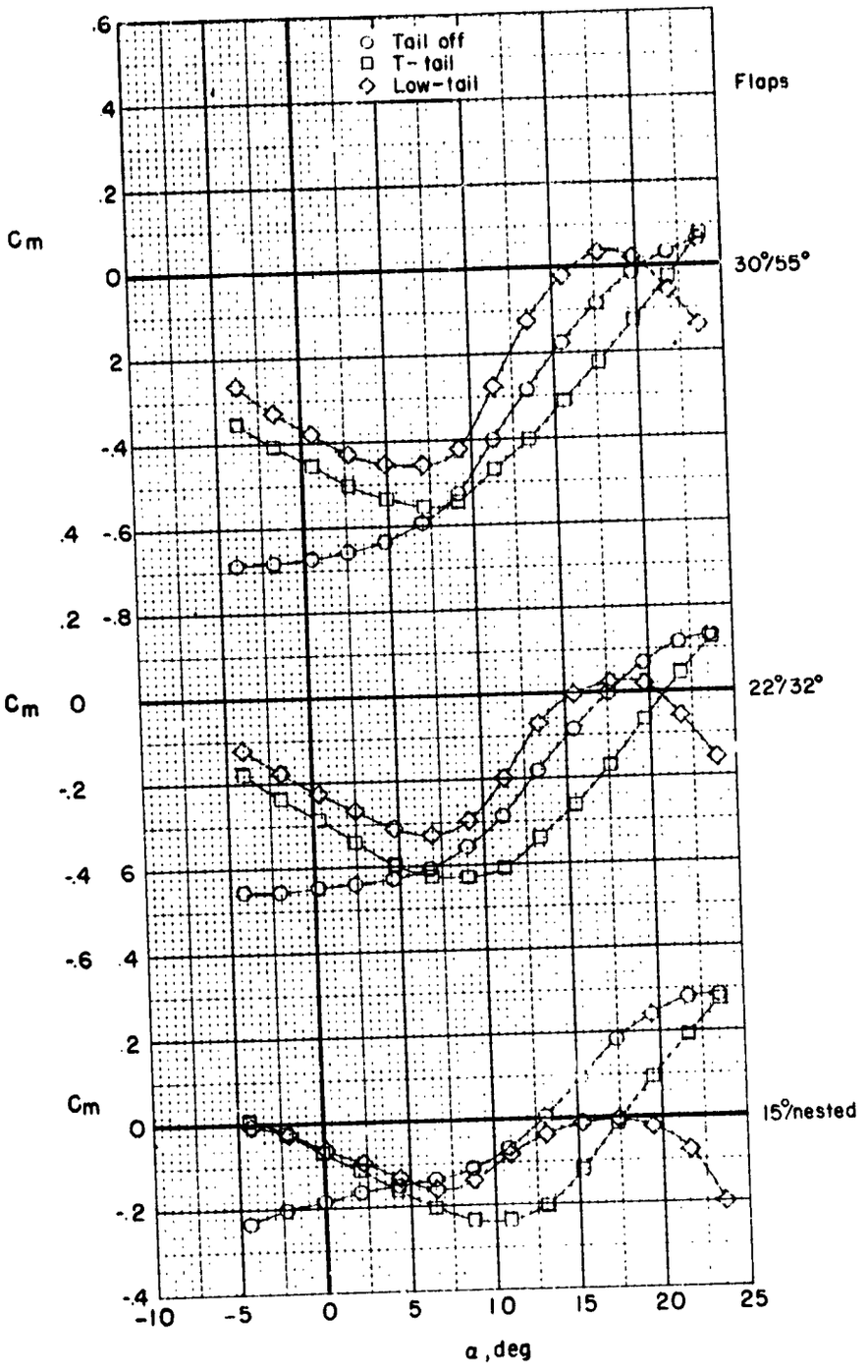

(b) Trailing-edge flap on; $\delta_s = 45^o$.

Figure 17.- Continued.

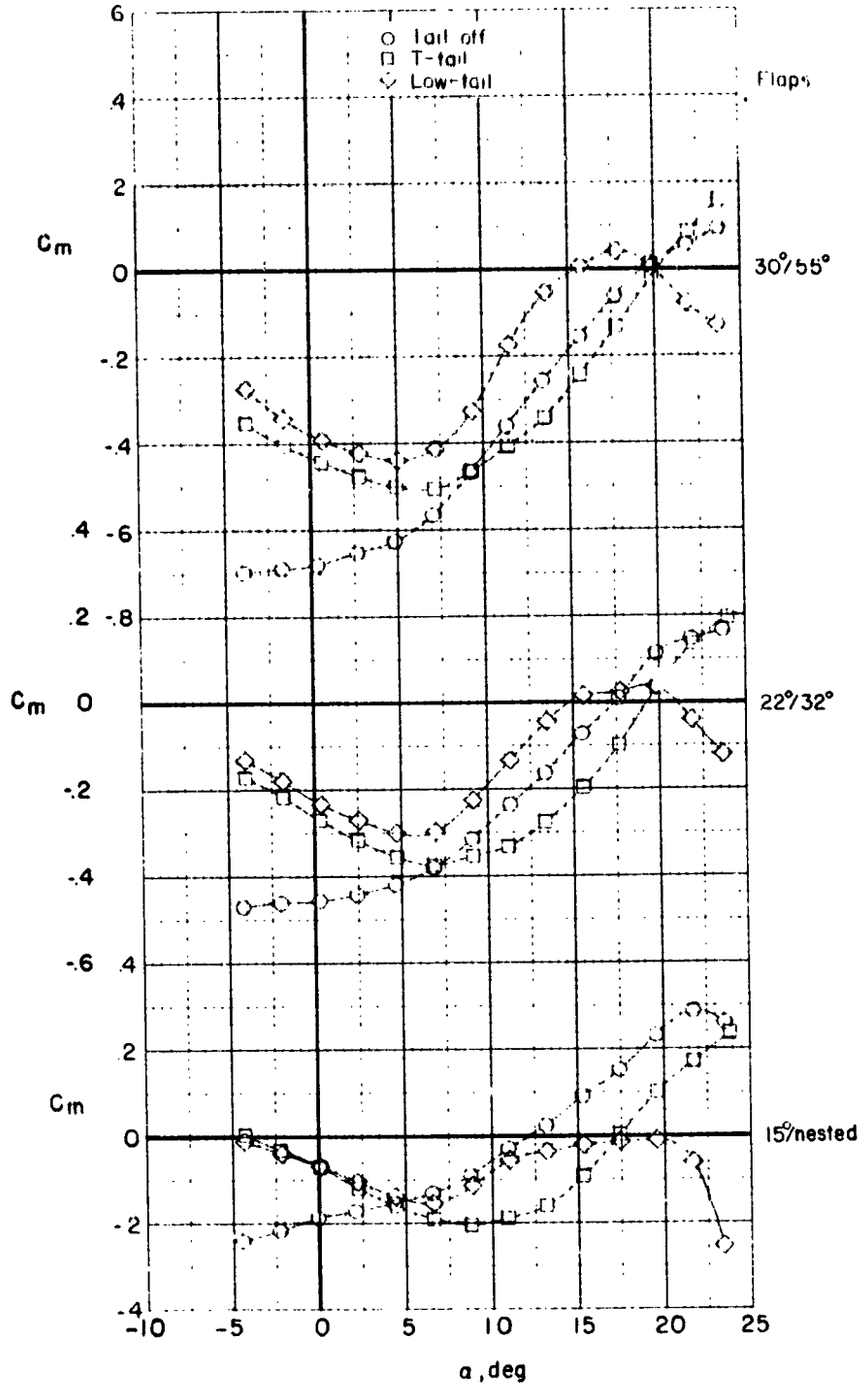

(c) Trailing-edge flap on; $\delta_K = 45^o$.

Figure 17.- Concluded.